NASA Contractor Report 4081

Analysis of the Vibratory Excitation Arising From Spiral Bevel Gears

William D. Mark

CONTRACT NAS3-23703
JULY 1987

NASA

NASA Contractor Report 4081

Analysis of the Vibratory Excitation Arising From Spiral Bevel Gears

William D. Mark
BBN Laboratories Incorporated
Cambridge, Massachusetts

Prepared for
Lewis Research Center
under Contract NAS3-23703

National Aeronautics
and Space Administration

**Scientific and Technical
Information Office**

1987

TABLE OF CONTENTS

TABLE OF CONTENTS (cont.)

SUMMARY

The static transmission error is widely recognized to be the principal source of vibratory excitation arising from meshing gear pairs. In this report, a generalized three-component transmission error of meshing spiral bevel gears is defined. Equations and computational procedures are developed for predicting the generalized transmission error components from their underlying causes.

First, it is shown that the traditional one-component transmission error is incapable of describing the vibratory excitation of spiral bevel gears arising from nonconjugate meshing action without making arbitrary, generally unjustifiable assumptions. A three-component generalized transmission error definition is introduced to rectify this deficiency. Contact between meshing teeth is assumed to take place in a plane surface containing the pitch element. Gears with spherical involute teeth exactly satisfy this assumption, and gears manufactured on the crown rack basis closely satisfy this assumption.

Equations are derived yielding the three components of the generalized transmission error in terms of deviations of tooth surfaces from equispaced perfect spherical involute surfaces and tooth/gearbody elastic deformations arising from the three components of the generalized force transmitted by the gears. It is explained how to incorporate these equations into the equations of motion of a gear system.

Equations are derived for the three components of the generalized force transmitted by the gears which are valid whenever inertial effects of the meshing gears and their supports are negligible. Bearing offsets from the positions occupied by the shaft centerlines of perfect spherical involute bevel gears and bearing/bearing support flexibilities enter into the computation of these forces. When these forces are used to predict the transmission error, one obtains the generalized static transmission error.

For given forces transmitted by the gears, the three components of the generalized transmission error are shown to be stationary with respect to small independent variations in the positions of the endpoints of the lines of tooth contact about their true values. One of these transmission error components is shown to take on a minimum value with respect to these variations. A computational procedure based on this extremum principle is described which is suitable for computing the zone of tooth contact in the plane of contact, the three components of the generalized static transmission error, and their spectra.

INTRODUCTION

For some time, lack of conjugate action (refs. 1,2) has been recognized to be the principal source of vibratory excitation arising from the meshing action of parallel-axis gear pairs (refs. 3-11). This lack of conjugate action is approximately characterized by the static transmission error (refs. 3,4), which is loosely defined (refs. 7,9) as the deviation from linearity of the angular position of a gear measured as a function of the angular position of the gear it meshes with when the gear pair is transmitting torque at low enough speed so that inertial effects are negligible. A more precise definition of the static transmission error is given by equation (1) of reference 9 and equation (2.1) of this report.

The static transmission error can be combined with the equations of motion of a gear system to predict responses of system elements of interest using the approximate method described on p. 1410 of reference 7 and pp. 13-18 of reference 12. An exact method for combining the transmission error with the quations of motion is described by equations (3.44) and (3.45) and the accompanying text of this report.

When characterizing the vibratory excitation of parallel-axis gear systems by the transmission error, there is an implied assumption that the shafts in a meshing gear pair remain parallel with one another even though they may be moving in relation to each other (refs. 7,9,12). Such motion is necessary for vibratory energy to be transmitted from the shafts into the bearings and gear casing - which, in turn, vibrates and radiates sound. However, in the case of nonparallel-axis gears, and spiral bevel gears in particular, it is shown in the present report in the text accompanying equations (2.3) and (2.4) that there would appear to be no physically justifiable assumption comparable to the assumption of the shafts of parallel-axis gears remaining parallel during their motions. Thus, in the present report, the traditional concept of the transmission error is generalized to a three-component transmission error. The three components completely characterize the vibratory excitation arising from arbitrary relative motions of the two gears of a meshing pair - provided that the surface of tooth contact is reasonably well approximated by a plane surface passing through the point occupied by the pitch cone apexes of the two meshing gears.

The generalization of the traditional one-component transmission error to the three-component generalized transmission error very substantially complicates transmission error analysis and its usage in the equations of motion of gear systems. Nevertheless, this generalization is necessary to avoid completely arbitrary assumptions characterizing the angular motions between nonparallel shafts.

However, the three-component generalized transmission error described herein retains another assumption employed in the traditional transmission error characterization; namely, that all tooth contact takes place in a plane surface. In the case of parallel-axis gears, this plane is the base plane (refs. 7-9), sometimes referred to as the plane of action. In the case of straight and spiral bevel gears, this surface is the base plane associated with spherical involute tooth generation (p. 199 of ref. 13) which is discussed in detail in the present report. The base plane also may be regarded as the plane containing the pitch element that is tangent to the true surface of tooth contact (pp. 1-4 and 1-16 of ref. 14). The octoid path of contact of gears manufactured on the crown rack basis (pp. 494-496 of ref. 15) is very nearly linear where actual tooth contact takes place (p. 322 of ref. 1; p. 1-15 of ref. 14). Thus, it is felt that the very substantial simplification achieved by assuming all tooth contact to take place in a plane surface containing the pitch element easily justifies this basic assumption. Even utilizing this assumption, the analysis required to understand and predict the generalized transmission error is very much more complicated than that required to understand and predict the traditional transmission error of parallel-axis gears.

The goals of the work described in this report have been to carry out an analysis of the generalized transmission error arising from spiral bevel gear pairs in sufficient detail (1) to gain a physical understanding of the factors that govern its magnitude and characteristics, and (2) to predict its magnitude and characteristics from these factors it depends on. It is shown that these physical factors include:

(1) deviations of tooth running surfaces from perfect conjugate surfaces

(2) tooth/gearbody stiffnesses

(3) deviations of gearshaft bearing centerline positions from the shaft centerline positions of perfect conjugate gears

(4) bearing/bearing support flexibilities, and

(5) the shaft input torque.

Appropriate descriptions of all of the above quantities are required to predict the generalized static transmission error of spiral bevel gears. Thus, all of the above quantities play important roles in controlling the magnitude and characteristics of the vibratory excitation arising from spiral bevel gear pairs.

In addition to the above-listed factors, the contact ratios play an important role in smoothing the lack of conjugate action contribution of individual teeth (refs. 7-9). Large contact ratios are helpful in reducing the transmission error.

THE GENERALIZED TRANSMISSION ERROR OF SPIRAL BEVEL GEARS

It is widely recognized (refs. 3-11) that the static transmission error (refs. 3,4) describes the principal source of vibratory excitation arising from meshing gear pairs. The static transmission error characterizes the deviation from conjugate action (refs. 13,16) of one gear with respect to its mating gear. The angular static transmission error can be defined loosely (refs. 7,9) as "the deviation $\delta\theta$ from linearity of the angular position θ of a gear measured as a function of the angular position of the gear it meshes with when the gear pair is transmitting a constant torque at low enough speed so that inertial effects are negligible." In gearing vibration analyses, it generally is more convenient to use a lineal equivalent $\zeta = R_b\delta\theta$ to the angular static transmission error, where R_b is the base circle radius of the gear whose angular transmission error is $\delta\theta$. The lineal static transmission error describes the deviation from conjugate action as a linear error in the plane of contact.

A slightly different <u>definition</u> of the lineal static transmission error useful for characterizing the vibratory excitation arising from a meshing gear pair of nominal involute design can be given (ref. 9, p. 57) as

$$\zeta \triangleq R_b^{(1)}\ \delta\theta^{(1)} - R_b^{(2)}\ \delta\theta^{(2)} \tag{2.1}$$

where $R_b^{(1)}$ and $R_b^{(2)}$ are the base circle radii of the two gears (1) and (2) of the pair and $\delta\theta^{(1)}$ and $\delta\theta^{(2)}$ are the angular deviations of gears (1) and (2) from the positions of their rigid perfect involute counterparts determined under the condition that lateral displacements $v^{(1)}$ and $v^{(2)}$ of the two gear shafts in the direction parallel to the plane of contact are zero (Fig. 1). The sign convention implied by equation (1)* and Fig. 1 is such that the lineal static transmission error ζ is positive when the deviations from perfect involute teeth are equivalent to <u>removal</u> of material from the running surfaces of the teeth.

In a gearing system in operation, the transmission error from each gear pair in the system arising from static and dynamic effects must be compensated for by rotational increments and torsional deformations of the shafting and/or lateral

---

*Reference to equations in the same section as the equation citation will be made without the section number in the citation.

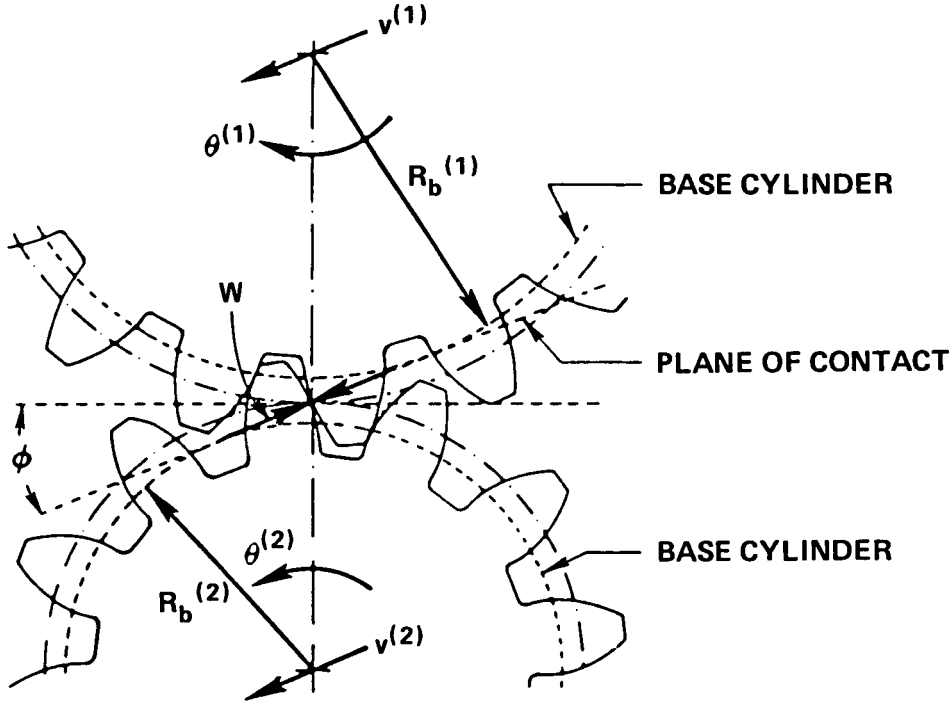

FIG. 1. PAIR OF MESHING PARALLEL-AXIS GEARS.

translational displacements $v^{(1)}$ and $v^{(2)}$ of the gear shafts in the direction parallel to the plane of contact (Fig. 1). This observation can be expressed (ref. 7, p. 1410) by the relation

$$R_b^{(1)}\,\delta'\theta^{(1)} + v^{(1)} - R_b^{(2)}\,\delta'\theta^{(2)} - v^{(2)} = \zeta \tag{2.2}$$

where the angular deviations $\delta'\theta^{(1)}$ and $\delta'\theta^{(2)}$ encountered under running conditions generally are different from the angular deviations $\delta\theta^{(1)}$ and $\delta\theta^{(2)}$, respectively, used in the definition (1) of the static transmission error.

In utilizing the static transmission error ζ as the vibratory excitation in the equations of motion of a gearing system, an equation of the form of equation (2) is written for each pair of parallel-axis gears in the system. Since the lateral shaft displacements $v^{(1)}$ and $v^{(2)}$ are required to predict the rate of vibratory energy flow into the gear supporting structure, accurate prediction of these displacements is very important in noise analyses. However, in equation (2) there is an implicit assumption that the shafts of gears (1) and (2) remain parallel when laterally displaced - i.e., that each displacement $v^{(1)}$ and $v^{(2)}$ is the same at the bearing locations at the two ends of the shaft. The simplification of the analyses that results from this assumption undoubtedly justifies its use in most cases involving parallel-axis gears.

In the case of bevel gears, however, there does not seem to be a simplifying assumption of comparable validity concerning lateral shaft displacements that would lead to a single relation analogous to equation (2) for each gear pair. To see this, we note first that, for either gear (1) or gear (2), the transmission error ζ in equation (2) can be compensated for by the term $R_b^{(\cdot)}\,\delta'\theta^{(\cdot)}$ arising from the angular deviation $\delta'\theta^{(\cdot)}$ or by the term $v^{(\cdot)}$ arising from the lateral shaft displacement of gear $(\cdot)$. For parallel-axis gears, the base circle radius $R_b^{(\cdot)}$ is a constant that is independent of axial location on the gear. In the case of bevel gears of nominal (spherical) involute design (ref. 13, p. 199; ref. 16, p. 128), however, the base cylinder of a parallel-axis gear is replaced by a base cone whose base circle radius varies in direct proportion to axial distance from the base cone apex. Thus, a single equation of the form of equation (2) could be made to apply to

bevel gears only if one were to assume that the quantity $\zeta - v^{(1)} + v^{(2)}$ varies axially in direct proportion to distance x' from the base cone apex - i.e., that

$$\zeta - v^{(1)} + v^{(2)} = ax', \tag{2.3}$$

where a is a constant. If the transmission error ζ is assumed to be independent of axial location x', this assumption would, in turn, require that shaft lateral displacements $v^{(1)}$ and $v^{(2)}$ vary with axial location x' as

$$v^{(1)} - v^{(2)} = \zeta - ax', \tag{2.4}$$

where ζ and a are independent of x'. It would be difficult to justify such an assumption on physical grounds.

In the present section, the need for such an assumption is removed by defining the generalized transmission error for spiral bevel gears of nominal spherical involute design. The generalization of the concept of the transmission error contained herein removes the need for all assumptions in gearing vibration analyses that would constrain the displacements of gear shafts from the positions occupied by the shafts of their rigid perfect involute counterparts.

Kinematics of Involute Spiral Bevel Gear Action

Geometric Description of Tooth Contact. Straight-tooth and spiral bevel gears transmit motion between nonparallel intersecting shafts. The motion transmitted by perfect bevel gear pairs is equivalent to that transmitted by perfect right circular cones with a common apex in pure rolling contact with no slipping (ref. 13, pp. 125-128). The ratio of the instantaneous angular velocities of the two cones about their axes is exactly constant. Such cones in rolling contact are referred to as pitch cones.

The teeth of a pair of involute bevel gears may be imagined to have been generated utilizing the base cones of the gears. The base cones are smaller than and concentric with the pitch cones. The base and pitch cones of both meshing gears have the same common apex A (Fig. 2). Let us imagine that the base cone of the upper gear in Fig. 2(a) is covered by a thin inextensible membrane which is unwrapped without slipping from the upper gear and rewrapped without slack onto the

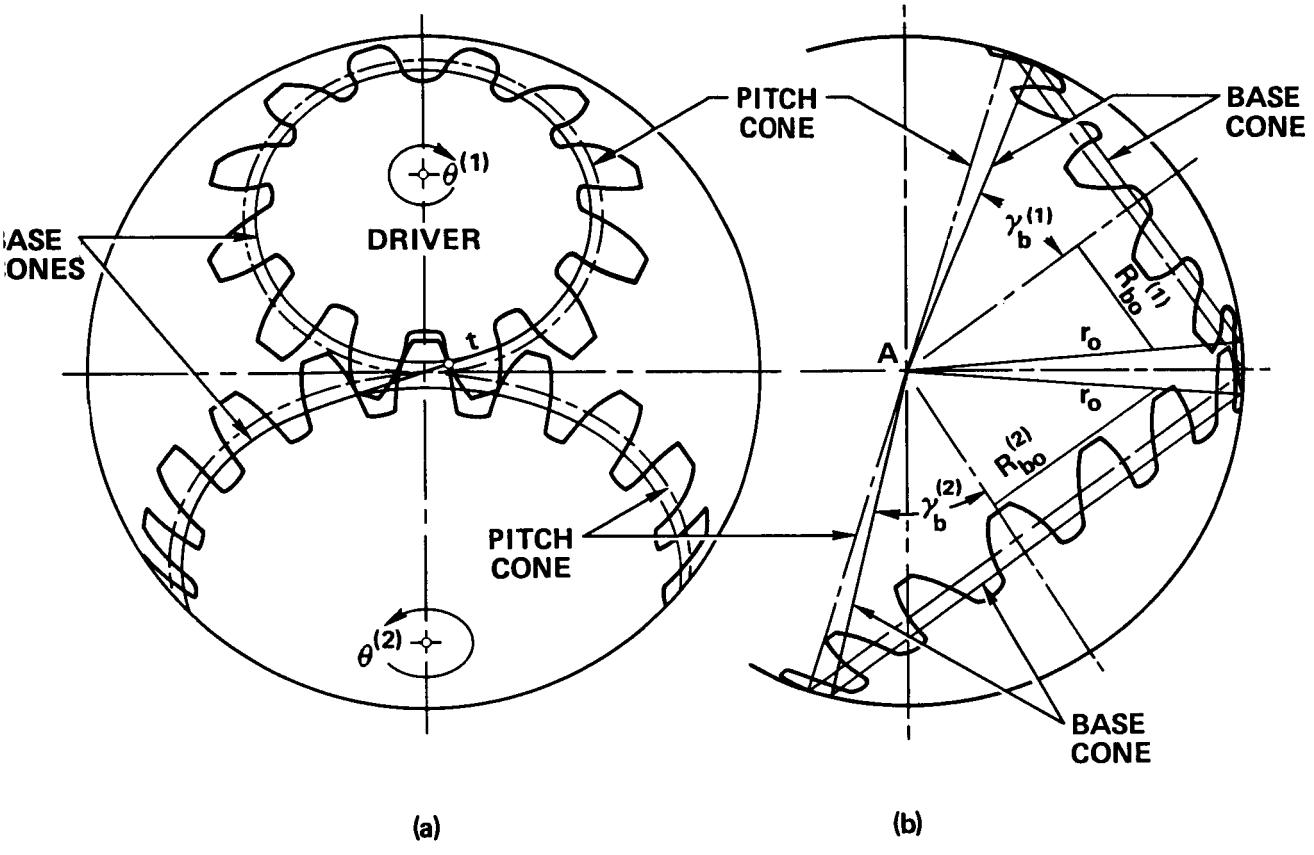

FIG. 2. SPHERICAL BASIS OF BEVEL GEAR ACTION (ADAPTED FROM FIG. 5.18 OF REF. 17 WITH PERMISSION).

base cone of the lower gear as the gears rotate. A point on this membrane traces out a spherical involute curve (ref. 13, pp. 197-199) as it is unwrapped from the base cone of the upper gear. As the membrane is unwrapped, such a point may be imagined to trace out the running suface of the tooth t as is indicated in Fig. 2(a). This process of generating a spherical involute is entirely analogous to the process of generating the involute of a circle (ref. 13, p. 163-167), except that the involute of a circle is generated by unwrapping a membrane from a right circular cylinder, whereas a spherical involute is generated by unwrapping a membrane from a right circular cone.

As the membrane is unwrapped from the base cone of the upper gear shown in Fig. 2(a) and rewrapped onto the base cone of the lower gear, a point on the membrane traces out a trajectory that lies on a spherical surface - as is indicated in the figure. Conversely, when the membrane is unwrapped from the cylinder in the generation of an involute of a circle, a point on the membrane travels in a plane that is perpendicular to the axis of the cylinder. This plane is called the transverse plane. Thus, the spherical surface with center at the base and pitch cone apex illustrated in Fig. 2 is the involute bevel gear counterpart to the transverse plane of involute parallel-axis gears (ref. 17, pp. 56-58). We shall call this spherical surface the transverse sphere.

Let us now imagine several concentric spherical sections of the type shown in Fig. 2, each located at a different radius from the common apex of the base and pitch cones. On each concentric sphere, the teeth of each of the two meshing gears are assumed to have been constructed as spherical involutes as described above. The loci of points connecting the spherical involute surface of a generic tooth t from one sphere to the next determine the shape of the running surface of that tooth. In the case of straight-tooth bevel gears, these loci of points are straight lines normal to the spheres which originate at the apex of the base and pitch cones. Straight-tooth bevel gears are the bevel gear counterparts to spur gears. In the case of spiral bevel gears, the loci of points connecting the surface of tooth t from one sphere to the next are curved or spiral lines which also originate at the apex of the cones, but which are not generally normal to the spheres.

Any spiral bevel gear may be imagined to have been generated from a straight-tooth bevel gear by cutting the straight-tooth gear into an (infinite) number of transverse spherical sections and rotating the sections relative to one another about

the axis of rotation of the gear. This operation produces the stepped bevel gear counterpart (ref. 13, p. 202) to the conceptual generation of a parallel-axis helical gear from a spur gear, which is carried out by cutting the spur gear into an (infinite) number of sections normal to the gear axis and rotating the sections reltive to one another (ref. 13, pp. 190,191). For any shape of tooth spiral, the kinematic action of an involute spiral bevel gear is identical in any transverse spherical section to that of an involute straight-tooth bevel gear.

The taut inextensible membrane connecting the base cones of the two meshing bevel gears (Fig. 2) is tangent to the conical surfaces of both base cones. The locus of points of tangency between each base cone and the membrane is a straight line. From the fact that these two straight lines of tangency intersect at the common apex of the two base cones it follows that the portion of the taut membrane lying between the two base cones is a plane surface tangent to both base cones. Furthermore, from the spherical involute construction of the tooth surfaces it follows that all tooth contact takes place in this plane of tangency for straight-tooth and spiral bevel involute gears. This plane of tangency is called the base plane (ref. 14, pp. 1-16).

At this juncture, it is convenient to replace the taut membrane by a rigid circular disk of infinitesimal thickness positioned in the plane of contact with center at the common apex of the base cones. The disk lies in the base plane and is tangent to both base cones (Fig. 3). As the two gears rotate, the base disk rotates about its center without slipping on either of the two base cones. The motion of the portion of the disk that momentarily lies between the lines of tangency to the base cones is identical to the motion of the taut inextensible membrane that it replaces.

Since all tooth contact takes place in the base plane, all instantaneous lines of tooth contact occur in the plane of the base disk. It follows from the spherical involute construction of the tooth surfaces that the circumferential distances separating the lines of tooth contact in the base plane do not change as the gears rotate. We may imagine that these lines of contact are drawn on the base disk. As the gears and base disk rotate about their respective axes, the true lines of tooth contact and the lines of contact drawn on the base disk exactly coincide in the region of the base plane where tooth contact occurs.

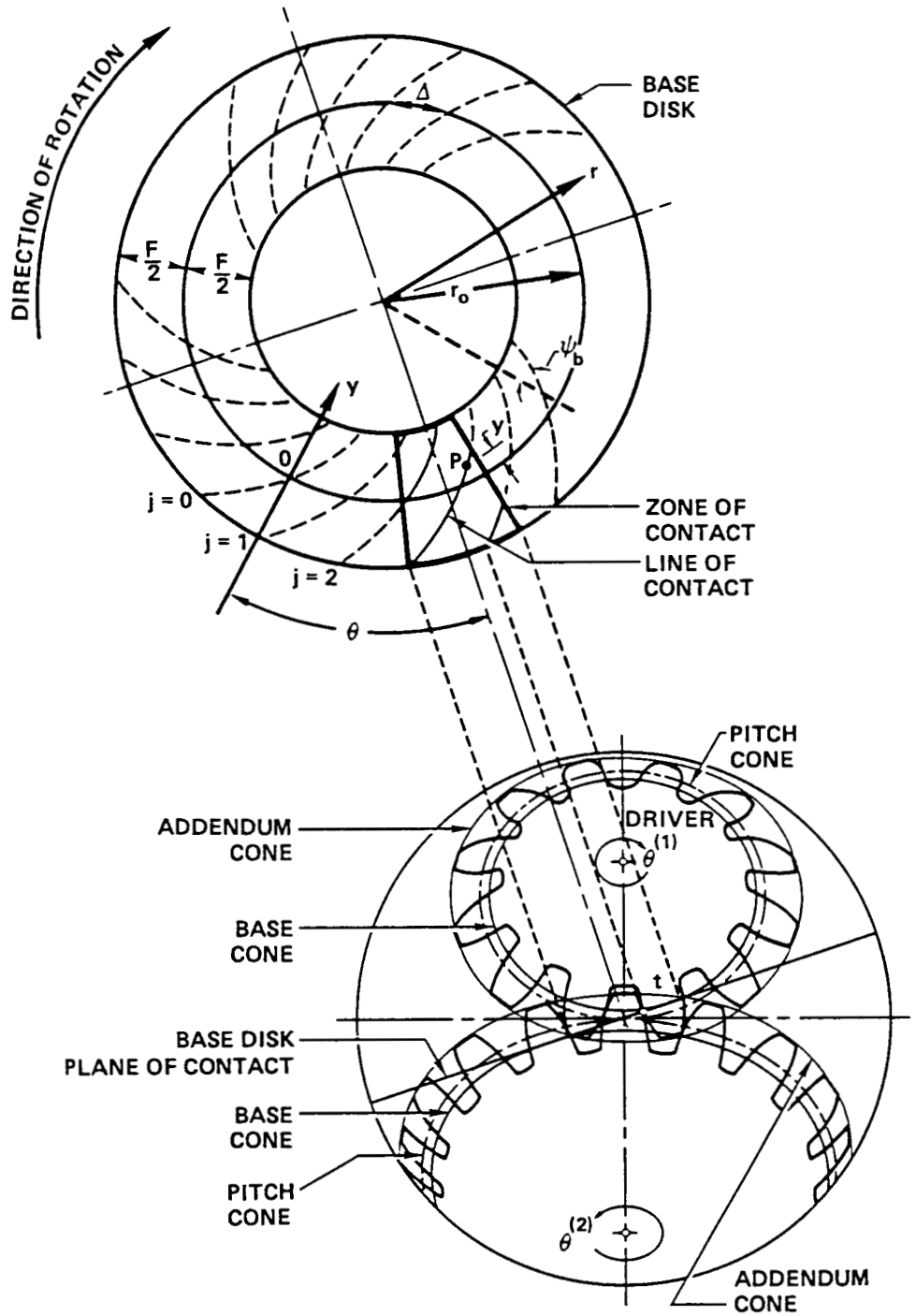

FIG. 3. LOWER FIGURE SHOWS BASE DISK TANGENT TO BASE CONES OF TWO MESHING PERFECT SPHERICAL INVOLUTE SPIRAL BEVEL GEARS. UPPER FIGURE SHOWS ZONE OF CONTACT IN BASE PLANE AND LINES OF CONTACT ON BASE DISK. (LOWER FIGURE ADAPTED FROM FIG. 5.18 OF REF. 17 WITH PERMISSION.)

Figure 3 also shows the addendum cones of the two gears which share a common apex with the base and pitch cones. Actual tooth contact takes place in the sector of the base plane located between the intersections of the two addendum cones with the base plane as is shown in Fig. 3. The two intersections delineating the zone of contact are straight radial lines that intersect at the common apex of the addendum, base, and pitch cones (Fig. 3).

The bevel gears are located between outer and inner spherical surfaces of the type illustrated in Figs. 2 and 3. If the spherical surfaces shown in Figs. 2 and 3 are taken to be the outer surface enclosing the two gears, then the zone of tooth contact in the base plane is the portion of the sector between the outer and inner radii drawn on the base disk in Fig. 3.

The lines of tooth contact in Fig. 3 are drawn solid within the zone of contact and dashed outside the zone of contact. As the gears and base disk rotate about their respective axes, the lines of tooth contact affixed to the base disk pass through the fixed zone of tooth contact as can readily be imagined with the aid of Fig. 3. This geometric model of spiral bevel gear action is an exact representation of the kinematic behavior of the lines of contact of perfect involute spiral bevel gears.

Tooth Contact Coordinates in the Base Plane. Concentric circles located at radii $r_o + (F/2)$ and $r_o - (F/2)$ on the base disk in Fig. 3 define the outer and inner radii of the zone of tooth contact in the base plane. Thus, the radial span of the zone of tooth contact in the base plane is F and the radial midpoint of this span is r_o. Let y denote a radial coordinate on the base disk in Fig. 3 defined by

$$y \triangleq r_o - r \ , \tag{2.5}$$

where r is the usual radial coordinate with origin at the center of the disk. From equation (5), it follows that the origin of y is located at $r = r_o$ and that y is positive for values of r less than r_o.

Lines of tooth contact on the base disk in Fig. 3 are designated by index values $j = 0,1,2,\cdots$. As the gears and base disk rotate about their respective axes, the angular position of tooth pair $j = 0$ relative to the center of the zone of contact is designated by θ, which is measured in radians. When the angular position of the line

of contact of tooth pair j = 0 at radial location y = 0 exactly coincides with the centerline of the zone of contact on the base disk, we have $\theta = 0$ as is readily apparent from Fig. 3.

Instead of dealing with the angular variable θ, we shall deal primarily with the lineal variable

$$x \triangleq r_o \theta, \tag{2.6}$$

where r_o and θ are defined above. Thus, x also determines the angular position of tooth pair j = 0 relative to the zone of contact centerline. Notice from Fig. 3 that x is the arc length in the base plane of the circular segment of radius r_o between the line of contact of tooth pair j = 0 and the centerline of the zone of contact. The tooth spacing Δ on the base disk in Fig. 3 also is measured on the same circular arc of radius r_o.

Consider the transverse spherical section that passes through the point P shown in the zone of contact on the base disk in Fig. 3. The radius of this spherical section is uniquely determined by the coordinate y that describes the position of P on the line of tooth contact in the base plane. For the particular value of $x = r_o\theta$ illustrated in Fig. 3, the point P determines a unique point located on the running surfaces of the two mating teeth. It follows that specification of a pair of coordinate values x,y determines a unique point of contact on the running surfaces of two mating teeth designated by index j.

Let $\theta^{(1)}$ and $\theta^{(2)}$ denote, respectively, the rotational positions of gears (1) and (2) about their axes of rotation. Consider infinitesimal increments $d\theta$, $d\theta^{(1)}$, and $d\theta^{(2)}$ in the rotational angles of the base disk and the two meshing gears. From the fact that the base disk may be imagined to be rotating without slipping on the two base cones illustrated in Fig. 2, it follows that the infinitesimal lineal increment dx is related to increments $d\theta$, $d\theta^{(1)}$, and $d\theta^{(2)}$ by

$$dx = r_o \, d\theta = R_{bo}^{(1)} d\theta^{(1)} = R_{bo}^{(2)} d\theta^{(2)} , \tag{2.7}$$

where $R_{bo}^{(1)}$ and $R_{bo}^{(2)}$ are the radii of the base cones of gears (1) and (2), respectively, that join the base cone generatrices at distances r_o from the common apex as illustrated in Fig. 2(b). The integral of equation (7) yields

$$x = r_o\theta = R_{bo}^{(1)}\theta^{(1)} = R_{bo}^{(2)}\theta^{(2)} \quad . \tag{2.8}$$

Dividing equation (8) by r_o and using elementary trigonometric relations arising from Fig. 2(b) yields, further,

$$(x/r_o) = \theta = \left(\sin\gamma_b^{(1)}\right)\theta^{(1)} = \left(\sin\gamma_b^{(2)}\right)\theta^{(2)}, \tag{2.9}$$

which relates the angular positions of the base disk and the two meshing gears using only the base cone angles $\gamma_b^{(1)}$ and $\gamma_b^{(2)}$ shown in Fig. 2(b).

Since $\gamma_b^{(1)}$ or $\gamma_b^{(2)}$ can be chosen more or less arbitrarily, it follows with reference to the base disk in Fig. 3 that $2\pi r_o/\Delta$ need not necessarily be an integer. Thus, once θ exceeds 2π, the positions of the lines of tooth contact on the base disk do not, in general, repeat.

The Generalized Transmission Error

We now consider deviation of the kinematic behavior of real bevel gear pairs of nominal spherical involute design from the above-described ideal behavior of rigid perfect involute gear pairs. The effects considered are those arising from geometric deviations of the unloaded tooth surfaces from perfect spherical involute surfaces and from elastic deformations of the teeth and gear bodies caused by tooth loading. In the case of parallel axis spur and helical gears, the above effects have been characterized (refs. 3-11) by the transmission error, which is a one-component scalar representation.

A more complete characterization of the above effects is provided by a three-component version of the transmission error, which we shall call the generalized transmission error. Let us consider the real gear counterparts to the perfect involute gears illustrated in Fig. 3. For any given value of x or θ, there exists a lineal force distribution along each of the lines of contact within the zone of contact shown in Fig. 3 which represents the continuous distribution of forces transmitted by the pair of teeth in contact. If we neglect the effects of friction between meshing teeth, then all such distributed force vectors are normal to the tooth surfaces and from involute construction therefore must lie in the plane of contact. The resultant total force transmitted by the mesh is the vector sum of all

forces transmitted by meshing tooth pairs; hence, the total transmitted resultant force vector also lies in the plane of contact.

This resultant force vector can be described by three scalar components - namely, two orthogonal force components that lie in the plane of contact, say W_t and W_r, and the moment, say τ, of the resultant total transmitted force taken about a specified point in the plane of contact. The directions of W_t and W_r will be chosen perpendicular and parallel to the zone of contact centerline, respectively. Moment τ will be taken about the point located at the mid-radial position $y = 0$ on the zone of contact centerline illustrated in Fig. 3. Force components W_t and W_r will be taken as positive when they result in tooth pairs being brought together (rather than separated). If the total transmitted resultant force vector is taken to be positive for this same condition, then τ will be taken as positive when the total resultant force vector passes through the zone of contact centerline at a negative value of $y = r_o - r$. This sign convention is illustrated in Fig. 4.

The above-described distributed tooth forces give rise to elastic deformations of the teeth and bodies of the two meshing gears. These elastic deformations result in displacements of the gear bodies "measured" at the gear shaft centerlines. Geometric deviations of the tooth running surfaces of the unloaded real gears from the spherical involute surfaces of their perfect involute counterparts give rise to additional displacements of the gear bodies at their shaft centerlines from the positions of their perfect involute counterparts. For a given value of x or θ and given loading components W_t, W_r, and τ, these displacements are characterized by the generalized transmission error which describes the composite change in position of the bodies of two meshing real gears at their shaft centerline locations from the positions of their rigid perfect involute counterparts.

In the present report, the total deviation of the loaded tooth surfaces of the real gears from the surfaces of their rigid perfect involute counterparts is assumed to be sufficiently small so that the surface of actual tooth contact can be assumed to be the plane of contact of their rigid perfect involute counterparts illustrated in Fig. 3. Thus, in comparing the positions of the loaded real gears with the positions of their perfect involute counterparts, we are concerned only with those differential position components that lie in the plane of contact. It follows that the generalized transmission error can be characterized by three displacement components - namely, two translation components that lie in the plane of contact and

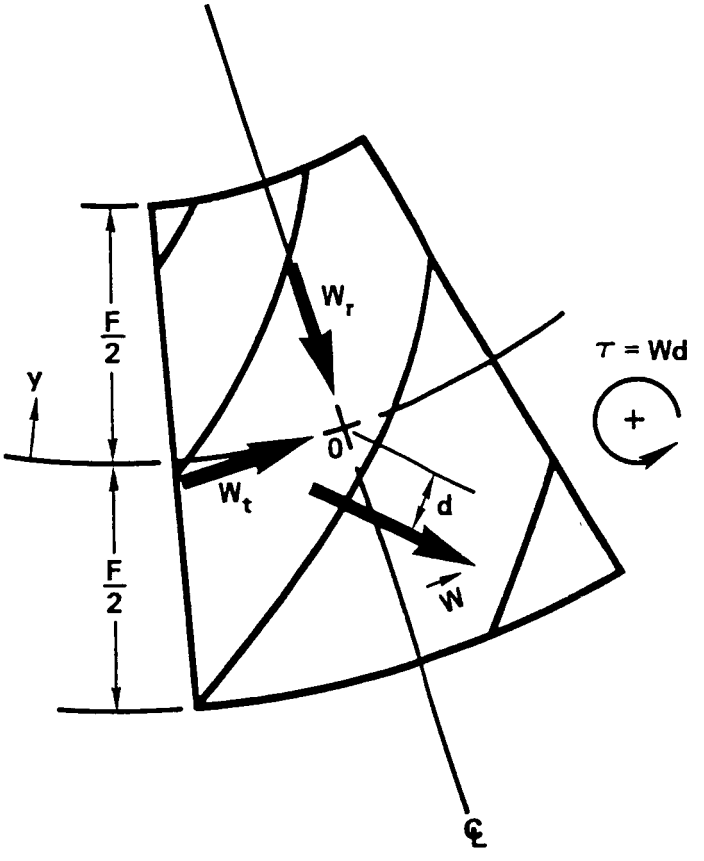

FIG. 4. SCALAR CHARACTERIZATION OF TOTAL FORCE $\vec{W}$ TRANSMITTED BY THE GEAR MESH. THE FIGURE ILLUSTRATES INSTANTANEOUS LINES OF TOOTH CONTACT AND ZONE OF CONTACT IN PLANE OF CONTACT WHICH IS PLANE OF PAPER. FORCE COMPONENTS SHOWN ARE POSITIVE AND ARE ACTING ON THE GEAR TO THE RIGHT. MOMENT τ IS POSITIVE WHEN $\vec{W}$ PASSES THROUGH ZONE OF CONTACT CENTERLINE AT A NEGATIVE VALUE OF y AS SHOWN IN THE FIGURE.

one rotation component about a specified axis in the plane of contact. Since these components represent small displacements, the rotation component of the generalized transmission error can be represented by a vector (ref. 18, pp. 107,108) which is normal to the plane of contact.

Each of these three displacement components of the generalized transmission error characterizes the composite displacement of both gears contributing to that component. The axis of rotation of the rotation component μ of the generalized transmission error will be taken to be the point 0 located on the zone of contact centerline at the value of $y = 0$ shown in Fig. 4. The rotation μ represents the sum of the rotations about the axis 0 of the two meshing gears from the positions of their perfect involute counterparts; μ is taken to be positive when the portions of the teeth in the negative y region of the zone of contact come together more, relative to their perfect involute counterparts, than the portions of the teeth in positive y region of the zone of contact. The directions of the two translation components ζ_t and ζ_r of the generalized transmission error are chosen to coincide, respectively, with the directions of the corresponding force components W_t and W_r illustrated in Fig. 4. Each component ζ_t and ζ_r represents the sum of the displacements of the two meshing gears from the positions of their perfect involute counterparts; ζ_t and ζ_r each is taken to be positive when it represents a displacement of the real gears "equivalent" to that caused by removal of material from the tooth surfaces of their perfect involute counterparts. Thus, positive values of W_t, W_r, and τ are associated with positive contributions of the elastic deformation components of ζ_t, ζ_r, and μ, respectively. The sign convention of the generalized transmission error components is illustrated in Fig. 5.

Expression for Generalized Transmission Error in Terms of Gear Displacements at Shaft Centerlines

The base cone and plane of contact of a generic bevel gear are shown in Fig. 6. Orthogonal components $x_1^{(\cdot)}$, $x_2^{(\cdot)}$, and $x_3^{(\cdot)}$ designate the three translation components of the shaft centerline position of gear $(\cdot)$ from the position of its rigid perfect involute counterpart. The origin of the $x_1^{(\cdot)}$, $x_2^{(\cdot)}$, $x_3^{(\cdot)}$ coordinate system is located at the common apex of the base cones of the involute counterparts of the two meshing gears. The $x_3^{(\cdot)}$ axis coincides with the axis of rotation of the involute counterpart of gear $(\cdot)$. The $x_1^{(\cdot)}$ axis lies in the plane of contact. Positive directions of the $x_1^{(\cdot)}$, $x_2^{(\cdot)}$, and $x_3^{(\cdot)}$ axes are indicated by the arrows on the ends

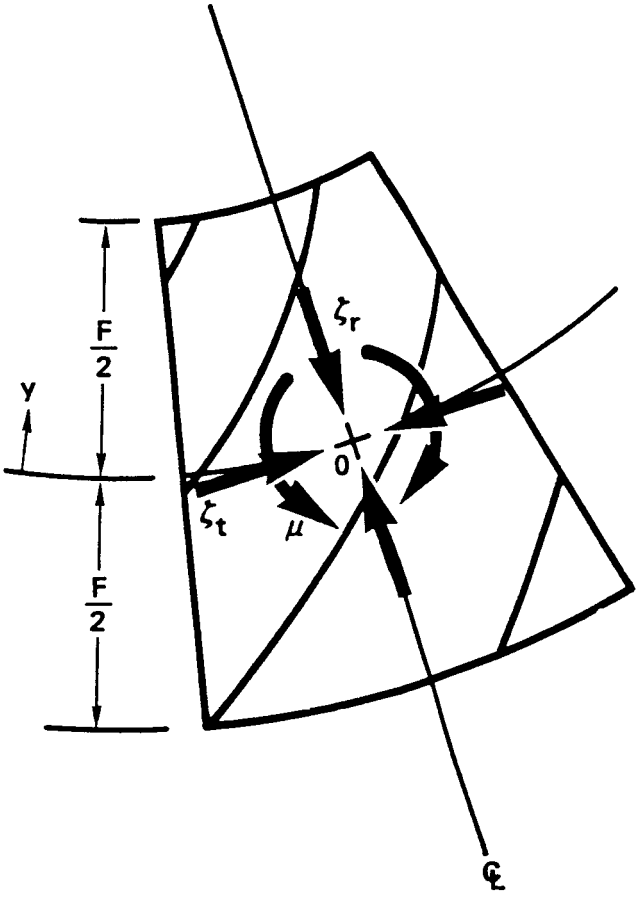

FIG. 5. COMPONENTS OF THE GENERALIZED TRANSMISSION ERROR. MUTUALLY APPROACHING ARROWS REPRESENT GEAR BODIES COMING TOGETHER RELATIVE TO THEIR PERFECT INVOLUTE COUNTERPARTS. DIRECTIONS SHOWN REPRESENT POSITIVE VALUES OF ζ_t, ζ_r, AND μ. EACH COMPONENT REPRESENTS THE SUM OF THE DISPLACEMENTS OF THE TWO MESHING GEARS RELATIVE TO THEIR PERFECT INVOLUTE COUNTERPARTS; THESE DISPLACEMENTS ARE "MEASURED" AT THE GEAR SHAFT CENTERLINES.

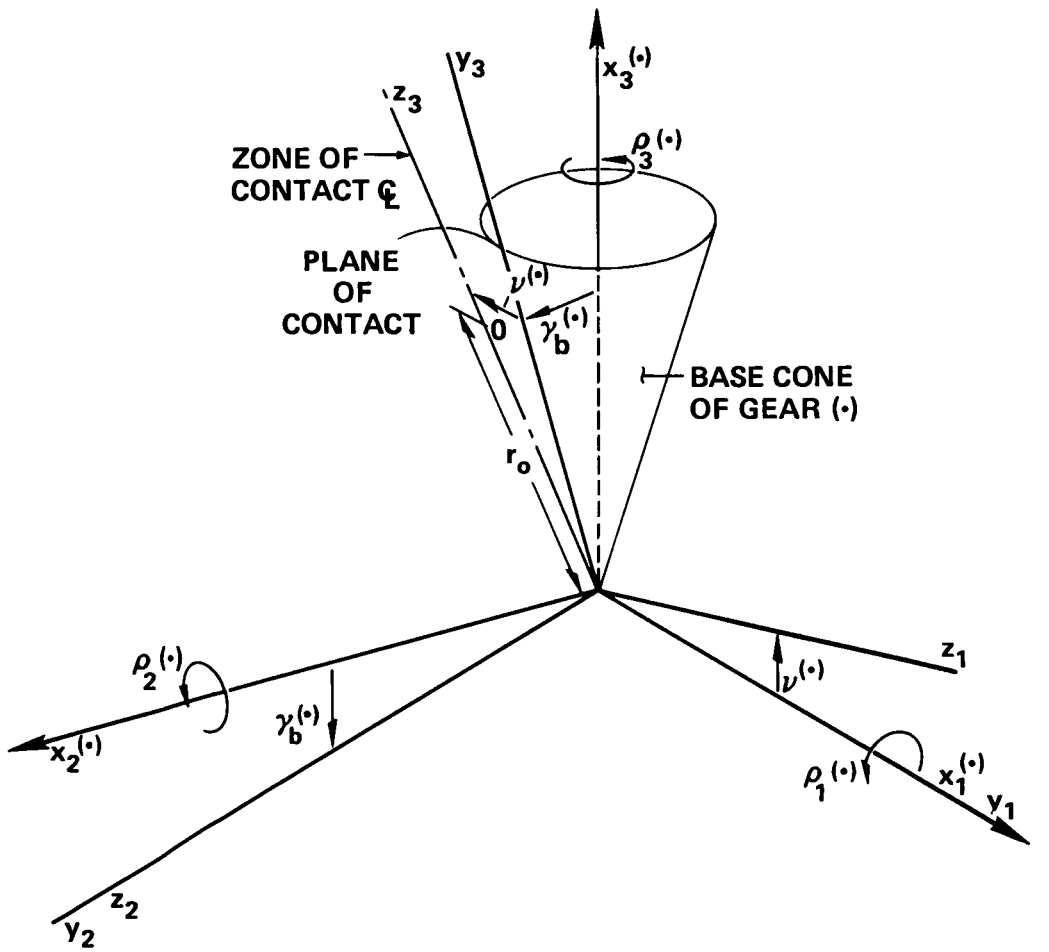

FIG. 6. BASE CONE AND PLANE OF CONTACT FOR A GENERIC BEVEL GEAR PAIR. COORDINATES $x_i^{(\cdot)}$ AND $\rho_i^{(\cdot)}$, i = 1,2,3 MEASURE THE DIFFERENCE IN POSITION OF THE SHAFT CENTERLINE OF GEAR (·) FROM THE POSITION OF ITS RIGID PERFECT INVOLUTE COUNTERPART. SIGN CONVENTIONS FOR THE $x_i^{(\cdot)}$ AND $\rho_i^{(\cdot)}$, i = 1,2,3 ARE ASSOCIATED WITH THE GEARS SHOWN IN FIG. 3 AND DESCRIBED IN THE FIRST TWO ROWS OF TABLE 1.

of the coordinate axes. These designations completely define the $x_1^{(\cdot)}$, $x_2^{(\cdot)}$, $x_3^{(\cdot)}$ coordinate system with respect to the location of the base cone of the rigid perfect involute counterpart of gear (•). The base cone of the mating gear lies to the left of the base cone shown in Fig. 6.

In addition to the three translation components $x_1^{(\cdot)}$, $x_2^{(\cdot)}$, and $x_3^{(\cdot)}$, three rotation components are required to describe arbitrary displacements of a real gear from the position of its perfect involute counterpart. Since such changes in position always are very small, the rotation components can be treated as vectors (ref. 18, pp. 107,108). We shall take the three rotation components to be the (small) rotations $\rho_1^{(\cdot)}$, $\rho_2^{(\cdot)}$, and $\rho_3^{(\cdot)}$ about the base cone axes $x_1^{(\cdot)}$, $x_2^{(\cdot)}$, and $x_3^{(\cdot)}$, respectively. Since the $x_1^{(\cdot)}$ axis lies <u>in</u> the plane of contact, small rotations $\rho_1^{(\cdot)}$ about this axis produce displacements at the plane of contact that are normal to that plane. Such displacements contribute nothing to the generalized transmission error, as indicated earlier. Thus, we shall be concerned only with the small rotations $\rho_2^{(\cdot)}$ and $\rho_3^{(\cdot)}$ about the axes $x_2^{(\cdot)}$ and $x_3^{(\cdot)}$.

To obtain the contributions of $x_1^{(\cdot)}$, $x_2^{(\cdot)}$, and $x_3^{(\cdot)}$ to the generalized transmission error, we require the contributions of these translations to the components ζ_t and ζ_r in the plane of contact shown in Fig. 5. These contributions can be obtained by transforming $x_1^{(\cdot)}$, $x_2^{(\cdot)}$, and $x_3^{(\cdot)}$ into the rectangular coordinate system z_1, z_2, z_3 illustrated in Fig. 6. The plane containing the z_1 and z_3 axes is the plane of contact; the z_3 axis coincides with the zone of contact centerline shown in Fig. 5. This transformation is carried out by two rotations - first, a rotation about the $x_1^{(\cdot)}$ axis through the base cone angle $\gamma_b^{(\cdot)}$ yielding displacements in the y_1, y_2, y_3 coordinate system followed by a rotation about the y_2 axis through the angle $\nu^{(\cdot)}$ yielding the desired displacements in the z_1, z_2, z_3 coordinate system. The resulting displacements along the z_1 axis contribute to ζ_t and the resulting displacements along the z_3 axis provide the contribution of gear (•) to ζ_r. Displacements along the z_2 axis are normal to the plane of contact and therefore do not contribute to the generalized transmission error.

The only rotation components contributing to the generalized transmission error are those components about the z_2 axis, since (small) rotations about the z_1 or the z_3 axis provide displacement components at the plane of contact that are normal to that plane. Small rotations $\rho_2^{(\cdot)}$ and $\rho_3^{(\cdot)}$ both contribute to the contribution of gear (•) to the generalized transmission error rotation component μ; in addition, $\rho_2^{(\cdot)}$ and

$\rho_3^{(\cdot)}$ both contribute to ζ_t, since ζ_t is the generalized transmission error translation component in the z_1 direction that passes through the z_3 axis a distance r_o from the base cone apex (Figs. 5 and 6).

The generalized transmission error components represent the sums of the contributions, as described above, from each of the two meshing gears. Let us designate the generalized transmission error by a column matrix or vector

$$\zeta(x) \triangleq \begin{Bmatrix} \mu(x) \\ \zeta_t(x) \\ \zeta_r(x) \end{Bmatrix} \tag{2.10}$$

and the rotational and translational components of the shaft centerline of gear $(\cdot)$ measured from the position of its rigid perfect involute counterpart by the generalized displacement column matrix or vector

$$\mathbf{q}^{(\cdot)}(x) \triangleq \begin{Bmatrix} \rho_1^{(\cdot)}(x) \\ \rho_2^{(\cdot)}(x) \\ \rho_3^{(\cdot)}(x) \\ x_1^{(\cdot)}(x) \\ x_2^{(\cdot)}(x) \\ x_3^{(\cdot)}(x) \end{Bmatrix} , \tag{2.11}$$

$(\cdot)$ = (1) or (2), as appropriate. It is shown in the appendix that $\zeta(x)$ can be obtained from the generalized displacements $\mathbf{q}^{(1)}(x)$ and $\mathbf{q}^{(2)}(x)$ of the two meshing gears by the matrix multiplications and summation

$$\zeta(x) = \mathbf{T}^{(1)}\mathbf{q}^{(1)}(x) + \mathbf{T}^{(2)}\mathbf{q}^{(2)}(x) , \tag{2.12}$$

where $\mathbf{T}^{(\cdot)}$, $(\cdot)$ = (1) or (2), is defined by

$$\mathbf{T}^{(\cdot)} \triangleq \begin{bmatrix} 0 & c\gamma_b^{(\cdot)} & -s\gamma_b^{(\cdot)} & 0 & 0 & 0 \\ 0 & r_o c\gamma_b^{(\cdot)} & -r_o s\gamma_b^{(\cdot)} & -c\nu^{(\cdot)} & -s\gamma_b^{(\cdot)} s\nu^{(\cdot)} & -c\gamma_b^{(\cdot)} s\nu^{(\cdot)} \\ 0 & 0 & 0 & \pm s\nu^{(\cdot)} & \mp s\gamma_b^{(\cdot)} c\nu^{(\cdot)} & \mp c\gamma_b^{(\cdot)} c\nu^{(\cdot)} \end{bmatrix}, \tag{2.13}$$

where c and s are abbreviations (ref. 18, p. 106) for cosine and sine operations, respectively, on the angles $\gamma_b^{(\cdot)}$ and $\nu^{(\cdot)}$. These angles and r_o are illustrated in Fig. 6.

The terms in the bottom row in the right-hand side of equation (13) have two signs. Determination of the appropriate sign is given in Table 1. The gear pair shown in Fig. 3 is represented by the first line in Table 1. If gear (2) in Fig. 3 becomes the driver rotating clockwise, the resulting configuration is represented by the second line in Table 1. The gear pair shown in Fig. 7 illustrates the other possible gearing configurations. Figure 8 displays the coordinate system used for each of the two gears shown in Fig. 7. The gear pair shown in Fig. 7 is represented by the third line in Table 1. If gear (2) in Fig. 7 becomes the driver rotating counterclockwise, the resulting configuration is represented by the fourth line in Table 1. Definitions of spiral directions are the same as those of screw threads (ref. 19, p. 241). Equations (10) through (13) and Table 1 can be regarded as the mathematical definition of the generalized transmission error for spiral bevel gear pairs.

Table 1 The upper or lower signs in the third row in equation (13) are chosen by the rules listed below. Each full line in the table represents one of the four possible configurations of spiral bevel gear pairs. Gear motions are observed from large end of base cone. The first two lines in the table are associated with Figs. 3 and 6 and the 3rd and 4th lines are associated with Figs. 7 and 8.

Upper Sign	Lower Sign
Driver clockwise, left-hand spiral	Follower counterclockwise, right-hand spiral
Follower counterclockwise, left-hand spiral	Driver clockwise, right-hand spiral
Driver counterclockwise, right-hand spiral	Follower clockwise, left-hand spiral
Follower clockwise, right-hand spiral	Driver counterclockwise, left-hand spiral

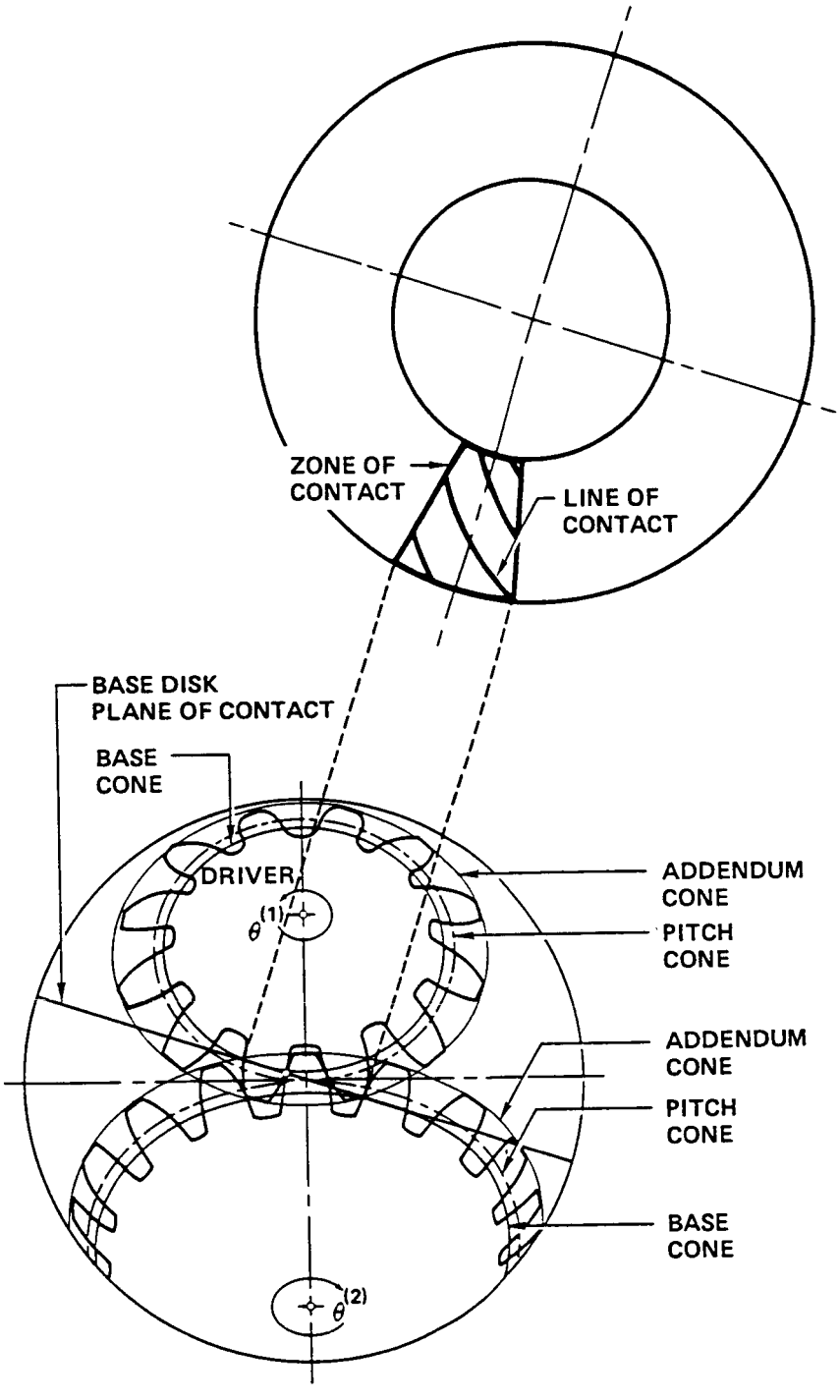

FIG. 7. ALTERNATIVE GEARING CONFIGURATION TO THAT SHOWN IN FIG. 3. CONFIGURATION SHOWN ABOVE IS ASSOCIATED WITH BASE CONE AND PLANE OF CONTACT CONFIGURATION SHOWN IN FIG. 8 AND DESCRIBED IN THE LAST TWO ROWS OF TABLE 1. (LOWER FIGURE ADAPTED FROM FIG. 5.18 OF REF. 17 WITH PERMISSION.)

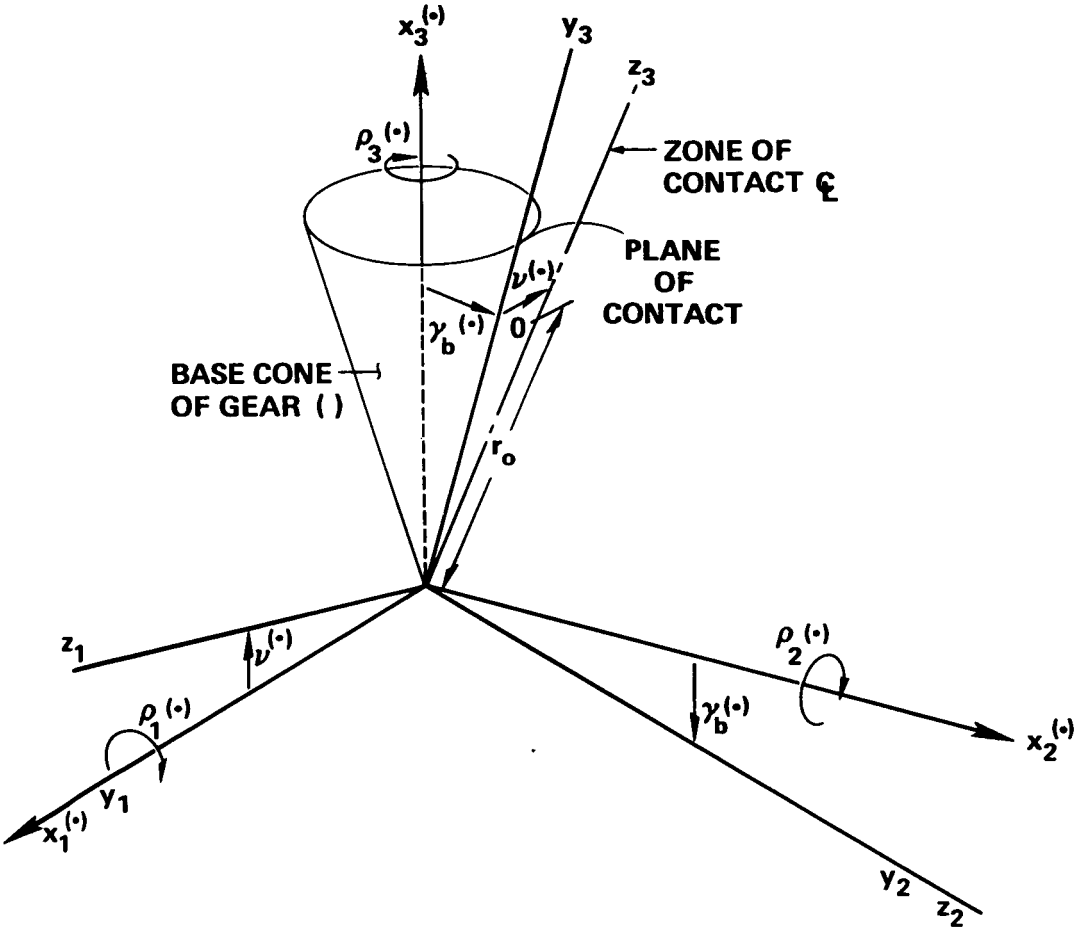

FIG. 8. BASE CONE AND PLANE OF CONTACT FOR BEVEL GEARS SHOWN IN FIG. 7 AND DESCRIBED IN THE LAST TWO ROWS OF TABLE 1. COORDINATES $x_i^{(\cdot)}$ AND $\rho_i^{(\cdot)}$, $i = 1,2,3$ MEASURE THE DIFFERENCE IN POSITION OF THE SHAFT CENTERLINE OF GEAR (•) FROM THE POSITION OF ITS RIGID PERFECT INVOLUTE COUNTERPART. NOTE ESPECIALLY THE SIGN CONVENTION FOR POSITIVE ρ_i, $i=1,2,3$. ABOVE CONFIGURATION IS THE MIRROR IMAGE OF FIG. 6.

USE OF THE GENERALIZED TRANSMISSION ERROR IN THE EQUATIONS OF MOTION OF GEAR SYSTEMS

In order to write the equations of motion of a gear system, one needs mathematical expressions for all forces and moments acting on each gear and each pinion in the system. Such forces and moments include those arising from bearing and shafting displacements and those transmitted by the teeth of the mating pinion or gear. Mathematical expressions for the bearing and shafting forces and moments can be written down in a relatively straightforward manner. In the present section, a methodology is developed for incorporating the forces and moments transmitted by the teeth of pairs of meshing gears into the equations of motion of gear systems. The effects of the nonuniform transmission of motion between meshing gears arising from shafting translational and rotational displacements, tooth and gear body elastic deformations, and deviations of the tooth running surfaces from perfect involute surfaces are included in this methodology.

For pairs of rigid perfect parallel-axis (refs. 7-9) and bevel involute gears, all tooth contact takes place in a fictitious plane called the plane of contact or base plane. If the forces of friction between the teeth are neglected, then the forces transmitted by the teeth lie normal to the tooth surfaces, and, therefore, in the plane of contact (ref. 7). It follows that the resultant total force transmitted by all teeth simultaneously in contact can be described by three scalar components - namely, two orthogonal force components that lie in the plane of contact and the moment of the resultant total transmitted force taken about a specified point in the plane of contact. These three components are the components of the generalized mesh force vector (Fig. 4).

In studying the vibratory excitation arising from a pair of meshing gears, we must be concerned with the unsteady behavior of the forces transmitted by the teeth. These unsteady forces are dependent on the tooth and gear body elasticity and the dynamic parameters of the gear system (inertias, stiffnesses, etc.) and therefore must be regarded as unknowns. In this section, a relationship is derived that relates the three-component generalized mesh force vector that describes these unsteady forces, the three-component generalized transmission error vector (Fig. 5) that describes the nonuniform transmission of motion, a three-component vector that describes the geometric deviations of the tooth running surfaces from perfect involute surfaces, and an appropriately defined mesh stiffness matrix. Combining

this relationship with the expression (2.12) for the generalized transmission error vector yields a matrix equation which is interpreted as an equation of constraint that relates the unknown vibratory displacements of the two meshing gears, the unknown mesh forces, and the geometric deviations of the tooth running surfaces from perfect involute surfaces which are assumed known. The relationship between the generalized transmission error vector, the generalized mesh force vector, and the geometric deviations of the tooth running surfaces from perfect involute surfaces is worked out in detail for spiral bevel gears of nominal (spherical) involute design and completely arbitrary spiral angle (19, p. 241). Earlier analyses along the same lines utilizing the one-component transmission error (refs. 3-12, 20) have been carried out for spur gears in refs. 6 and 20 and for helical gears in refs. 7 and 9.

Equations for Generalized Transmission Error in Terms of Mesh Loading and Geometric Tooth Surface Deviations

We now derive a set of equations for the generalized transmission error of spiral bevel gears that involves the mesh loading components illustrated in Fig. 4 and the geometric deviations of the tooth running surfaces from perfect spherical involute surfaces. This material is an extension to the three-component generalized transmission error for spiral bevel gears of a much simpler derivation (ref. 7, pp. 1412, 1413) of the one-component transmission error for helical gears.

Force Deformation Relations. In the previous section, it was pointed out with the aid of Fig. 3 and equation (2.6) that specification of the pair of coordinate values x,y determines a unique point of contact on the running surfaces of two mating teeth designated by index j. Let $u_{nj}^{(\bullet)}(x,y)$ denote the elastic deformation of the running surface of tooth j of gear $(\bullet)$ under such a contact point, $(\bullet) = 1$ or 2. The direction of $u_{nj}^{(\bullet)}(x,y)$ is taken <u>normal</u> to the tooth surface and, therefore, in the plane of contact normal to the line of contact, as can be envisaged with the aid of Fig. 3; $u_{nj}^{(\bullet)}(x,y)$ is defined to be positive when it is "equivalent" to removal of material from the running surface of the tooth. Thus, $u_{nj}^{(\bullet)}(x,y)$ always is non-negative. Let $u_{nj}(x,y)$ denote the sum of the elastic deformations of two mating teeth in contact - i.e.,

$$u_{nj}(x,y) \triangleq u_{nj}^{(1)}(x,y) + u_{nj}^{(2)}(x,y) \ , \tag{3.1}$$

and let $K_{nj}^{(\cdot)}(x,y)$ denote the local stiffness of tooth pair j per unit length of line of contact as defined in Appendix B, where subscript n again denotes that these quantities refer to deformations normal to the common point of tangency of the two mating teeth which is located by the coordinate values x,y. The superscript (•) on $K_{nj}^{(\cdot)}(x,y)$ will be used to distinguish the different definitions of local tooth-pair stiffness that are established in Appendix B and used later in this section. Then

$$dW_{nj}(x,y) = K_{nj}^{(\cdot)}(x,y)\, u_{nj}(x,y)\, d\ell \tag{3.2}$$

is the normal force increment transmitted by the differential length $d\ell$ of the line of contact of tooth pair j as illustrated in Fig. 9. From Fig. 9, we can see that

$$d\ell = \sec \psi_b(y)\, dy \; ; \tag{3.3}$$

hence,

$$dW_{nj}(x,y) = \sec \psi_b(y)\, K_{nj}^{(\cdot)}(x,y)\, u_{nj}(x,y)\, dy \; . \tag{3.4}$$

The angle $\psi_b(y)$ is the base plane spiral angle (ref. 19, p. 241) illustrated in Fig. 9 which can vary in a rather general, but specified, way as a function of $y = r_o - r$.

Let $dW_{nj}(x,y)$ be resolved into tangential and radial components $dW_{tj}(x,y)$ and $dW_{rj}(x,y)$ that are perpendicular and parallel, respectively, to the zone of contact centerline as shown in Fig. 9. From the figure, it is readily seen that the differential tangential and radial forces are related to the differential normal force by

$$\begin{aligned} dW_{tj} &= \sin\{\tfrac{\pi}{2} - [\psi_b(y) - \lambda_j(x,y)]\}\, dW_{nj} \\ &= \cos[\psi_b(y) - \lambda_j(x,y)]\, dW_{nj} \end{aligned} \tag{3.5}$$

and

$$\begin{aligned} dW_{rj} &= \cos\{\tfrac{\pi}{2} - [\psi_b(y) - \lambda_j(x,y)]\}\, dW_{nj} \\ &= \sin[\psi_b(y) - \lambda_j(x,y)]\, dW_{nj}, \end{aligned} \tag{3.6}$$

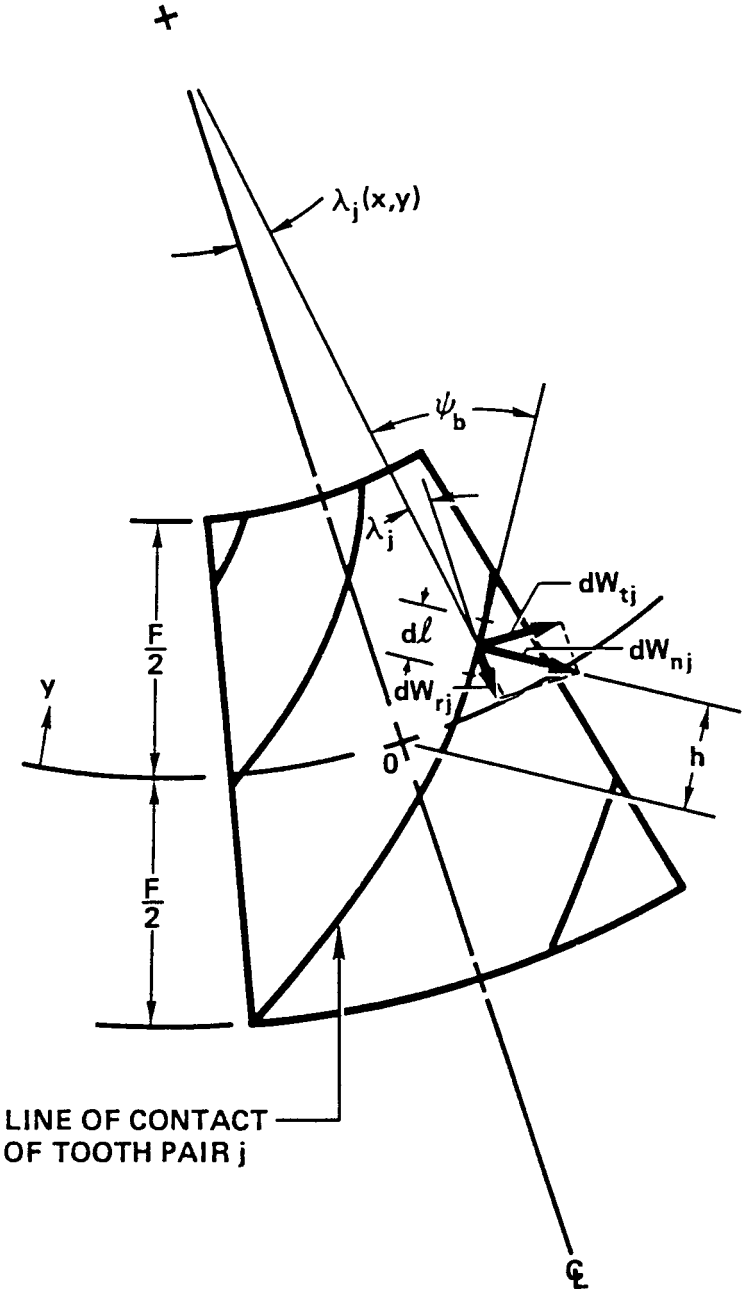

FIG. 9. RESOLUTION OF DIFFERENTIAL NORMAL FORCE INCREMENT $dW_{nj}(x,y)$ INTO COMPONENTS $dW_{tj}(x,y)$ and $dW_{rj}(x,y)$ PERPENDICULAR AND PARALLEL TO ZONE OF CONTACT CENTERLINE. FOR LOCATION OF ZONE OF CONTACT IN PLANE OF CONTACT, SEE FIG. 3.

where $\lambda_j(x,y)$ is the angle in the base plane between the zone of contact centerline and the radial line passing through the differential force element with vertex at the base cone apex as illustrated in Fig. 9. The contributions $W_{tj}(x)$ and $W_{rj}(x)$ from the force transmitted by tooth pair j to the tangential and radial components $W_t(x)$ and $W_r(x)$ of the total force transmitted by the mesh are obtained by (Stieltjes) integrations of dW_{tj} and dW_{rj}, respectively, over the total line of contact of tooth pair j:

$$W_{tj}(x) = \int_{y_A}^{y_B} dW_{tj}(x,y) \tag{3.7}$$

and

$$W_{rj}(x) = \int_{y_A}^{y_B} dW_{rj}(x,y) \ , \tag{3.8}$$

where y_A and y_B denote the endpoints in the coordinate y of the line of contact of tooth pair j.

Let h denote the distance measured perpendicular to $dW_{nj}(x,y)$ between the zone of contact center $\underline{0}$ and the line of action of the differential normal force $dW_{nj}(x,y)$ as illustrated in Fig. 9. Then, using the sign convention for moments illustrated in Fig. 4, it follows that the contribution $\tau_j(x)$ from the force transmitted by tooth pair j to the total moment $\tau(x)$ about the zone of contact center $\underline{0}$ is

$$\tau_j(x) = - \int_{y_A}^{y_B} h(x,y)\ dW_{nj}(x,y) \ . \tag{3.9}$$

The tangential and radial components $W_t(x)$ and $W_r(x)$ of the total force transmitted by the mesh and the total moment $\tau(x)$ about the point $\underline{0}$ illustrated in Fig. 4 are given by the sums of $W_{tj}(x)$, $W_{rj}(x)$, and $\tau_j(x)$ over all tooth pairs in contact:

$$W_t(x) = \sum_j W_{tj}(x) \tag{3.10}$$

$$W_r(x) = \sum_j W_{rj}(x) \tag{3.11}$$

$$\tau(x) = \sum_j \tau_j(x) \ . \tag{3.12}$$

Inserting equations (4) and (5) into equation (7) gives

$$W_{tj}(x) = \int_{y_A}^{y_B} \sec \psi_b(y)\, K_{nj}^{(t)}(x,y)\, \cos[\psi_b(y)-\lambda_j(x,y)]\, u_{nj}(x,y)dy \ , \tag{3.13}$$

and inserting equations (4) and (6) into equation (8) gives

$$W_{rj}(x) = \int_{y_A}^{y_B} \sec\psi_b(y)\, K_{nj}^{(r)}(x,y)\, \sin[\psi_b(y)-\lambda_j(x,y)]\, u_{nj}(x,y)dy \ , \tag{3.14}$$

where $K_{nj}^{(t)}(x,y)$ and $K_{nj}^{(r)}(x,y)$ are defined in Appendix B. In Appendix C, it is shown that

$$h(x,y) = r_o\cos[\psi_b(y)-\lambda_j(x,y)] - (r_o-y)\cos\psi_b(y) \ . \tag{3.15}$$

Finally, inserting equations (4) and (15) into equation (9) yields

$$\tau_j(x) = -r_o \int_{y_A}^{y_B} \sec\psi_b(y)\, K_{nj}^{(t)}(x,y)\, \cos[\psi_b(y)-\lambda_j(x,y)]\, u_{nj}(x,y)dy$$

$$+ \int_{y_A}^{y_B} (r_o-y)\, K_{nj}^{(\mu)}(x,y)\, u_{nj}(x,y)dy \ , \tag{3.16}$$

where $K_{nj}^{(\mu)}(x,y)$ also is defined in Appendix B.

Force-Transmission Error Relations. Let $\eta_{nj}^{(\bullet)}(x,y)$, $(\bullet)$=1 or 2, denote the geometric deviation of the unloaded running surface of tooth j of gear $(\bullet)$ from the surface of its perfect spherical involute counterpart at the point of contact on the surface determined by the pair of coordinate values x,y. The deviation $\eta_{nj}^{(\bullet)}(x,y)$ is measured in a direction <u>normal</u> to the tooth surface and, therefore, in the plane of contact normal to the line of contact; $\eta_{nj}^{(\bullet)}(x,y)$ is taken to be positive when it is equivalent to removal of material from the surface of its perfect involute counterpart. Let $\eta_{nj}(x,y)$ denote the sum of the geometric deviations of two mating teeth in contact - i.e.,

$$\eta_{nj}(x,y) \triangleq \eta^{(1)}_{nj}(x,y) + \eta^{(2)}_{nj}(x,y) \ , \tag{3.17}$$

which is the geometric deviation counterpart to the corresponding relation (1) that applies to elastic deformations. Let $\zeta_{nj}(x,y)$ denote the local transmission error of tooth pair j defined in the same direction and with the same sign convention as $u_{nj}(x,y)$ and $\eta_{nj}(x,y)$. The local transmission error is defined as the sum of the elastic deformation $u_{nj}(x,y)$ and the geometric deviation $\eta_{nj}(x,y)$ of the tooth pair at the point of contact determined by x,y:

$$\zeta_{nj}(x,y) \triangleq u_{nj}(x,y) + \eta_{nj}(x,y) \ . \tag{3.18}$$

In Fig. 10, the local transmission error $\zeta_{nj}(x,y)$ of tooth pair j is shown resolved into local tangential and radial components $\zeta_t - a\mu$ and $\zeta_r - b\mu$ that are perpendicular and parallel to the zone of contact centerline, respectively. The sign convention of the transmission error components shown in Fig. 10 coincides with the displacement of the gear on the left-hand side of the zone of contact shown in Fig. 5. The local tangential component $\zeta_t - a\mu$ contains contributions from the global tangential and rotational components ζ_t and μ that are illustrated in Fig. 5; the local radial component $\zeta_r - b\mu$ contains contributions from the global radial and rotational components ζ_r and μ also shown in Fig. 5. From Fig. 11, one can readily show that the distances a and b (in Fig. 10) of the contact point from the center O of the zone of contact are

$$a = r_o[1-\cos\lambda_j(x,y)] + y\cos\lambda_j(x,y) \tag{3.19}$$

$$b = (r_o-y)\sin\lambda_j(x,y) \ . \tag{3.20}$$

Thus, the local tangential and radial components of the transmission error are

$$\zeta_t(x) - a\mu(x) = \zeta_t(x) - \{r_o[1-\cos\lambda_j(x,y)] + y\cos\lambda_j(x,y)\}\,\mu(x) \tag{3.21}$$

and

$$\zeta_r(x) - b\mu(x) = \zeta_r(x) - [(r_o-y)\sin\lambda_j(x,y)]\,\mu(x) \ . \tag{3.22}$$

Recognizing the geometric similarity between the force resolution in Fig. 9 and the local transmission error resolution in Figs. 10 and 11, it follows from equations (5)

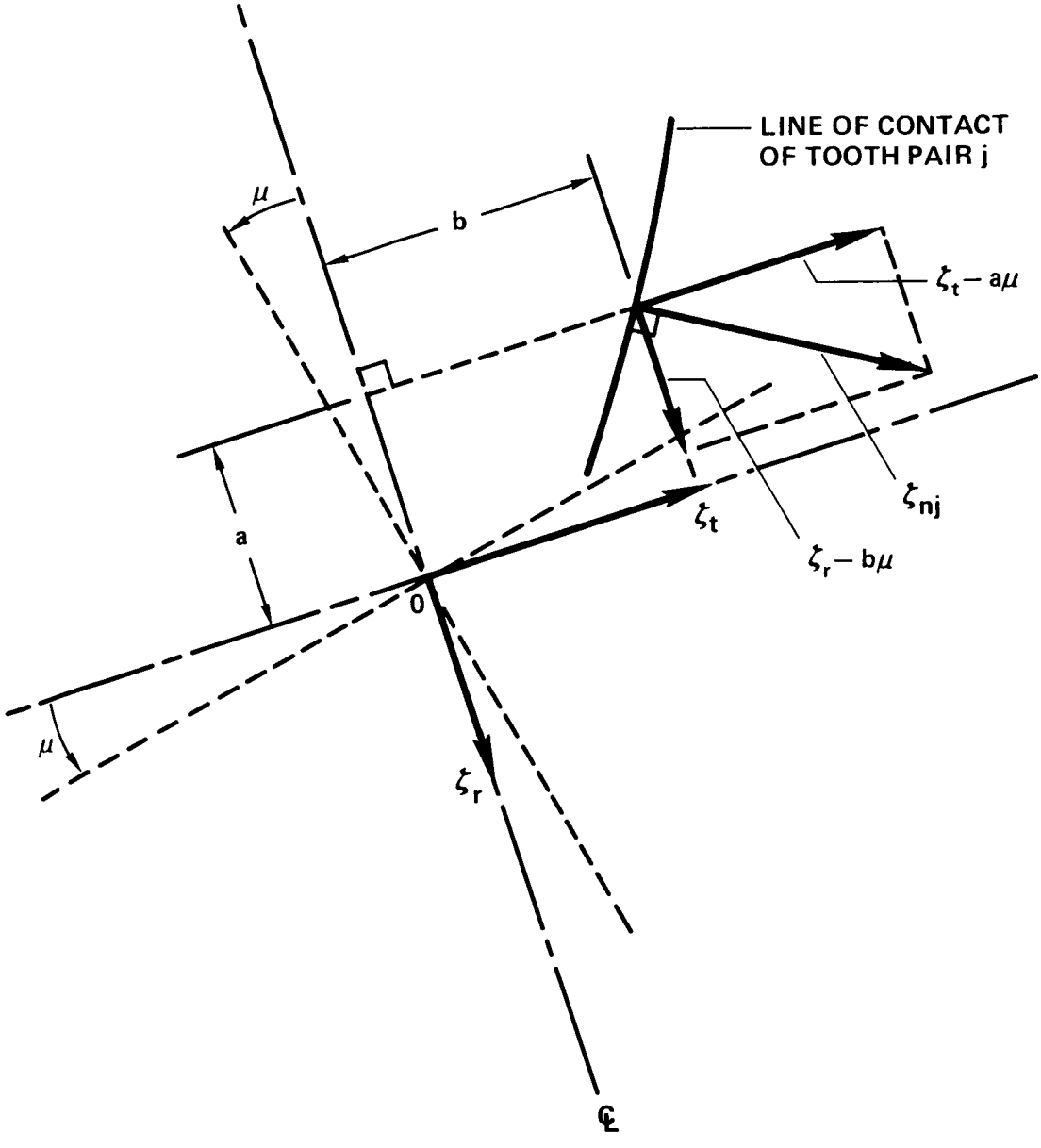

FIG. 10. RESOLUTION OF LOCAL TRANSMISSION ERROR $\zeta_{nj}(x,y)$ INTO LOCAL TANGENTIAL AND RADIAL COMPONENTS $\zeta_t - a\mu$ AND $\zeta_r - b\mu$ PERPENDICULAR AND PARALLEL TO ZONE OF CONTACT CENTERLINE, RESPECTIVELY. DISPLACEMENTS SHOWN COINCIDE WITH MOTION OF GEAR ON THE LEFT-HAND SIDE OF THE ZONE OF CONTACT SHOWN IN FIG. 5.

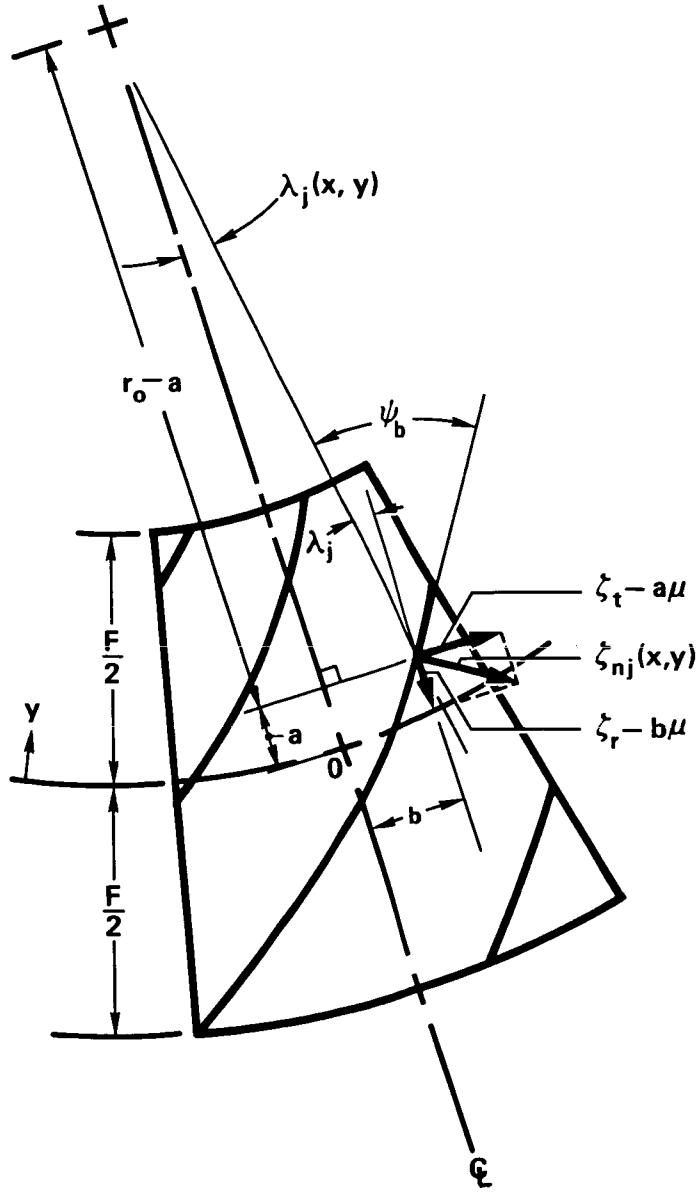

FIG. 11. GEOMETRY OF POINT OF CONTACT LOCAL TRANSMISSION ERROR AND ZONE OF CONTACT ORIGIN 0.

and (6) that the tangential and radial components of the local transmission error are related to the normal component by

$$\zeta_t(x) - a\mu(x) = \cos[\psi_b(y) - \lambda_j(x,y)]\ \zeta_{nj}(x,y) \tag{3.23}$$

and

$$\zeta_r(x) - b\mu(x) = \sin[\psi_b(y) - \lambda_j(x,y)]\ \zeta_{nj}(x,y)\ . \tag{3.24}$$

It is possible, now, to express the (unknown) elastic deformation component $u_{nj}(x,y)$ in equations (13), (14), and (16) in terms of the geometric deviations $\eta_{nj}(x,y)$ of the tooth running surfaces and the three generalized transmission error components $\mu(x)$, $\zeta_t(x)$, and $\zeta_r(x)$. Solving equation (18) for $u_{nj}(x,y)$ gives

$$u_{nj}(x,y) = \zeta_{nj}(x,y) - \eta_{nj}(x,y)\ . \tag{3.25}$$

Multiplying equation (25) by $\cos[\psi_b(y) - \lambda_j(x,y)]$ and combining the resulting expression with equations (21) and (23) to eliminate $\zeta_{nj}(x,y)$ gives

$$\cos[\psi_b(y) - \lambda_j(x,y)]\ u_{nj}(x,y) = \zeta_t(x) - \{r_o[1 - \cos\lambda_j(x,y)] + y\cos\lambda_j(x,y)\}\ \mu(x)$$
$$- \cos[\psi_b(y) - \lambda_j(x,y)]\ \eta_{nj}(x,y)\ . \tag{3.26}$$

Multiplying equation (25) by $\sin[\psi_b(y) - \lambda_j(x,y)]$ and combining the resulting expression with equations (22) and (24) to eliminate $\zeta_{nj}(x,y)$ gives

$$\sin[\psi_b(y) - \lambda_j(x,y)]\ u_{nj}(x,y) = \zeta_r(x) - [(r_o - y)\sin\lambda_j(x,y)]\ \mu(x)$$
$$- \sin[\psi_b(y) - \lambda_j(x,y)]\ \eta_{nj}(x,y)\ . \tag{3.27}$$

Dividing equation (26) by $\cos[\psi_b(y) - \lambda_j(x,y)]$ gives

$$u_{nj}(x,y) = \sec[\psi_b(y) - \lambda_j(x,y)]\{\zeta_t(x) - \{r_o[1-\cos\lambda_j(x,y)] + y\cos\lambda_j(x,y)\}\ \mu(x)\}$$
$$- \eta_{nj}(x,y)\ . \tag{3.28}$$

Finally, substituting equations (26), (27), and (28) into equations (16), (13), and (14), as required, yields the desired expressions for $\tau_j(x)$, $W_{tj}(x)$, and $W_{rj}(x)$:

$$\tau_j(x) = -r_o \int_{y_A}^{y_B} \sec \psi_b(y)\, K_{nj}^{(t)}(x,y)\{\zeta_t(x) - \{r_o[1-\cos\lambda_j(x,y)]$$

$$+ y\cos\lambda_j(x,y)\}\,\mu(x) - \cos[\psi_b(y) - \lambda_j(x,y)]\,\eta_{nj}(x,y)\}\,dy$$

$$+ \int_{y_A}^{y_B} (r_o - y)\, K_{nj}^{(\mu)}(x,y)[\sec[\psi_b(y)-\lambda_j(x,y)]\{\zeta_t(x)$$

$$- \{r_o[1-\cos\lambda_j(x,y)] + y\cos\lambda_j(x,y)\}\,\mu(x)\} - \eta_{nj}(x,y)]\,dy\,, \qquad (3.29)$$

$$W_{tj}(x) = \int_{y_A}^{y_B} \sec\psi_b(y)\, K_{nj}^{(t)}(x,y)\{\zeta_t(x) - \{r_o[1-\cos\lambda_j(x,y)] + y\cos\lambda_j(x,y)\}\,\mu(x)$$

$$- \cos[\psi_b(y) - \lambda_j(x,y)]\,\eta_{nj}(x,y)\}\,dy\,, \qquad (3.30)$$

and

$$W_{rj}(x) = \int_{y_A}^{y_B} \sec\psi_b(y) K_{nj}^{(r)}(x,y)\{\zeta_r(x) - [(r_o-y)\sin\lambda_j(x,y)]\,\mu(x)$$

$$-\sin[\psi_b(y)-\lambda_j(x,y)]\,\eta_{nj}(x,y)\}\,dy. \qquad (3.31)$$

Let us define

$$\tilde{K}_{c^{-1}j}^{(\cdot)}(x;\psi_b) \triangleq \int_{y_A}^{y_B} \sec\psi_b(y)\, K_{nj}^{(\cdot)}(x,y)\,dy \qquad (3.32a)$$

$$\tilde{K}_{c^{-1}j}^{(\cdot)}(x;\psi_b-\lambda_j) \triangleq \int_{y_A}^{y_B} \sec[\psi_b(y) - \lambda_j(x,y)]\, K_{nj}^{(\cdot)}(x,y)\,dy \qquad (3.32b)$$

$$\tilde{K}_{c^{-1}sj}^{(\cdot)}(x;\psi_b,\lambda_j) \triangleq \int_{y_A}^{y_B} \sec\psi_b(y)\sin\lambda_j(x,y)\, K_{nj}^{(\cdot)}(x,y)\,dy \qquad (3.32c)$$

$$\tilde{K}^{(\cdot)}_{c^{-1}(1-c)j}(x;\psi_b,\lambda_j) \triangleq \int_{y_A}^{y_B} \sec\psi_b(y)[1-\cos\lambda_j(x,y)]\, K^{(\cdot)}_{nj}(x,y)\, dy \tag{3.32d}$$

$$\tilde{K}^{(\cdot)}_{c^{-1}(1-c)j}(x;\psi_b-\lambda_j,\lambda_j) \triangleq \int_{y_A}^{y_B} \sec[\psi_b(y)-\lambda_j(x,y)][1-\cos\lambda_j(x,y)]\, K^{(\cdot)}_{nj}(x,y)\, dy \tag{3.32e}$$

$$\tilde{K}^{(\cdot)}_{yc^{-1}j}(x;\psi_b-\lambda_j) \triangleq \int_{y_A}^{y_B} y\sec[\psi_b(y)-\lambda_j(x,y)]\, K^{(\cdot)}_{nj}(x,y)\, dy \tag{3.32f}$$

$$\tilde{K}^{(\cdot)}_{yc^{-1}cj}(x;\psi_b,\lambda_j) \triangleq \int_{y_A}^{y_B} y\sec\psi_b(y)\cos\lambda_j(x,y)\, K^{(\cdot)}_{nj}(x,y)\, dy \tag{3.32g}$$

$$\tilde{K}^{(\cdot)}_{yc^{-1}cj}(x;\psi_b-\lambda_j,\lambda_j) \triangleq \int_{y_A}^{y_B} y\sec[\psi_b(y)-\lambda_j(x,y)]\cos\lambda_j(x,y)\, K^{(\cdot)}_{nj}(x,y)\, dy \tag{3.32h}$$

$$\tilde{K}^{(\cdot)}_{yc^{-1}sj}(x;\psi_b,\lambda_j) \triangleq \int_{y_A}^{y_B} y\sec\psi_b(y)\sin\lambda_j(x,y)\, K^{(\cdot)}_{nj}(x,y)\, dy \tag{3.32i}$$

$$\tilde{K}^{(\cdot)}_{yc^{-1}(1-c)j}(x;\psi_b-\lambda_j,\lambda_j) \triangleq \int_{y_A}^{y_B} y\sec[\psi_b(y)-\lambda_j(x,y)][1-\cos\lambda_j(x,y)]\, K^{(\cdot)}_{nj}(x,y)\, dy \tag{3.32j}$$

$$\tilde{K}^{(\cdot)}_{y^2c^{-1}cj}(x;\psi_b-\lambda_j,\lambda_j) \triangleq \int_{y_A}^{y_B} y^2\sec[\psi_b(y)-\lambda_j(x,y)]\cos\lambda_j(x,y)\, K^{(\cdot)}_{nj}(x,y)\, dy \tag{3.32k}$$

$$\tilde{\eta}^{(\cdot)}_{Kj}(x) \triangleq \int_{y_A}^{y_B} K^{(\cdot)}_{nj}(x,y)\, \eta_{nj}(x,y)\, dy \tag{3.32ℓ}$$

$$\tilde{\eta}^{(\cdot)}_{Kc^{-1}cj}(x;\psi_b,\psi_b-\lambda_j) \triangleq \int_{y_A}^{y_B} K^{(\cdot)}_{nj}(x,y)\ \sec\psi_b(y)\ \cos[\psi_b(y)-\lambda_j(x,y)]\ \eta_{nj}(x,y)\ dy \tag{3.32m}$$

$$\tilde{\eta}^{(\cdot)}_{Kc^{-1}sj}(x;\psi_b,\psi_b-\lambda_j) \triangleq \int_{y_A}^{y_B} K^{(\cdot)}_{nj}(x,y)\ \sec\psi_b(y)\ \sin[\psi_b(y)-\lambda_j(x,y)]\ \eta_{nj}(x,y)\ dy \tag{3.32n}$$

$$\tilde{\eta}^{(\cdot)}_{yKj}(x) \triangleq \int_{y_A}^{y_B} y\ K^{(\cdot)}_{nj}(x,y)\ \eta_{nj}(x,y)\ dy\ . \tag{3.32o}$$

The above notational convention is easy to remember once it is understood. Each of the above fifteen definitions is an integral over the full line of contact of tooth pair j. The integration is represented by the tilde over the symbols on the left-hand side - since the tilde has the approximate form of an integral sign (rotated 90°). The fact that the integration is taken over the line of contact of tooth pair j is represented by the last of the subscripts, j, on the symbol the tilde has been placed over. The first eleven of the definitions are regarded as weighted integrals of the stiffness $K^{(\cdot)}_{nj}(x,y)$ and the remaining four are regarded as weighted integrals of the deviation $\eta_{nj}(x,y)$, which explains the symbols that the tildes have been placed over. The subscripts following these symbols represent the weighting functions in the integrals, where c^{-1} represents sec = cos $^{-1}$, s represents sin, c represents cos, 1-c represents 1-cos, and K represents $K^{(\cdot)}_{nj}(x,y)$. Each of the fifteen integrals is a function of $x = r_o\theta$, which accounts for the symbol x in the arguments on the left-hand sides. The remaining symbols after the semicolons in the arguments on the left-hand sides represent the arguments of the subscripted trigonometric functions, in the same order as the subscripts, with the last argument on the left-hand side after the semicolon in each of the definitions representing the argument of the last subscripted function before the j. Each superscript (•) in the left-hand side represents the superscript (•) in $K^{(\cdot)}_{nj}(x,y)$ in the right-hand side, (•) = (t), (r), or (μ), as appropriate.

By utilizing the definitions (32a) - (32o), equations (29), (30), and (31) can be expressed as

$$\tau_j(x) = -r_o\zeta_t(x)\,\tilde{K}^{(t)}_{c^{-1}j}(x;\psi_b) + r_o^2\mu(x)\,\tilde{K}^{(t)}_{c^{-1}(1-c)j}(x;\psi_b,\lambda_j)$$

$$+r_o\mu(x)\,\tilde{K}^{(t)}_{yc^{-1}cj}(x;\psi_b,\lambda_j) + r_o\tilde{\eta}^{(t)}_{Kc^{-1}cj}(x;\psi_b,\psi_b-\lambda_j)$$

$$+r_o\zeta_t(x)\,\tilde{K}^{(\mu)}_{c^{-1}j}(x;\psi_b-\lambda_j) - \zeta_t(x)\,\tilde{K}^{(\mu)}_{yc^{-1}j}(x;\psi_b-\lambda_j)$$

$$-r_o^2\mu(x)\,\tilde{K}^{(\mu)}_{c^{-1}(1-c)j}(x;\psi_b-\lambda_j,\lambda_j) + r_o\mu(x)\,\tilde{K}^{(\mu)}_{yc^{-1}(1-c)j}(x;\psi_b-\lambda_j,\lambda_j)$$

$$-r_o\mu(x)\,\tilde{K}^{(\mu)}_{yc^{-1}cj}(x;\psi_b-\lambda_j,\lambda_j) + \mu(x)\,\tilde{K}^{(\mu)}_{y^2c^{-1}cj}(x;\psi_b-\lambda_j,\lambda_j)$$

$$-r_o\tilde{\eta}^{(\mu)}_{Kj}(x) + \tilde{\eta}^{(\mu)}_{yKj}(x)\ , \qquad (3.33)$$

$$W_{tj}(x) = \zeta_t(x)\,\tilde{K}^{(t)}_{c^{-1}j}(x;\psi_b) - r_o\mu(x)\,\tilde{K}^{(t)}_{c^{-1}(1-c)j}(x;\psi_b,\lambda_j)$$

$$-\mu(x)\,\tilde{K}^{(t)}_{yc^{-1}cj}(x;\psi_b,\lambda_j) - \tilde{\eta}^{(t)}_{Kc^{-1}cj}(x;\psi_b,\psi_b-\lambda_j)\ , \qquad (3.34)$$

and

$$W_{rj}(x) = \zeta_r(x)\,\tilde{K}^{(r)}_{c^{-1}j}(x;\psi_b) - r_o\mu(x)\,\tilde{K}^{(r)}_{c^{-1}sj}(x;\psi_b,\lambda_j)$$

$$+\mu(x)\,\tilde{K}^{(r)}_{yc^{-1}sj}(x;\psi_b,\lambda_j) - \tilde{\eta}^{(r)}_{Kc^{-1}sj}(x;\psi_b,\psi_b-\lambda_j)\ . \qquad (3.35)$$

The total moment $\tau(x)$ and forces $W_t(x)$ and $W_r(x)$ transmitted by the mesh are obtained by summing equations (33), (34), and (35) over all tooth pairs j in contact, as indicated by equations (10), (11), and (12). If the sums over j of the quantities defined by equations (32a) - (32o) are denoted by the same symbols with the subscripts j that are not included within the parentheses omitted - i.e.,

$$\tilde{K}^{(\cdot)}_{c^{-1}}(x;\psi_b) \triangleq \sum_j \tilde{K}^{(\cdot)}_{c^{-1}j}(x;\psi_b) \tag{3.36a}$$

$$\tilde{K}^{(\cdot)}_{c^{-1}}(x;\psi_b-\lambda_j) \triangleq \sum_j \tilde{K}^{(\cdot)}_{c^{-1}j}(x;\psi_b-\lambda_j) \tag{3.36b}$$

$$\vdots$$

$$\tilde{\eta}^{(\cdot)}_{yK}(x) \triangleq \sum_j \tilde{\eta}^{(\cdot)}_{yKj}(x) \ , \tag{3.36o}$$

then the total moment and forces transmitted by the mesh are expressed in a form identical to equations (33), (34), and (35) with the subscripts omitted as indicated in equations (10) - (12) and (36a) - (36o). The coefficients of $\mu(x)$, $\zeta_t(x)$, and $\zeta_r(x)$ in the resulting equations can be factored out to yield the following set of equations for the generalized transmission error components:

$$\mu(x)\{\tilde{K}^{(\mu)}_{y^2c^{-1}c}(x;\psi_b-\lambda_j,\lambda_j) + r_o[\tilde{K}^{(t)}_{yc^{-1}c}(x;\psi_b,\lambda_j) - \tilde{K}^{(\mu)}_{yc^{-1}c}(x;\psi_b-\lambda_j,\lambda_j)]$$

$$+ r_o\{\tilde{K}^{(\mu)}_{yc^{-1}(1-c)}(x;\psi_b-\lambda_j,\lambda_j) + r_o[\tilde{K}^{(t)}_{c^{-1}(1-c)}(x;\psi_b,\lambda_j) - \tilde{K}^{(\mu)}_{c^{-1}(1-c)}(x;\psi_b-\lambda_j,\lambda_j)]\}\}$$

$$- \zeta_t(x)\{\tilde{K}^{(\mu)}_{yc^{-1}}(x;\psi_b-\lambda_j) + r_o\,[\tilde{K}^{(t)}_{c^{-1}}(x;\psi_b) - \tilde{K}^{(\mu)}_{c^{-1}}(x;\psi_b-\lambda_j)]\}$$

$$= \tau(x) - \tilde{\eta}^{(\mu)}_{yK}(x) + r_o[\tilde{\eta}^{(\mu)}_{K}(x) - \tilde{\eta}^{(t)}_{Kc^{-1}c}(x;\psi_b,\psi_b-\lambda_j)] \ , \tag{3.37}$$

$$-\mu(x)[\tilde{K}^{(t)}_{yc^{-1}c}(x;\psi_b,\lambda_j) + r_o\tilde{K}^{(t)}_{c^{-1}(1-c)}(x;\psi_b,\lambda_j)] + \zeta_t(x)\tilde{K}^{(t)}_{c^{-1}}(x;\psi_b)$$

$$= W_t(x) + \tilde{\eta}^{(t)}_{Kc^{-1}c}(x;\psi_b,\psi_b-\lambda_j) \ , \tag{3.38}$$

and

$$-\mu(x)\left[r_o \tilde{K}^{(r)}_{c^{-1}s}(x;\psi_b,\lambda_j) - \tilde{K}^{(r)}_{yc^{-1}s}(x;\psi_b,\lambda_j)\right] + \zeta_r(x)\tilde{K}^{(r)}_{c^{-1}}(x;\psi_b)$$

$$= W_r(x) + \tilde{\eta}^{(r)}_{Kc^{-1}s}(x;\psi_b,\psi_b-\lambda_j) \ . \tag{3.39}$$

Equations (37) and (38) are a pair of simultaneous linear algebraic equations for the rotational and tangential components, $\mu(x)$ and $\zeta_t(x)$, of the generalized transmission error illustrated in Fig. 5. The coefficients of the unknowns defined in equations (32a) - (32k) are functions of the gear mesh geometry and the tooth-pair stiffnesses $K^{(\cdot)}_{nj}(x,y)$, $(\cdot) = (t)$ or (μ) . The right-hand sides contain the forcing terms $\tau(x)$ and $W_t(x)$ illustrated in Fig. 4 and the stiffness weighted geometric deviations of the tooth running surfaces from perfect involute surfaces defined in equations (32ℓ) - (32o). Equation (39), the third in the set, can be regarded as an equation for the radial component $\zeta_r(x)$ of the generalized transmission error in terms of $\mu(x)$ and the forcing and geometric deviation terms that are written on its right-hand side.

Use of Generalized Transmission Error in Equations of Motion

The set of equations (37) - (39) for the generalized transmission error components $\mu(x)$, $\zeta_t(x)$, and $\zeta_r(x)$ can be written in matrix form as

$$\mathbf{K}(x)\ \boldsymbol{\zeta}(x) = \mathbf{W}(x) + \eta_K(x) \ , \tag{3.40}$$

where $\boldsymbol{\zeta}(x)$ is the generalized transmission error vector defined by equation (2.10), $\mathbf{W}(x)$ is the generalized mesh force vector

$$\mathbf{W}(x) \triangleq \begin{Bmatrix} \tau(x) \\ W_t(x) \\ W_r(x) \end{Bmatrix} \ , \tag{3.41}$$

and $\eta_K(x)$ is the vector that describes the stiffness weighted geometric deviations of the tooth surfaces from perfect involute surfaces:

$$\eta_K(x) \triangleq \left\{ \begin{array}{l} \tilde{\eta}^{(\mu)}_{yK}(x) + r_o[\tilde{\eta}^{(\mu)}_{K}(x) - \tilde{\eta}^{(t)}_{Kc^{-1}c}(x;\psi_b,\psi_b-\lambda_j)] \\ \\ \tilde{\eta}^{(t)}_{Kc^{-1}c}(x;\psi_b,\psi_b-\lambda_j) \\ \\ \tilde{\eta}^{(r)}_{Kc^{-1}s}(x;\psi_b,\psi_b-\lambda_j) \end{array} \right\} . \tag{3.42}$$

The matrix $\mathbf{K}(x)$ is the 3 × 3 element coefficient matrix readily written down from the left-hand sides of equations (37) - (39).

Let us define the inverse $\mathbf{C}(x)$ of the mesh stiffness matrix $\mathbf{K}(x)$ by

$$\mathbf{C}(x) \triangleq \mathbf{K}^{-1}(x) . \tag{3.43}$$

An expression for $\mathbf{C}(x)$ is derived in Appendix D. Premultiplying equation (40) by $\mathbf{K}^{-1}(x)$ gives

$$\zeta(x) = \mathbf{C}(x)\mathbf{W}(x) + \mathbf{C}(x)\eta_K(x) , \tag{3.44}$$

where the definition (43) has been used. Equating the right-hand sides of equations (2.12) and (44) yields

$$\mathbf{T}^{(1)}\mathbf{q}^{(1)}(x) + \mathbf{T}^{(2)}\mathbf{q}^{(2)}(x) = \mathbf{C}(x)\mathbf{W}(x) + \mathbf{C}(x)\eta_K(x) \tag{3.45a}$$

or

$$\mathbf{T}^{(1)}\mathbf{q}^{(1)}(x) + \mathbf{T}^{(2)}\mathbf{q}^{(2)}(x) - \mathbf{C}(x)\mathbf{W}(x) = \mathbf{C}(x)\eta_K(x) , \tag{3.45b}$$

which is the final result.

Each gear and pinion in a simple or complex gearing system possesses 6 degrees-of-freedom when modeled as a rigid body. These 6 degrees-of-freedom can be taken to be the $x_i^{(\cdot)}$ and $\rho_i^{(\cdot)}$, i = 1,2,3 illustrated in Figs. 6 or 8, as appropriate. The differential equations of motion of each such gear or pinion can be expressed in terms of these 6 coordinates and their first and second temporal derivatives, the elastic restoring forces and moments of the bearing supports which depend on these same 6 coordinates, and the shafting forces and moments that also may depend on the comparable coordinates that describe the position of a neighboring gear or pinion. In

addition to these elastic forces, the three components of the mesh force vector **W**, equation (41) and Fig. 4, also act on the gear. The temporal variations of the components of the mesh force vector **W** depend on the dynamic properties of the gearing system (masses, stiffnesses, etc.); therefore, they must be treated as dependent variables or unknowns whose time-dependent behavior also must be obtained from solution of the equations of motion of the gearing system.

Treatment of the three components of **W** as unknowns requires the addition of three equations to the equations of motion of the gearing system for each pair of meshing gears in the system. The three scalar components of the matrix equation (45b) are these three additional equations. If, for each pair of meshing gears in the system, we consider the components of **W** as three additional generalized coordinates (ref. 21, p. 12), then the scalar components of equation (45b) have the form of holonomic constraints (ref. 21, pp. 10-14; ref. 22, pp. 24-27). When a matrix equation of the form of equation (45b) is included for each pair of meshing gears in the system, it is evident that the vibratory excitation of the system arising from each gear pair is a displacement form of excitation provided by the three components of the vector $\mathbf{C}(x)\boldsymbol{\eta}_K(x)$together with the three components of the vector $\mathbf{C}(x)\mathbf{W}(x)$ that provide a parametric excitation of the system through the periodic dependence on x of the matrix **C**(x).

Denoting the nominal angular velocity of gear (•) by $\omega^{(\bullet)}$ rad/sec, it follows from equation (2.8) that

$$x = R_{bo}^{(\bullet)} \left(\theta^{(\bullet)} - \theta_o^{(\bullet)}\right) = R_{bo}^{(\bullet)} \omega^{(\bullet)}(t - t_o) , \tag{3.46}$$

where $\theta_o^{(\bullet)}$ and t_o denote appropriate initial conditions. From equation (46) it follows that **C**(x) can be regarded as a function of time t. Hence, the equation of constraint (45b) has time-dependent coefficients which sometimes are referred to as rheonomic constraints (ref. 22, p. 32). When included as part of the equations of motion of a gearing system, it seems appropriate to refer to the matrix equation (45b) as the mesh constraint equation. However, from a physical perspective, equation (45b) is a geometric compatibility relation (ref. 23, pp. 99, 100) involving the gear axes vectorial displacements $\mathbf{q}^{(1)}(x)$ and $\mathbf{q}^{(2)}(x)$, the elastic deformations of the gear teeth and bodies characterized by the matrix product $\mathbf{C}(x)\mathbf{W}(x)$, and the geometric

deviations of the tooth running surfaces from perfect involute surfaces characterized by the matrix product $C(x)\eta_K(x)$ - as is readily understood from equations (2.11) and (2.12), and equations (44) and (45) above.

EFFECTS OF BEARING OFFSET AND FLEXIBILITY ON THE MESH FORCE DISTRIBUTION

In the preceding section, a method is outlined for determining the values of the three generalized force components W_t, W_r, and τ. This method is valid for elastic teeth of modified spherical involute design if the true surface of tooth contact is reasonably well approximated by a plane surface passing through the common apex of the base and pitch cones of the meshing bevel gears. The method outlined in the text following equation (3.45b) includes contributions to W_t, W_r, and τ from the inertial forces of the gear bodies arising from their transverse and axial vibratory motions, and contributions from the torsional vibratory motions of the gears which depend on the torsional dynamic properties of all gearing elements in the system.

In the present section, equations are derived for the generalized mesh force components W_t, W_r, and τ under the assumption that the gear body inertial forces and the inertial forces associated with the "effective" bearing mass are negligible in comparison with the bearing/bearing support elastic reaction forces. When the values of these generalized mesh force components are used in equations (3.41) and (3.44), the value of the generalized transmission error determined therefrom as a function of the rotational positions of the gears is the generalized static transmission error. However, contributions from the torsional vibratory motions of the gears are readily taken into account when using the equations derived herein, since the component of mesh torque coinciding with the gear axis is an "input" to the equations for W_t, W_r, and τ. The temporal variations of this torque component can be determined from the torsional equations of motion of the gearing system.

In the subsection below, the generalized mesh force vector is transformed into a coordinate system suitable for use in writing the equations of motion of the gear bodies. This transformation is useful in applying the methodology outlined following equation (3.45b) which takes into full account the inertial forces associated with transverse and axial gear body motions.

Expression for Mesh Forces in Gear Coordinates

The scalar components W_t, W_r, and τ of the resultant total force $\vec{W}$ transmitted by the gear teeth can be represented by the generalized mesh force column matrix or vector defined by equation (3.41) and illustrated in Fig. 4,

$$W \triangleq \begin{Bmatrix} \tau \\ W_t \\ W_r \end{Bmatrix}. \tag{4.1}$$

According to Newton's third law, this system of forces acts on each member of the pair of meshing spiral bevel gears.

We require a representation in "gear coordinates" of the mesh force system W_t, W_r, and τ acting on a generic spiral bevel gear $(\cdot)$. These gear coordinates are provided by the generalized displacement column matrix or vector $q^{(\cdot)}$ defined by equation (2.11),

$$q^{(\cdot)} \triangleq \begin{Bmatrix} \rho_1^{(\cdot)} \\ \rho_2^{(\cdot)} \\ \rho_3^{(\cdot)} \\ x_1^{(\cdot)} \\ x_2^{(\cdot)} \\ x_3^{(\cdot)} \end{Bmatrix}, \tag{4.2}$$

where each $\rho_i^{(\cdot)}$, $i = 1,2,3$ represents the (small) rotational deviation about the base cone coordinate axis $x_i^{(\cdot)}$ of the position of the shaft centerline of gear $(\cdot)$ from the position of its rigid perfect involute counterpart. Orthogonal coordinates $x_1^{(\cdot)}$, $x_2^{(\cdot)}$, and $x_3^{(\cdot)}$ represent translations of the shaft centerline position of gear $(\cdot)$ from the position of its rigid perfect involute counterpart. This six degree-of-freedom system of coordinates is illustrated in Fig. 12 or its mirror image Fig. 13, whichever is appropriate.

We can associate a generalized force column matrix or vector

$$Q^{(\cdot)} \triangleq \begin{Bmatrix} \tau_1^{(\cdot)} \\ \tau_2^{(\cdot)} \\ \tau_3^{(\cdot)} \\ F_1^{(\cdot)} \\ F_2^{(\cdot)} \\ F_3^{(\cdot)} \end{Bmatrix} \tag{4.3}$$

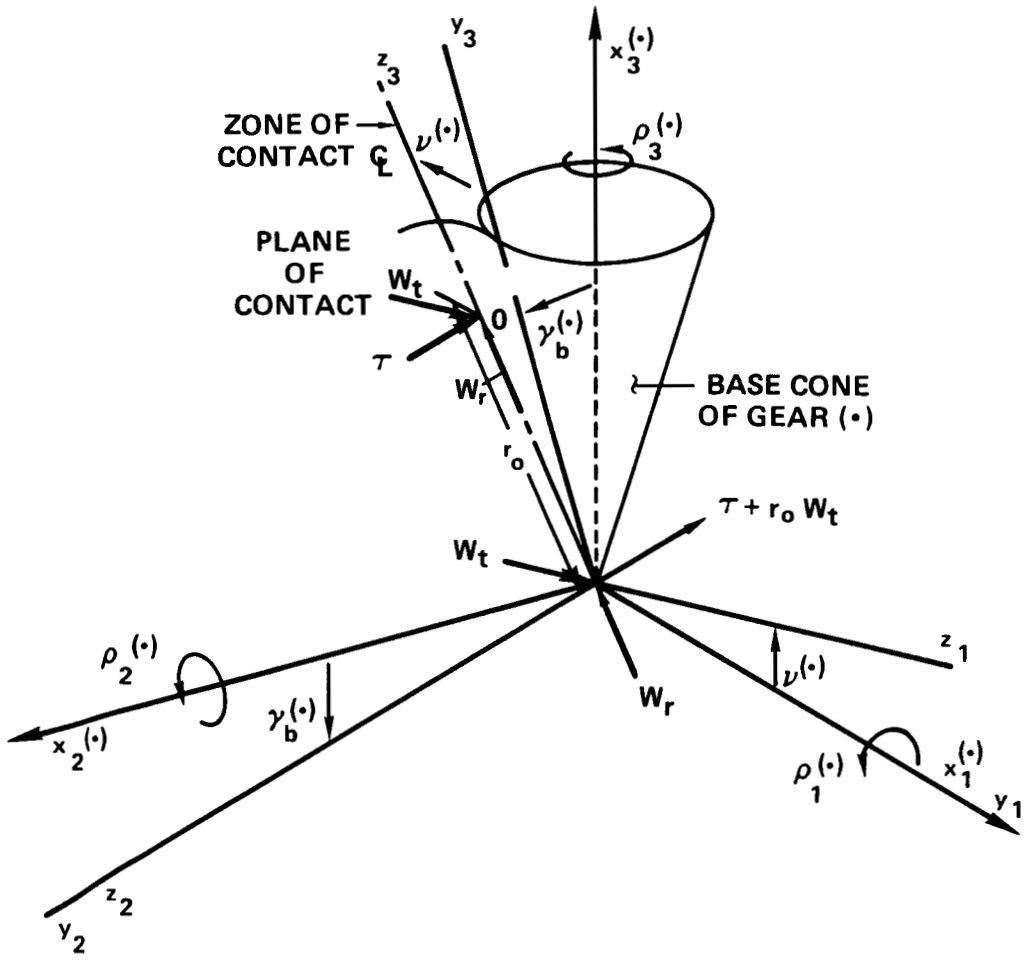

FIG. 12. GEAR COORDINATE SYSTEM CONSISTING OF ROTATIONS $\rho_i^{(\cdot)}$, i = 1,2,3 AND TRANSLATIONS $x_i^{(\cdot)}$, i = 1,2,3 REPRESENTING DEVIATIONS OF POSITION OF GEAR (•) FROM POSITION OF ITS RIGID PERFECT INVOLUTE COUNTERPART. CARTESIAN COORDINATES z_i, i = 1,2,3 ARE ORIENTED WITH RESPECT TO PLANE OF CONTACT WHICH IS z_1, z_3 PLANE WITH z_3 AXIS PASSING THROUGH ZONE OF CONTACT CENTER 0. FORCE SYSTEM LOCATED AT 0 SHOWS FORCES EXERTED ON GEAR (•) BY ITS MATING GEAR WITH MOMENT τ OF RESULTANT TOTAL FORCE TAKEN ABOUT 0. FORCE SYSTEM LOCATED AT BASE CONE APEX SHOWS EQUIVALENT FORCES WITH MOMENT $\tau + r_o W_t$ OF RESULTANT TOTAL FORCE TAKEN ABOUT BASE CONE APEX. VECTOR REPRESENTATION OF MOMENTS τ and $\tau + r_o W_t$ IS GOVERNED BY RIGHT-HAND RULE.

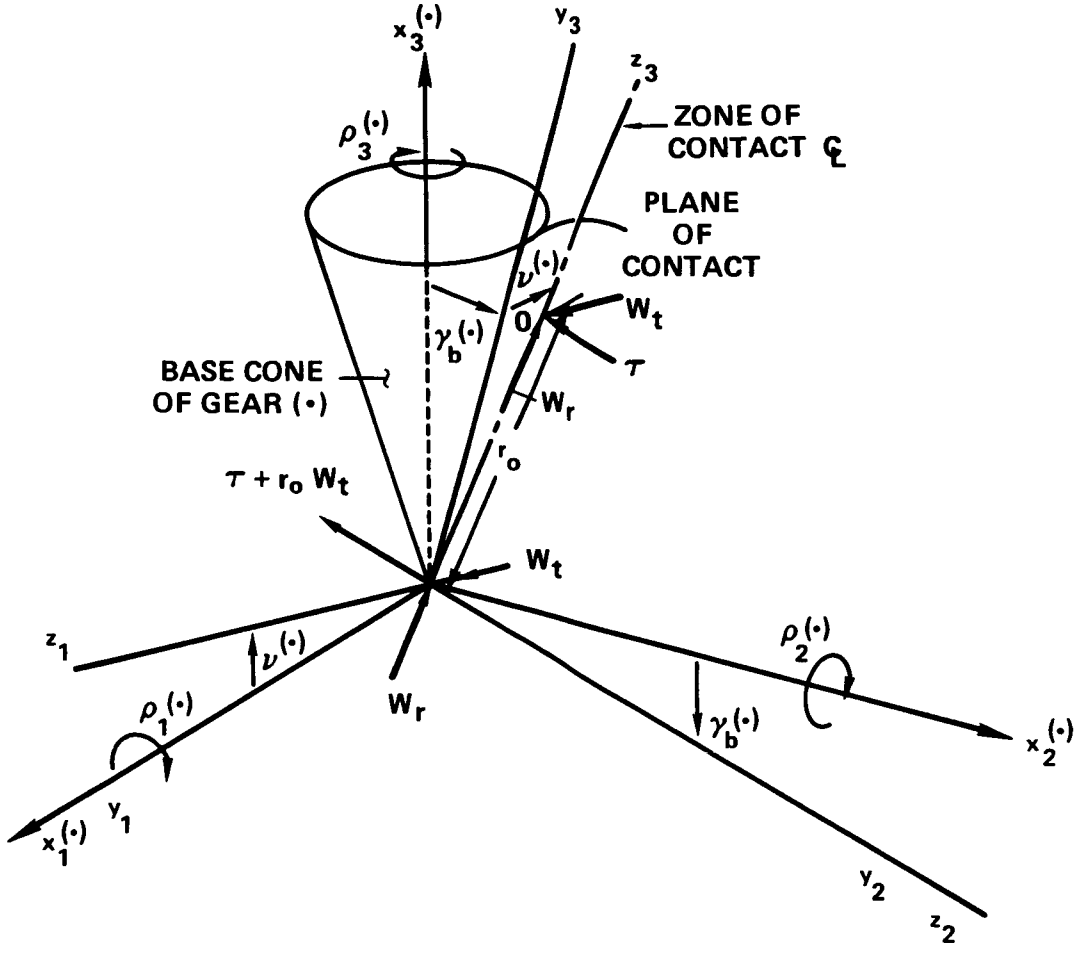

FIG. 13. MIRROR IMAGE OF FIG. 12. SEE CAPTION OF FIG. 12. HERE, VECTOR REPRESENTATION OF MOMENTS τ and $\tau + r_o W_t$ IS GOVERNED BY LEFT-HAND RULE.

with the generalized displacement vector $q^{(\cdot)}$ given by equation (2). The generalized force vector $Q^{(\cdot)}$ has three moment or torque components $\tau_i^{(\cdot)}$, i = 1,2,3 and three force components $F_i^{(\cdot)}$, i = 1,2,3. These components are not the generalized forces normally associated with Lagrange's equations.

Each $\tau_i^{(\cdot)}$, i = 1,2,3 is the component of torque taken about the axis $x_i^{(\cdot)}$. Positive values of the $\tau_i^{(\cdot)}$ correspond to positive values of the (small) rotations $\rho_i^{(\cdot)}$. The directions of positive $\rho_i^{(\cdot)}$, i = 1,2,3 are illustrated in Fig. 12 or Fig. 13, as appropriate. From Figs. 12 or 13, we may conclude that each torque component $\tau_i^{(\cdot)}$ is taken about the point occupied by the base cone apex. From Fig. 12, one may observe that for each i = 1,2,3 the relationship between the sign of $\rho_i^{(\cdot)}$, and hence $\tau_i^{(\cdot)}$, and the sign of $x_i^{(\cdot)}$ is governed by the well-known right-hand rule; whereas, from Fig. 13, which is the mirror image of Fig. 12, the relationship between the sign of $\rho_i^{(\cdot)}$, and hence $\tau_i^{(\cdot)}$, and the sign of $x_i^{(\cdot)}$ is governed by the left-hand rule. This difference in sign convention between Figs. 12 and 13 is a necessary consequence of the mirror image property.

Each $F_i^{(\cdot)}$, i = 1,2,3 in equation (3) is the component of force in the direction of $x_i^{(\cdot)}$. Positive values of the $F_i^{(\cdot)}$ correspond to positive values of the displacements $x_i^{(\cdot)}$.

For a generic spiral bevel gear (·), it is shown in Appendix E that the generalized force vector $Q^{(\cdot)}$ in gear coordinates is related to the generalized mesh force vector W by the matrix transformation

$$Q^{(\cdot)} = -\tilde{T}^{(\cdot)} W \,, \tag{4.4}$$

where $\tilde{T}^{(\cdot)}$ is the transpose of the matrix $T^{(\cdot)}$ defined by equation (2.13) and Table 1,

$$\tilde{T}^{(\cdot)} \triangleq \begin{bmatrix} 0 & 0 & 0 \\ c\gamma_b^{(\cdot)} & r_o c\gamma_b^{(\cdot)} & 0 \\ -s\gamma_b^{(\cdot)} & -r_o s\gamma_b^{(\cdot)} & 0 \\ 0 & -c\nu^{(\cdot)} & \pm s\nu^{(\cdot)} \\ 0 & -s\gamma_b^{(\cdot)} s\nu^{(\cdot)} & \mp s\gamma_b^{(\cdot)} c\nu^{(\cdot)} \\ 0 & -c\gamma_b^{(\cdot)} s\nu^{(\cdot)} & \mp c\gamma_b^{(\cdot)} c\nu^{(\cdot)} \end{bmatrix} , \tag{4.5}$$

where c and s are abbreviations (ref. 18, p. 106) for cosine and sine operations, respectively, on the angles $\gamma_b^{(\cdot)}$ and $\nu^{(\cdot)}$. These angles and r_o are illustrated in Figs. 12 and 13. Determination of the appropriate sign for the terms in the third column of $\tilde{\mathbf{T}}^{(\cdot)}$ is governed by the rules for determination of the appropriate sign for the terms in the third row of $\mathbf{T}^{(\cdot)}$ that are described in Table 1. Further explanation of the gearing configurations described in Table 1 may be found following equation (2.13).

The transformation provided by equations (4) and (5) yields the three torque components $\tau_i^{(\cdot)}$ and three force components $F_i^{(\cdot)}$, i = 1,2,3 associated with the three rotations $\rho_i^{(\cdot)}$ and three displacements $x_i^{(\cdot)}$, i = 1,2,3 with positive torques and forces associated with positive rotations and displacements, respectively. These are the torque and force components applied to gear (•) by its mating gear expressed in the gear coordinate system defined by equation (2) and Figs. 12 or 13, as appropriate.

Expression for Generalized Transmission Error in Terms of Bearing Offset and Flexibility Matrices

The expression given by equation (2.12),

$$\zeta(x) = \mathbf{T}^{(1)}\mathbf{q}^{(1)}(x) + \mathbf{T}^{(2)}\mathbf{q}^{(2)}(x) \ , \tag{4.6}$$

describes the generalized transmission error $\zeta(x)$ of a meshing pair of spiral bevel gears in terms of the generalized displacement vectors $\mathbf{q}^{(1)}(x)$ and $\mathbf{q}^{(2)}(x)$ of the shaft centerline positions of gears (1) and (2), respectively, measured from the positions of their rigid perfect involute counterparts. The generalized transmission error is defined by equation (2.10) and Fig. 5; the matrix $\mathbf{T}^{(\cdot)}$, (•) = (1) or (2), is defined by equation (2.13) and Table 1; and, the vectors $\mathbf{q}^{(\cdot)}$, (•) = (1) or (2), are defined by equation (2).

Geometric compatibility requires that the shaft centerline positions of gears (1) and (2) coincide with their respective bearing centerline positions. The bearing centerline positions also are described using the generalized displacement vectors $\mathbf{q}^{(1)}(x)$ and $\mathbf{q}^{(2)}(x)$ that characterize the deviations of the actual centerline positions from the positions of the rigid perfect involute counterparts to the gears under consideration. These deviations have three vector contributions. The first of

these contributions is the generalized displacement vector $\mathbf{q}_{\mathbf{0}}^{(\bullet)}$, $(\bullet) = (1)$ or (2), that describes the deviation of the bearing centerline position when the gears are transmitting negligible load. This bearing "offset" from the position occupied by the shaft centerline of the rigid perfect involute counterpart may be intentional or unintentional. The second contribution $\mathbf{q}_{\mathbf{W}}^{(\bullet)}$ describes the component attributable to the bearing and bearing support elastic deformations caused by the generalized force $\mathbf{W}$ transmitted by the gear mesh. Neither of the vector contributions $\mathbf{q}_{\mathbf{0}}^{(\bullet)}$ or $\mathbf{q}_{\mathbf{W}}^{(\bullet)}$, by definition, includes a nonzero component $q_3^{(\bullet)} = \rho_3^{(\bullet)}$ of the generalized displacement vector $\mathbf{q}^{(\bullet)}$ that describes the pure rotational deviation of the shaft of gear $(\bullet)$ about its axis from the position of its rigid perfect involute counterpart. The vector describing this third contribution is $\{\delta_{i3}\rho_3^{(\bullet)}\}$ where δ_{i3} is Kronecker's delta (ref. 24). Hence, the third component $\rho_3^{(\bullet)}$ of each vector $\mathbf{q}_{\mathbf{0}}^{(\bullet)}$ and $\mathbf{q}_{\mathbf{W}}^{(\bullet)}$ is, by definition, zero. The deviation vector for gear $(\bullet)$ that describes the sum of these three contributions is

$$\mathbf{q}^{(\bullet)} = \mathbf{q}_{\mathbf{0}}^{(\bullet)} + \mathbf{q}_{\mathbf{W}}^{(\bullet)} + \{\delta_{i3}\rho_3^{(\bullet)}\} \ . \tag{4.7}$$

Let $\mathbf{A}_{\mathbf{0}}^{(\bullet)}$ denote the 6×6 element bearing/bearing support flexibility matrix $[A_{ij}^{(\bullet)}]$, where each flexibility influence coefficient $A_{ij}^{(\bullet)}$ represents the contribution to the generalized displacement component $q_i^{(\bullet)}$ from a unit torque or force component $Q_j^{(\bullet)}$ of the generalized force vector described by equations (3) and (4). Since the component $q_3^{(\bullet)} = \rho_3^{(\bullet)}$ of $\mathbf{q}^{(\bullet)}$ is being handled separately by the term $\{\delta_{i3}\rho_3^{(\bullet)}\}$ in equation (7), the third row in the flexibility matrix $\mathbf{A}_{\mathbf{0}}^{(\bullet)}$ is, by definition, filled with zeros; i.e.,

$$A_{3j}^{(\bullet)} \triangleq 0 \ , \quad j = 1,2,\ldots,6 \ . \tag{4.8}$$

Furthermore, it will be assumed that the reaction of the shaft of gear $(\bullet)$ to the pure torque component $Q_3^{(\bullet)} = \tau_3^{(\bullet)}$ is not coupled to the bearing supports, which implies that

$$A_{i3}^{(\bullet)} \triangleq 0, \quad i = 1,2,\ldots,6 \tag{4.9}$$

since $A_{33}^{(\bullet)} = 0$ by virtue of equation (8). Thus, the bearing/bearing support flexibility matrix $[A_{ij}^{(\bullet)}]$ is symmetric (ref. 23, pp. 4,5). The subscript $\mathbf{0}$ on $\mathbf{A}_{\mathbf{0}}^{(\bullet)}$

is used as a reminder of the requirements (8) and (9). From the definitions of $q_W^{(\cdot)}$ and $A_0^{(\cdot)}$, there follows

$$q_W^{(\cdot)} = A_0^{(\cdot)} Q^{(\cdot)} \tag{4.10a}$$

$$= -A_0^{(\cdot)} \tilde{T}^{(\cdot)} W \ , \tag{4.10b}$$

where $Q^{(\cdot)}$ is defined by equation (3), and equation (4) has been used in going from equation (10a) to equation (10b). Equation (10b) gives the vector contribution of the deviation of the bearing centerline position attributable to the generalized mesh force vector **W**. From equations (9), (10a), and (3) it follows that $q_W^{(\cdot)}$ contains no contribution from the component $Q_3^{(\cdot)} = \tau_3^{(\cdot)}$ of torque about the axis of gear $(\cdot)$, which may be determined from equations (4), (5), and (1) to be $\tau_3^{(\cdot)} = (\tau + r_o W_t) \sin\gamma_b^{(\cdot)}$.

For $(\cdot) = (1)$ or (2), let us define the matrix

$$\Phi^{(\cdot)} \triangleq T^{(\cdot)} A_0^{(\cdot)} \tilde{T}^{(\cdot)} \ , \tag{4.11}$$

and the matrix

$$\Phi \triangleq \Phi^{(1)} + \Phi^{(2)} \ . \tag{4.12}$$

Using equation (10b), we have

$$T^{(1)} q_W^{(1)} + T^{(2)} q_W^{(2)} = -[T^{(1)} A_0^{(1)} \tilde{T}^{(1)} + T^{(2)} A_0^{(2)} \tilde{T}^{(2)}] W \tag{4.13}$$

$$= -\Phi W \ ,$$

where the definitions (11) and (12) have been used. Combining equations (6), (7), and (13) gives

$$\zeta(x) = T^{(1)} q_0^{(1)} + T^{(2)} q_0^{(2)} - \Phi W(x) + T^{(1)} \{\delta_{i3} \rho_3^{(1)}(x)\} + T^{(2)} \{\delta_{i3} \rho^{(2)}(x)\} \ , \tag{4.14}$$

where dependence on the rotational positions of the gears is denoted by the variable x. Equation (14) expresses the generalized transmission error $\zeta(x)$ defined by

equation (2.10) in terms of the bearing centerline offset vectors $\mathbf{q}_0^{(1)}$ and $\mathbf{q}_0^{(2)}$, the generalized mesh force vector $\mathbf{W}(x)$, and the gear shaft rotations $\rho_3^{(1)}(x)$ and $\rho_3^{(2)}(x)$ about their axes illustrated in Figs. 12 or 13, as appropriate.

The matrix Φ in equation (14) characterizes the composite bearing/bearing support flexibility of gears (1) and (2). Each of the two matrices $\Phi^{(1)}$ and $\Phi^{(2)}$ that contributes to Φ in equation (12) is the negative of the bearing/bearing support flexibility matrix that yields the contribution to the generalized transmission error vector ζ from the bearing/bearing support elastic displacements caused by the generalized mesh force vector $\mathbf{W}$. It follows by forming the transpose of $\Phi^{(\cdot)}$ that each of these matrices is symmetric; i.e.,

$$\tilde{\Phi}^{(\cdot)} \equiv \left(\mathbf{T}^{(\cdot)}\mathbf{A}_0^{(\cdot)}\tilde{\mathbf{T}}^{(\cdot)}\right)^T = \left(\mathbf{A}_0^{(\cdot)}\tilde{\mathbf{T}}^{(\cdot)}\right)^T\left(\mathbf{T}^{(\cdot)}\right)^T$$

$$= \left(\tilde{\mathbf{T}}^{(\cdot)}\right)^T\left(\mathbf{A}_0^{(\cdot)}\right)^T\left(\mathbf{T}^{(\cdot)}\right)^T \equiv \mathbf{T}^{(\cdot)}\tilde{\mathbf{A}}_0^{(\cdot)}\tilde{\mathbf{T}}^{(\cdot)} \; ; \tag{4.15}$$

hence, it follows from the symmetry of $\mathbf{A}_0^{(\cdot)}$ and the definitions (11) and (12) that $\Phi^{(\cdot)}$ and Φ are symmetric. Each of the matrices $\Phi^{(1)}$, $\Phi^{(2)}$, and Φ has three rows and three columns.

Equations for Generalized Mesh Force Components

Consider the last two terms in the right-hand side of equation (14). Utilizing equation (2.13) to evaluate these two terms, we have

$$\mathbf{T}^{(1)}\{\delta_{i3}\rho_3^{(1)}(x)\} + \mathbf{T}^{(2)}\{\delta_{i3}\rho_3^{(2)}(x)\}$$

$$= \begin{Bmatrix} -s\gamma_b^{(1)}\rho_3^{(1)}(x) - s\gamma_b^{(2)}\rho_3^{(2)}(x) \\ -r_o s\gamma_b^{(1)}\rho_3^{(1)}(x) - r_o s\gamma_b^{(2)}\rho_3^{(2)}(x) \\ 0 \end{Bmatrix} \tag{4.16a}$$

$$= -\left[\rho_3^{(1)}(x)\sin\gamma_b^{(1)} + \rho_3^{(2)}(x)\sin\gamma_b^{(2)}\right]\begin{Bmatrix} 1 \\ r_o \\ 0 \end{Bmatrix} \tag{4.16b}$$

$$= -\begin{Bmatrix} \rho_{3b}(x) \\ r_o \rho_{3b}(x) \\ 0 \end{Bmatrix} , \qquad (4.16c)$$

where, in going from equation (16b) to equation (16c), we have defined

$$\rho_{3b}(x) \triangleq \rho_3^{(1)}(x)\sin\gamma_b^{(1)} + \rho_3^{(2)}(x)\sin\gamma_b^{(2)} . \qquad (4.17)$$

Figure 14 shows the torque component $\tau + r_o W_t$ at the base cone apex of gear $(\cdot)$ resolved into components $(\tau + r_o W_t)\sin\gamma_b^{(\cdot)}$ and $(\tau + r_o W_t)\cos\gamma_b^{(\cdot)}$ parallel to the $x_3^{(\cdot)}$ and $-x_2^{(\cdot)}$ axes, respectively. In the absence of gear rotational inertial effects, it follows that the torque applied to gear $(\cdot)$ by its shaft, which coincides with the $x_3^{(\cdot)}$ axis, must have a magnitude of $(\tau + r_o W_t)\sin\gamma_b^{(\cdot)}$ positive in the direction of $-\rho_3^{(\cdot)}$. Examination of Figs. 12 and 13 shows this conclusion to be valid for all gear configurations listed in Table 1. Let us denote by $M^{(\cdot)}$ the value of this torque applied to the shaft of gear $(\cdot)$; i.e.,

$$M^{(\cdot)} \triangleq (\tau + r_o W_t)\sin\gamma_b^{(\cdot)} , \qquad (4.18)$$

which we may regard as being known. Then, from equation (18), we have

$$\tau = M^{(\cdot)}\csc\gamma_b^{(\cdot)} - r_o W_t , \qquad (4.19)$$

from which it follows that the generalized mesh force vector, equation (1), can be expressed as

$$\mathbf{W}(x) = \begin{Bmatrix} M^{(\cdot)}\csc\gamma_b^{(\cdot)} - r_o W_t(x) \\ W_t(x) \\ W_r(x) \end{Bmatrix} , \qquad (4.20)$$

where the dependence of $\mathbf{W}(x)$, $W_t(x)$, and $W_r(x)$ on the rotational positions of the gears has been explicitly denoted by their dependence on x.

Equation 14 expresses the generalized transmission error $\zeta(x)$ in terms of bearing offsets, bearing/bearing support flexibilities, and shaft rotational displacements. In contrast, equation (3.40),

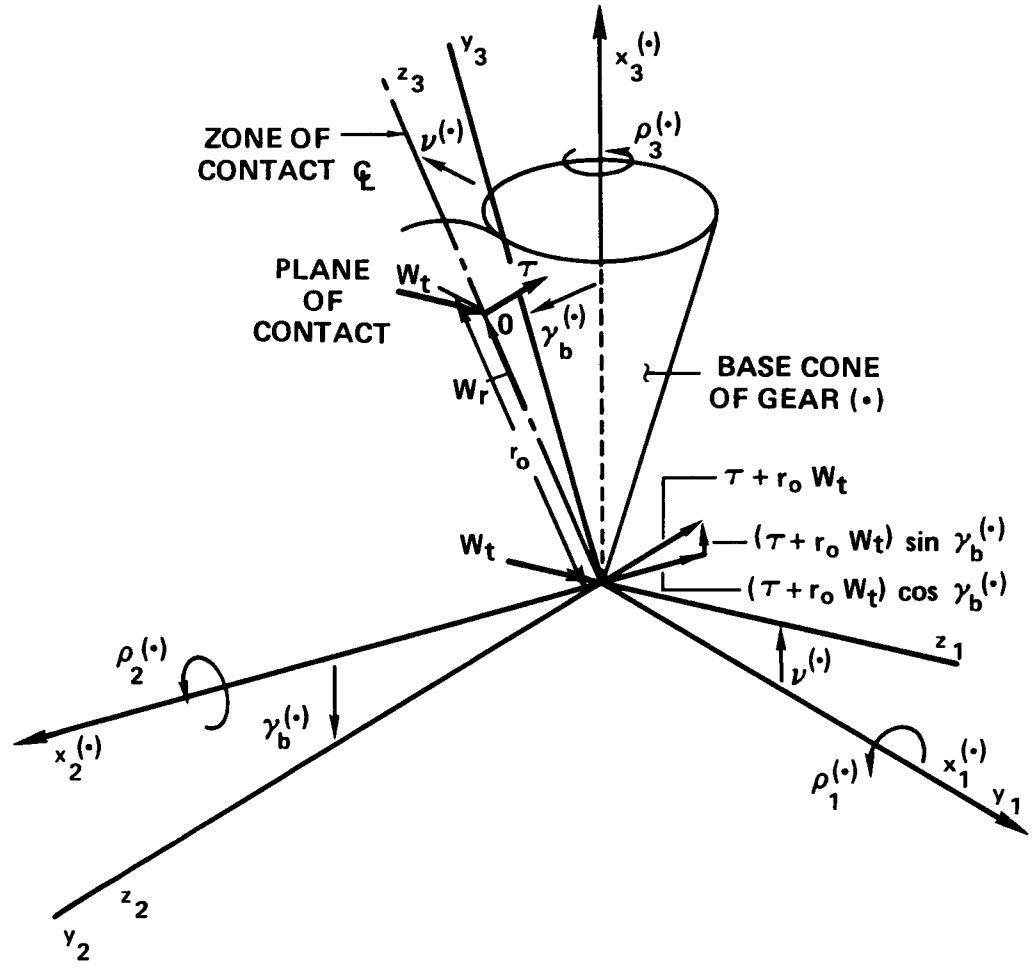

FIG. 14. GENERALIZED MESH FORCE COMPONENTS W_t, W_r, AND τ SHOWN IN FIG. 4 EXERTED ON GEAR (•) BY ITS MATING GEAR. GEAR (•) IS GEAR (1) IN FIG. 3. RIGHT-HAND RULE APPLIES TO VECTOR REPRESENTATION OF MOMENTS. MOMENT OF $\vec{W}$ ABOUT ZONE OF CONTACT CENTER 0 IS τ. MOMENT OF $\vec{W}$ ABOUT BASE CONE APEX IS $\tau + r_o W_t$ WHICH HAS COMPONENTS $(\tau + r_o W_t)\sin\gamma_b^{(\cdot)}$ AND $(\tau + r_o W_t)\cos\gamma_b^{(\cdot)}$ IN THE $x_3^{(\cdot)}$ AND $-x_2^{(\cdot)}$ DIRECTIONS, RESPECTIVELY.

$$\mathbf{K}(x)\boldsymbol{\zeta}(x) = \mathbf{W}(x) + \boldsymbol{\eta}_{\mathbf{K}}(x) \ , \tag{4.21}$$

is an equation for the generalized transmission error in terms of the stiffness weighted geometric deviations $\boldsymbol{\eta}_{\mathbf{K}}(x)$ of the tooth surfaces from perfect spherical involute surfaces defined by equation (3.42), and the tooth pair/gear body stiffness matrix $\mathbf{K}(x)$ defined by the coefficients of the left-hand sides of equations (3.37) through (3.39). By combining equations (14) and (21) to eliminate $\boldsymbol{\zeta}(x)$, we can obtain a matrix algebraic equation for the generalized mesh force vector $\mathbf{W}(x)$.

Substituting equation (16c) into equation (14) and the resulting expression into equation (21), we obtain

$$\mathbf{K}(x)\left[\mathbf{T}^{(1)}\mathbf{q}_0^{(1)} + \mathbf{T}^{(2)}\mathbf{q}_0^{(2)} - \boldsymbol{\Phi}\mathbf{W}(x) - \begin{Bmatrix} \rho_{3b}(x) \\ r_o\rho_{3b}(x) \\ 0 \end{Bmatrix}\right] = \mathbf{W}(x) + \boldsymbol{\eta}_{\mathbf{K}}(x) \ , \tag{4.22}$$

or, by rearranging terms and introducing the identity matrix $\mathbf{I}$,

$$[\mathbf{K}(x)\boldsymbol{\Phi} + \mathbf{I}]\mathbf{W}(x) + \mathbf{K}(x)\begin{Bmatrix} \rho_{3b}(x) \\ r_o\rho_{3b}(x) \\ 0 \end{Bmatrix} = \mathbf{K}(x)\{\mathbf{T}^{(1)}\mathbf{q}_0^{(1)} + \mathbf{T}^{(2)}\mathbf{q}_0^{(2)}\} - \boldsymbol{\eta}_{\mathbf{K}}(x) \ . \tag{4.23}$$

Introducing equation (20) into equation (23) and again rearranging terms, we have

$$[\mathbf{K}(x)\boldsymbol{\Phi} + \mathbf{I}]\begin{Bmatrix} -r_o W_t(x) \\ W_t(x) \\ W_r(x) \end{Bmatrix} + \mathbf{K}(x)\begin{Bmatrix} \rho_{3b}(x) \\ r_o\rho_{3b}(x) \\ 0 \end{Bmatrix}$$

$$= \mathbf{K}(x)\{\mathbf{T}^{(1)}\mathbf{q}_0^{(1)} + \mathbf{T}^{(2)}\mathbf{q}_0^{(2)}\} - \boldsymbol{\eta}_{\mathbf{K}}(x) - [\mathbf{K}(x)\boldsymbol{\Phi}+\mathbf{I}]\begin{Bmatrix} M^{(\cdot)}\csc\gamma_b^{(\cdot)} \\ 0 \\ 0 \end{Bmatrix}. \tag{4.24}$$

Equation (24) is the desired matrix equation for the components $W_t(x)$ and $W_r(x)$ of the generalized mesh force vector $\mathbf{W}(x)$ defined by equation (1). Once $W_t(x)$ and $W_r(x)$ are obtained, the component $\tau(x)$ of $\mathbf{W}(x)$ may be determined from equation (19) using the shaft input torque $M^{(\cdot)}$, which is assumed known.

The matrix equation (24) represents three simultaneous linear algebraic equations for the three unknowns $W_t(x)$, $W_r(x)$, and $\rho_{3b}(x)$. The (small) angular displacement vector component $\rho_{3b}(x)$ defined by equation (17) is the total contribution from both meshing gears to the rotational vector component normal to the base plane (plane of contact) arising from the angular deviation components $\rho_3^{(1)}$ and $\rho_3^{(2)}$ of the shafts of gears (1) and (2), respectively, from the positions of their rigid perfect involute counterparts. The value of $\rho_{3b}(x)$ is of interest in the present investigation only in the supplementary role it plays in equation (24) as a contribution to our ability to compute $W_t(x)$ and $W_r(x)$. The parameter r_o is defined by equation (2.5) and the neighboring text.

The matrix $\mathbf{K}(x)$ is the composite tooth pair/gear body stiffness matrix of the two meshing gears defined by the coefficients of the left-hand sides of the set of simultaneous equations (3.37) through (3.39), as one may see by comparing this set of equations with equation (3.40). The bearing/bearing support flexibility matrix defined by equations (11) and (12) occurs in equation (24) only as the second term in the matrix product $\mathbf{K}(x)\boldsymbol{\Phi}$ which collectively characterizes the elastic properties of the meshing gears (including the teeth) and the bearings and bearing supports. The matrix $\mathbf{K}(x)$, the matrix product $\mathbf{K}(x)\boldsymbol{\Phi}$, and the identity matrix $\mathbf{I}$ all are of dimension 3×3.

The right-hand side of the matrix equation (24) contains contributions from three sources: (a) the bearing offset generalized displacement vectors $\mathbf{q}_0^{(1)}(x)$ and $\mathbf{q}_0^{(2)}(x)$ from gears (1) and (2), respectively, (b) the vector $\eta_K(x)$ defined by equation (3.42) which characterizes the stiffness weighted geometric deviations of the tooth running surfaces from their perfect spherical involute counterparts, and (c) the torque $M^{(\cdot)}\csc\gamma_b^{(\cdot)}$, where $M^{(\cdot)}$ may be taken as the driving torque of either gear $(\cdot)$ of the meshing pair when the rotational inertial effects of gear $(\cdot)$ are negligible, and $\gamma_b^{(\cdot)}$ is the angle associated with the same gear $(\cdot)$ illustrated in either Fig. 12 or Fig. 13, as appropriate. The bearing offset vectors $\mathbf{q}_0^{(1)}(x)$ and $\mathbf{q}_0^{(2)}(x)$ are represented in the generalized displacement coordinates defined by equation (2) and Fig. 12 or Fig. 13, as appropriate. The matrix $\mathbf{T}^{(\cdot)}$ is defined by

equation (2.13) and Table 1. It is the transpose of the matrix $\tilde{T}^{(\cdot)}$ defined by equation (5). Equation (24) readily can be solved using Cramer's rule (ref. 24).

The location of the force vector $\vec{W}$ representing the resultant total force transmitted by the mesh is illustrated in Fig. 4. Dimension d shown in the figure measures the distance between the nominal zone of contact center $\underline{0}$ located by r_o in Figs. 12 or 13 and the path of $\vec{W}$. The value of d is readily computed from the three components τ, W_t, and W_r of the generalized mesh force $\mathbf{W}$ described by equation (1). Since $\tau = |W|d$, it follows with the aid of equation (19) that

$$d = \frac{\tau}{|W|} = \frac{\tau}{\left[W_t^2 + W_r^2\right]^{1/2}} = \frac{M^{(\cdot)} \csc\gamma_b^{(\cdot)} - r_o W_t(x)}{\left[W_t^2(x) + W_r^2(x)\right]^{1/2}}, \tag{4.25}$$

where $W_t(x)$ and $W_r(x)$ are solutions to equation (24). Since these solutions are functions of the rotational positions of the gears, as indicated by their dependence on x, it follows that the distance d also is a function of the rotational positions of the gears.

Case of Nonnegligible Gear Body Inertias. In deriving equation (24), the inertial forces arising from transverse and axial vibrations of the gear bodies were assumed to be negligible. This assumption was employed when the forces applied to the bearings by the gear bodies (or shafts) were set equal to the appropriate mesh forces; that is, when the generalized force vector $Q^{(\cdot)}$ describing the forces applied to the bearings by the gear bodies (or shafts) was set equal to the right-hand side of equation (4). That step occurred in passing from equation (10a) to equation (10b). An assumption of negligible gear train inertia also was employed when the shaft input torque $M^{(\cdot)}$, equation (18), was assumed to be known and independent of the rotational positions of the gears and of time as in equation (20). In addition, characterizing the relationship between the generalized force vector $Q^{(\cdot)}$ applied to the bearings and the generalized bearing displacement vector $q_w^{(\cdot)}$ by the bearing/bearing support flexibility matrix $A_0^{(\cdot)} = [A_{ij}^{(\cdot)}]$, as in equation (10a), ignores the inertia of the bearings and their supporting structure. When inertial effects are not negligible, a further complication arises from the fact that the mesh force components τ, W_t, and W_r will be functions not only of the rotational positions of the gears characterized by the variable x, but also of time and the rotational speed

of the gear train which controls the temporal behavior of the gear train vibratory excitation.

A general methodology for computing the components of the mesh force vector $\mathbf{W}$ in cases where inertial effects are not negligible is outlined in the text following equation (3.45b). Equations (4) and (5), which describe the components, equation (3), of the generalized force vector $Q^{(\bullet)}$ in terms of the mesh force vector $\mathbf{W}$, are useful for describing the mesh excitation torques and forces on the gear bodies in these cases. Furthermore, in these cases one would describe the bearing/bearing support elastic deformations $q_w^{(\bullet)}$ by

$$q_w^{(\bullet)} = q^{(\bullet)} - q_0^{(\bullet)} , \tag{4.26}$$

where the meanings of $q^{(\bullet)}$, $q_0^{(\bullet)}$, and $q_w^{(\bullet)}$ are the same as those in equation (7).

Equation (24) remains valid if the input torque $M^{(\bullet)}$ defined by equation (18) is allowed to vary with time. In such applications, $M^{(\bullet)}$ is to be interpreted as the component of the mesh torque coinciding with the axis of gear $(\bullet)$. The temporal variations of $M^{(\bullet)}$ can be determined by solving the torsional equations of motion of the gear system. If the temporal variations of $M^{(\bullet)}$, correctly determined in this manner, are used in equation (24), the time dependent values of W_t and W_r obtained therefrom, and the values of τ obtained from $M^{(\bullet)}$ and W_t using equation (19), will include the inertial effects associated with torsional vibratory motions of the gear system. It is likely that these inertial effects are more important than those arising from transverse and axial vibrations of the gear bodies, or from bearing/bearing support motions.

AN EXTREMUM PRINCIPLE FOR COMPUTATION OF THE ZONE OF TOOTH CONTACT AND GENERALIZED TRANSMISSION ERROR

A set of linear algebraic equations, equations (4.24) and (4.19), has been derived for computing the three mesh force components under "static" loading conditions where inertial effects are negligible. The resulting mesh force components are dependent on the bearing/bearing support flexibilities, tooth/gear body stiffnesses, and other factors. When these mesh force components are used to evaluate the three transmission error components, they yield the generalized static transmission error components.

To carry out the above-described computations, the positions of the endpoints of the lines of tooth contact must be known for all rotational positions of the gears. However, for tooth running surfaces that have been substantially modified from the "ideal" spherical involute toothform (ref. 13), these endpoint positions generally will have to be computed.

In the present section, a method is developed for computing the positions of the endpoints of the lines of tooth contact and the three components of the generalized transmission error. For a given set of forces transmitted by the mesh, it is shown first that each of the three components of the generalized transmission error is stationary (ref. 22) with respect to small independent variations in the endpoint positions of all lines of tooth contact about their true values. For given forces transmitted by the mesh, this property implies that the value of each of the generalized transmission error components is insensitive to small errors in the endpoint positions of the lines of tooth contact.

It then is shown that the tangential component of the generalized transmission error takes on a minimum value when the endpoint positions are given their true values. This property is the basis of a computational procedure utilizing the method of steepest descent (ref. 25) that is described for computing the true values of the endpoint positions and the generalized transmission error components. Alternative methods for computing the contact regions of the teeth of parallel-axis gears have been developed by Seager (ref. 26) and Conry and Seireg (refs. 27, 28).

The computational procedure described herein is based on the assumption that along every path of tooth contact on a tooth running surface, the tooth surface modification from a perfect spherical involute surface is a monotonic strictly

increasing function (ref. 29) in both directions along this path away from some interior unmodified region which may be of negligible size. The modification is considered positive when it is equivalent to removal of material from a perfect spherical involute surface. However, one tooth of a meshing pair of teeth is permitted to be completely unmodified. If both teeth are unmodified, the zone of contact is the ideal geometric zone of tooth contact shown in Fig. 3. It will be assumed that the tooth running surface modifications from equispaced perfect spherical involute surfaces are sufficiently small so that the true surface of tooth contact is well approximated by a plane surface passing through the common location of the apexes of the pitch cones of the two meshing gears as illustrated in Fig. 3.

Stationary Property of Generalized Transmission Error

As the gears in a meshing spiral bevel pair rotate, the lines of contact of meshing pairs of teeth pass through the nominal zone of contact, as one can see from Fig. 3. The variable x, defined by equation (2.6) and Fig. 3, describes the rotational positions of the gears and the locations of the lines of tooth contact in the plane of contact. Our aim is to determine the true locations of the endpoints of these lines of contact for a generic fixed value of x. When these endpoint locations are determined for all tooth pairs j in contact for all values of x within the range $-(\Delta/2) \leq x < (\Delta/2)$ where Δ is the tooth spacing interval in the variable x, the locus of points traced out by the endpoints of the lines of contact of all tooth pairs j as x is varied determines the zone of tooth contact in the plane of contact. This zone of contact is illustrated in Fig. 15. For a fixed value of x, the positions of the endpoints for tooth pair j are described by the values y_{Aj} and y_{Bj} where y is the radial coordinate

$$y \triangleq r_o - r \tag{5.1}$$

illustrated in Fig. 3.

For a given generic value of x, it is shown below that each of the components $\zeta_t(x)$, $\mu(x)$, and $\zeta_r(x)$ of the generalized transmission error is stationary with respect to small independent variations in the values of the endpoints y_{Aj} and y_{Bj} of all lines j of tooth contact of all pairs of teeth in contact, where these variations are taken about the true values of y_{Aj} or y_{Bj}. In carrying out these variations in

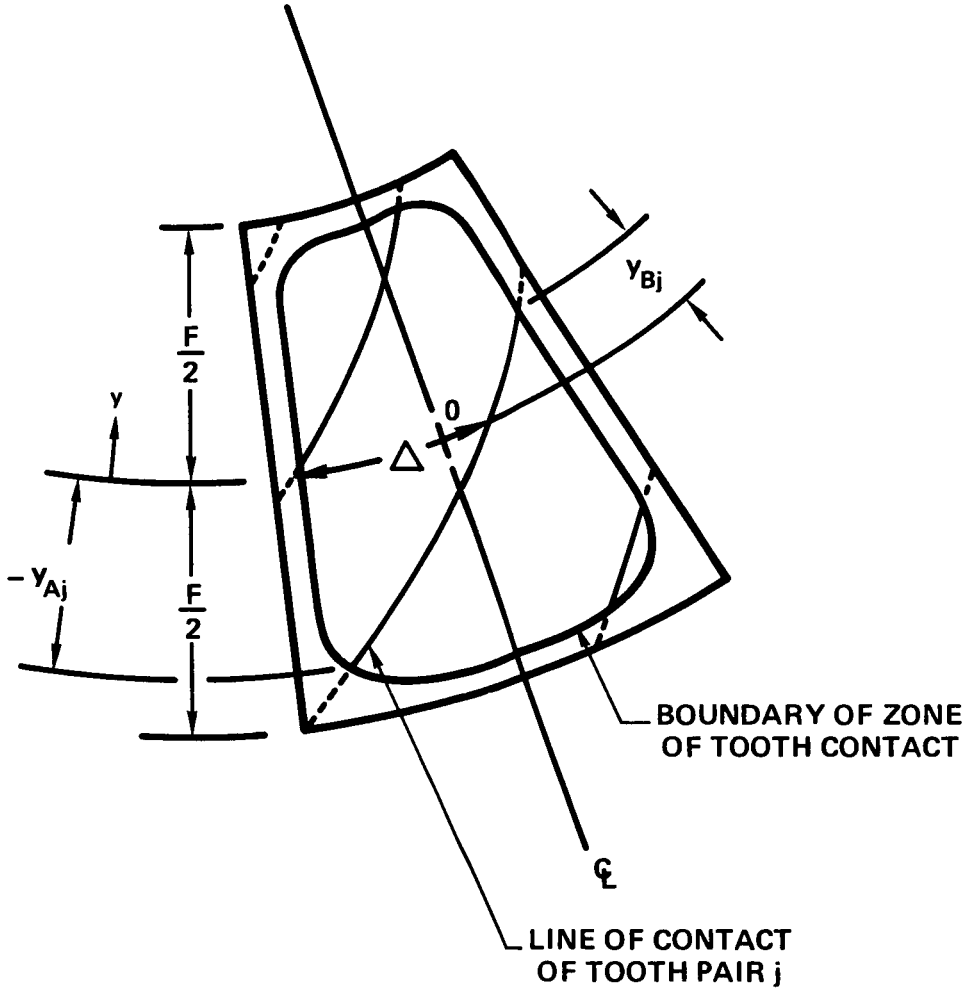

FIG. 15. ZONE OF TOOTH CONTACT IN PLANE OF CONTACT TRACED OUT BY ENDPOINT POSITIONS y_{Aj} AND y_{Bj} OF LINES OF TOOTH CONTACT.

the endpoint positions y_{Aj} or y_{Bj}, all other parameters and variables, including the generalized force components W_t, τ, and W_r transmitted by the mesh, are held fixed.

Furthermore, in carrying out these variations, negative values of the elastic deformations $u_{nj}(x,y)$ normal to the tooth surfaces are permitted, where a positive value of $u_{nj}(x,y)$ is associated with compressive forces between the teeth. The mathematical artifact of allowing negative values of $u_{nj}(x,y)$ to occur along the lines of contact outside the actual contact range determined by the true endpoint values of y_{Aj} and y_{Bj} will be seen later in this section to guarantee that the transmission error component $\zeta_t(x)$ takes on a strong local minimum (ref. 30) with respect to both positive and negative variations in the endpoint positions about their true values. The procedure developed to compute the true values of the endpoint positions and the transmission error component $\zeta_t(x)$ also allows negative values of $u_{nj}(x,y)$ beyond the true range of tooth contact.

Stationary Property of $\zeta_t(x)$. Equations (3.37) and (3.38) are a pair of simultaneous algebraic equations for the generalized transmission error components $\mu(x)$ and $\zeta_t(x)$. These equations are of the form

$$a_1\mu + a_2\zeta_t = r_a \tag{5.2}$$

$$b_1\mu + b_2\zeta_t = r_b \,, \tag{5.3}$$

where the right-hand sides are of the form

$$r_a = \tau + \eta_a \tag{5.4}$$

$$r_b = W_t + \eta_b \,, \tag{5.5}$$

where all quantities in equations (2) through (5) are functions of the variable x which describes the rotational position of the gears. The terms τ and W_t in equations (4) and (5), respectively, are two of the components of the generalized force transmitted by the mesh. Expressions for the terms a_1, a_2, η_a; and b_1, b_2, and η_b are readily obtained by comparing equations (2) through (5) with equations (3.37) and (3.38). Each of these latter six terms is an explicit function of the endpoint positions y_{Aj} and y_{Bj} of all of the tooth pairs j in contact at the rotational position of the gears designated by the value of x, as one can see from

equations (3.37) and (3.38), (3.36a) through (3.36o), and (3.32a) through (3.32o), where dependence of the endpoint positions y_{Aj} and y_{Bj} on tooth pair index j has been suppressed. Thus, the generalized transmission error components μ and ζ_t, determined by the solution of equations (2) and (3), also must be regarded as functions of the endpoint positions of all tooth pairs in contact. The generalized mesh force components τ and W_t are considered here to be known and fixed.

Equations (2) and (3) are readily solved for the tangential generalized transmission error component ζ_t:

$$\zeta_t = \frac{\begin{vmatrix} a_1 & r_a \\ b_1 & r_b \end{vmatrix}}{\begin{vmatrix} a_1 & a_2 \\ b_1 & b_2 \end{vmatrix}} = \frac{a_1 r_b - b_1 r_a}{a_1 b_2 - b_1 a_2} \quad . \tag{5.6}$$

Let y_{ej} denote either endpoint position y_{Aj} or y_{Bj} of a generic tooth pair j in contact. In order to show that ζ_t is stationary with respect to small independent variations in the endpoint positions y_{ej}, it is necessary to show that $(\partial\zeta_t/\partial y_{ej}) = 0$ at the true values of the endpoint positions for all such endpoint positions y_{ej}. The generalized mesh force components τ and W_t are to be held fixed while carrying out these partial derivatives.

We shall let primes denote partial derivatives with respect to a single generic endpoint position y_{ej}. Forming the partial derivative of equation (6) with respect to y_{ej} gives

$$\frac{\partial\zeta_t}{\partial y_{ej}} = \frac{\left[\begin{matrix}(a_1b_2-b_1a_2)(a_1r'_b+a'_1r_b-b_1r'_a-b'_1r_a) \\ -(a_1r_b-b_1r_a)(a_1b'_2+a'_1b_2-b_1a'_2-b'_1a_2)\end{matrix}\right]}{(a_1b_2-b_1a_2)^2} \tag{5.7a}$$

$$= \frac{(a_1r'_b+a'_1r_b-b_1r'_a-b'_1r_a) - \zeta_t(a_1b'_2+a'_1b_2-b_1a'_2-b'_1a_2)}{a_1b_2 - b_1a_2} \tag{5.7b}$$

$$= \frac{a_1(r'_b-b'_2\zeta_t) - b'_1(r_a-a_2\zeta_t) - b_1(r'_a-a'_2\zeta_t) + a'_1(r_b-b_2\zeta_t)}{a_1b_2 - b_1a_2} \, , \tag{5.7c}$$

where equation (6) was used in going from equation (7a) to equation (7b). However, from equations (2) and (3) we have $r_a - a_2\zeta_t = a_1\mu$ and $r_b - b_2\zeta_t = b_1\mu$, respectively, which when combined with equation (7c) gives

$$\frac{\partial \zeta_t}{\partial y_{ej}} = \frac{a_1(r'_b - b'_2\zeta_t - b'_1\mu) - b_1(r'_a - a'_2\zeta_t - a'_1\mu)}{a_1 b_2 - b_1 a_2} . \tag{5.8}$$

From equations (3.37), (3.38), (3.36a) through (3.36o), and (3.32a) through (3.32o), it follows that the coefficients and right-hand sides of equations (2) and (3) can be expressed as

$$a_1 = \sum_j a_{1j} , \quad a_2 = \sum_j a_{2j} , \quad r_a = \tau + \sum_j \eta_{aj} \tag{5.9a,b,c}$$

and

$$b_1 = \sum_j b_{1j} , \quad b_2 = \sum_j b_{2j} , \quad r_b = W_t + \sum_j \eta_{bj} , \tag{5.10a,b,c}$$

where equations (4) and (5) have been used in equations (9c) and (10c). Each term a_{1j}, a_{2j}, η_{aj}, b_{1j}, b_{2j}, and η_{bj} in equations (9a,b,c) and (10a,b,c) is dependent on only the endjoints y_{Aj} and y_{Bj} of the single mating tooth pair j. Moreover, these six terms are independent of τ and W_t. Hence, continuing to denote partial derivatives with respect to y_{ej} by primes, we have by differentiating equations (9a,b,c) and (10a,b,c) with respect to y_{ej} while holding τ and W_t fixed,

$$a'_1 = a'_{1j}, \quad a'_2 = a'_{2j} , \quad (\partial r_a / \partial y_{ej})_\tau = \eta'_{aj} \tag{5.11a,b,c}$$

and

$$b'_1 = b'_{1j}, \quad b'_2 = b'_{2j} , \quad (\partial r_b / \partial y_{ej})_{W_t} = \eta'_{bj} , \tag{5.12a,b,c}$$

where the subscripts τ and W_t denote that these quantities have been held constant while evaluating the derivatives. Combining equations (11a,b,c) and (12a,b,c) with equation (8) gives

$$\left(\frac{\partial \zeta_t}{\partial y_{ej}}\right)_{\tau, W_t} = \frac{a_1(\eta'_{bj} - b'_{2j}\zeta_t - b'_{1j}\mu) - b_1(\eta'_{aj} - a'_{2j}\zeta_t - a'_{1j}\mu)}{a_1 b_2 - b_1 a_2} , \tag{5.13}$$

where the subscript τ, W_t on the left-hand side denotes that τ and W_t have been held constant while evaluating the partial derivative $\partial \zeta_t / \partial y_{ej}$.

From equations (3.12) and (3.10), we see that the generalized mesh force components τ and W_t can be expressed as

$$\tau = \sum_j \tau_j , \qquad W_t = \sum_j W_{tj} , \tag{5.14a,b}$$

where τ_j and W_{tj} are the components of τ and W_t, respectively, transmitted by tooth pair j. It follows from the discussion between equations (3.33) and (3.37) and equations (2), (3), (9a,b,c), (10a,b,c), and (14a,b) above that τ_j and W_{tj} can be expressed as

$$\tau_j = a_{1j}\mu + a_{2j}\zeta_t - \eta_{aj} , \tag{5.15}$$

and

$$W_{tj} = b_{1j}\mu + b_{2j}\zeta_t - \eta_{bj} , \tag{5.16}$$

which are abbreviated forms of equations (3.33) and (3.34), respectively. Forming the partial derivatives of equations (15) and (16) with respect ot y_{ej} while holding the generalized transmission error components μ and ζ_t constant gives

$$\left(\frac{\partial \tau_j}{\partial y_{ej}}\right)_{\mu,\zeta_t} = a'_{1j}\mu + a'_{2j}\zeta_t - \eta'_{aj} \tag{5.17}$$

and

$$\left(\frac{\partial W_{tj}}{\partial y_{ej}}\right)_{\mu,\zeta_t} = b'_{1j}\mu + b'_{2j}\zeta_t - \eta'_{bj} , \tag{5.18}$$

where primes denote partial derivatives with respect to y_{ej}, as before. Substituting equations (17) and (18) into equation (13), we have

$$\left(\frac{\partial \zeta_t}{\partial y_{ej}}\right)_{\tau,W_t} = -(a_1 b_2 - b_1 a_2)^{-1}\left[a_1\left(\frac{\partial W_{tj}}{\partial y_{ej}}\right)_{\mu,\zeta_t} - b_1\left(\frac{\partial \tau_j}{\partial y_{ej}}\right)_{\mu,\zeta_t}\right]. \tag{5.19}$$

From equations (3.13) and (3.16), respectively, it follows that W_{tj} and τ_j can be expressed as

$$W_{tj} = \int_{y_{Aj}}^{y_{Bj}} g_{1j}(x,y)u_{nj}(x,y)dy \tag{5.20}$$

and

$$\tau_j = r_o \int_{y_{Aj}}^{y_{Bj}} [g_{2j}(x,y) - g_{1j}(x,y)]u_{nj}(x,y)dy \ , \tag{5.21}$$

where

$$g_{1j}(x,y) \triangleq \sec\psi_b(y)K_{nj}^{(t)}(x,y)\cos[\psi_b(y) - \lambda_j(x,y)] \tag{5.22}$$

and

$$g_{2j}(x,y) \triangleq [1-(y/r_o)]K_{nj}^{(\mu)}(x,y) \ , \tag{5.23}$$

where r_o and y are defined in Fig. 3, x is defined by equation (2.6) and Fig. 3, angles $\psi_b(y)$ and $\lambda_j(x,y)$ are defined in Fig. 9, $K_{nj}^{(t)}(x,y)$ and $K_{nj}^{(\mu)}(x,y)$ are local stiffnesses of tooth pair j per unit length of line of contact defined in Appendix B, and $u_{nj}(x,y)$ is the local combined elastic deformation of the running surfaces of both teeth of tooth pair j evaluated at location y along the line of contact, as described by equation (3.1) and the accompanying text.

According to equation (19), μ and ζ_t must be held constant when evaluating the partial derivatives of the right-hand sides of equations (20) and (21). From equation (3.28), it follows that the elastic deformation $u_{nj}(x,y)$ must be treated as a constant when μ and ζ_t are held fixed. Furthermore, in the steepest descent procedure used to compute the endpoint positions y_{Aj} and y_{Bj} and the generalized transmission error components μ, ζ_t, and ζ_r, the local tooth pair stiffnesses $K_{nj}^{(t)}(x,y)$ and $K_{nj}^{(\mu)}(x,y)$ will be assumed to be independent of y_{Aj} and y_{Bj} during any descent. Forming the partial derivatives of equations (20) and (21) with respect to the general endpoint variable y_{ej} and treating $K_{nj}^{(t)}(x,y)$ and $K_{nj}^{(\mu)}(x,y)$ as independent of y_{Aj} and y_{Bj}, we thus find

$$\left(\frac{\partial W_{tj}}{\partial y_{ej}}\right)_{\mu,\zeta_t} = \pm\, g_{1j}(x,y_{ej})u_{nj}(x,y_{ej}) \tag{5.24}$$

and

$$\left(\frac{\partial \tau_j}{\partial y_{ej}}\right)_{\mu,\zeta_t} = \pm\, r_o[g_{2j}(x,y_{ej}) - g_{1j}(x,y_{ej})]u_{nj}(x,y_{ej}) \ , \tag{5.25}$$

where the upper (plus) signs apply to the case $y_{ej} = y_{Bj}$ and the lower (minus) signs apply to the case $y_{ej} = y_{Aj}$.

Finally, substituting equations (24) and (25) into equation (19), we obtain

$$\left(\frac{\partial \zeta_t}{\partial y_{ej}}\right)_{\tau,W_t} = \mp \left.\frac{a_1 g_{1j} - r_o b_1 (g_{2j} - g_{1j})}{a_1 b_2 - b_1 a_2}\right|_{y=y_{ej}} u_{nj}(x,y_{ej}) \ , \tag{5.26}$$

where the upper (minus) sign applies to the case $y_{ej} = y_{Bj}$ and the lower (plus) sign applies to the case $y_{ej} = y_{Aj}$. The quantities a_1, a_2, b_1, and b_2 are the coefficients in equations (2) and (3) which are readily determined by comparing these two equations with equations (3.37) and (3.38), respectively. The quantities g_{1j} and g_{2j} are defined by equations (22) and (23). Each of these six quantities is dependent on the endpoint value y_{ej} under consideration and is to be evaluated at that value in equation (26) as is indicated.

For a fixed rotational position of the meshing bevel gear pair designated by the variable x, as we proceed along a generic line of tooth contact j from the interior of the contact region outward in either possible direction, the composite local elastic deformation $u_{nj}(x,y)$ of the tooth pair diminishes from a positive value in the interior of the contact region to a value of zero at the boundary $y = y_{ej}$ of that region. Thus, when the local tooth pair stiffnesses $K^{(t)}_{nj}(x,y)$ and $K^{(\mu)}_{nj}(x,y)$ are considered to be independent of the endpoint positions $y = y_{Aj}$ and $y = y_{Bj}$ of the line of contact of tooth pair j, equation (26) shows that the tangential component ζ_t of the generalized transmission error is stationary with respect to small variations in the endpoint positions of the line of contact of tooth pair j about their true values when the components τ and W_t of the generalized force transmitted by the mesh are held constant while the endpoint positions are varied. Furthermore, since

equation (26) applies to any tooth pair j in contact, we have shown that ζ_t is stationary (ref. 22) with respect to small independent variations in the line of contact endpoint positions of all tooth pairs in contact.

Stationary Property of $\mu(x)$. The symmetry in the relationships leading to equation (26) enables us to write an expression for $(\partial\mu/\partial y_{ej})_{\tau,W_t}$ directly from the result (26). To see this, we note first that the derivation of equation (19) is based entirely on the relationships described by equations (2) through (5), (9a,b,c), (10a,b,c), (14a,b), (15), and (16). If the members in each of the five pairs of quantities (μ,ζ_t), (a_1,a_2), (b_1,b_2), (a_{1j},a_{2j}), and (b_{1j}, b_{2j}) are exchanged with one another, the above set of relationships remains unchanged except for some of the equation numbers. Making these same exchanges in equation (19) yields

$$\left(\frac{\partial\mu}{\partial y_{ej}}\right)_{\tau,W_t} = -(a_2b_1-b_2a_1)^{-1}\left[a_2\left(\frac{\partial W_{tj}}{\partial y_{ej}}\right)_{\zeta_t,\mu} - b_2\left(\frac{\partial\tau_j}{\partial y_{ej}}\right)_{\zeta_t,\mu}\right], \tag{5.27}$$

where the order of the quantities ζ_t and μ in the subscript ζ_t,μ is of no consequence. Furthermore, equations (20) through (25) remain unchanged when the members in each of the above-mentioned five pairs of quantities are exchanged with one another. Hence, we obtain a valid relationship by exchanging the members in each of the above five pairs of quantities in equation (26), which yields

$$\left(\frac{\partial\mu}{\partial y_{ej}}\right)_{\tau,W_t} = \mp\left.\frac{a_2g_{1j}-r_ob_2(g_{2j}-g_{1j})}{a_2b_1-b_2a_1}\right|_{y=y_{ej}} u_{nj}(x,y_{ej}), \tag{5.28}$$

where the upper (minus) sign applies to the case $y_{ej} = y_{Bj}$ and the lower (plus) sign applies to the case $y_{ej} = y_{Aj}$. It follows from equation (28) that the rotational component μ of the generalized transmission error is stationary with respect to small independent variations in the endpoint positions of the lines of contact of all tooth pairs in contact about their true values for the same reason given in the discussion of equation (26).

Stationary Property of $\zeta_r(x)$. Equation (3.39) is of the form

$$c_1\mu + c_3\zeta_r = W_r + \eta_c, \tag{5.29}$$

where ζ_r is the third component of the generalized transmission error and W_r is the third component of the generalized force transmitted by the mesh. Expressions for c_1, c_3, and η_c are obtained by comparing equation (29) with equation (3.39). Each of these three terms is an explicit function of the endpoint positions y_{Aj} and y_{Bj} of all of the tooth pairs j in contact, as one can see from equations (3.39), (3.36a) through (3.36o), and (3.32a) through (3.32o). Thus, μ and ζ_r are functions of these endpoint positions. Furthermore, from equations (2) through (5) we have seen that μ must be regarded as an implicit function of the generalized mesh force components τ and W_t. It follows then from equation (29) that ζ_r must be regarded as a function of all three mesh force components τ, W_t, and W_r.

Forming the partial derivative of equation (29) with respect to a single generic endpoint position y_{ej} while holding all three mesh force components τ, W_t, and W_r constant, we have

$$c_1\left(\frac{\partial\mu}{\partial y_{ej}}\right)_{\tau,W_t} + c_1'\mu + c_3\left(\frac{\partial\zeta_r}{\partial y_{ej}}\right)_{\tau,W_t,W_r} + c_3'\zeta_r = \eta_c' \,, \tag{5.30}$$

where primes denote partial derivatives with respect to y_{ej}, as before. Rearranging the terms in equation (30), we have

$$c_3\left(\frac{\partial\zeta_r}{\partial y_{ej}}\right)_{\tau,W_t,W_r} = -c_1\left(\frac{\partial\mu}{\partial y_{ej}}\right)_{\tau,W_t} - \left(c_1'\mu + c_3'\zeta_r - \eta_c'\right) \tag{5.31a}$$

$$= -c_1\left(\frac{\partial\mu}{\partial y_{ej}}\right)_{\tau,W_t} - \left(\frac{\partial W_r}{\partial y_{ej}}\right)_{\mu,\zeta_r} \,, \tag{5.31b}$$

where equation (29) was used in going to the second line and subscripts following parentheses in equations (30) and (31a,b) denote quantities to be treated as constants in evaluating the partial derivatives.

From equation (3.11), we see that the component W_r of the generalized mesh force can be expressed as

$$W_r = \sum_j W_{rj} \,. \tag{5.32}$$

Furthermore, from equation (3.35) it follows that W_{rj} can be expressed as

$$W_{rj} = c_{1j}\mu + c_{3j}\zeta_r - \eta_{cj} \,, \tag{5.33}$$

where by comparing equations (3.35), (3.36a) through (3.36o), and (3.39) with equations (33), (32), and (29) above, we see that

$$c_1 = \sum_j c_{1j} , \qquad c_3 = \sum_j c_{3j} , \qquad \eta_c = \sum_j \eta_{cj} , \tag{5.34a,b,c}$$

where each term c_{1j}, c_{3j}, and η_{cj} is dependent on only the endpoint positions y_{Aj} and y_{Bj} of the single tooth pair j. Hence, from equations (29) and (32) through (34c) it follows that

$$\left(\frac{\partial W_r}{\partial y_{ej}}\right)_{\mu,\zeta_r} = \left(\frac{\partial W_{rj}}{\partial y_{ej}}\right)_{\mu,\zeta_r} . \tag{5.35}$$

From equation (3.14), it follows that W_{rj} can be expressed as

$$W_{rj} = \int_{y_{Aj}}^{y_{Bj}} g_3(x,y)u_{nj}(x,y)dy , \tag{5.36}$$

where

$$g_3(x,y) \triangleq \sec\psi_b(y)K_{nj}^{(r)}(x,y)\sin[\psi_b(y) - \lambda_i(x,y)] , \tag{5.37}$$

where the local tooth pair stiffness $K_{nj}^{(r)}(x,y)$ is defined in Appendix B. Furthermore, it follows from equation (3.27) that $u_{nj}(x,y)$ is independent of y_{Aj} and y_{Bj} when μ and ζ_r are held constant. Hence, considering $K_{nj}^{(r)}(x,y)$ to be independent of y_{Aj} and y_{Bj}, it follows from equations (36) and (37) that

$$\left(\frac{\partial W_{rj}}{\partial y_{ej}}\right)_{\mu,\zeta_r} = \pm g_3(x,y_{ej})u_{nj}(x,y_{ej}) , \tag{5.38}$$

where the upper (plus) sign applies to the case $y_{ej} = y_{Bj}$ and the lower (minus) sign applies to the case $y_{ej} = y_{Aj}$.

Finally, combining equations (31b), (28), (35), and (38), we have

$$\left(\frac{\partial \zeta_r}{\partial y_{ej}}\right)_{\tau,W_t,W_r} = \pm \frac{1}{c_3}\left\{c_1\left[\frac{a_2g_{1j} - r_ob_2(g_{2j}-g_{1j})}{a_2b_1 - b_2a_1}\right] - g_3\right\}\Bigg|_{y = y_{ej}} u_{nj}(x,y_{ej}) , \tag{5.39}$$

where the upper (plus) sign applies to the case $y_{ej} = y_{Bj}$ and the lower (minus) sign applies to the case $y_{ej} = y_{Aj}$. It follows from equation (39) that the radial component ζ_r of the generalized transmission error is stationary with respect to small independent variations in the endpoint positions of the lines of tooth contact about their true values for the same reason given in the discussion of equation (26).

Minimum Property of Generalized Transmission Error Component ζ_t

In order to show that the tangential component ζ_t of the generalized transmission error takes on a minimum value when the endpoint positions y_{Aj} and y_{Bj} of the lines of contact of all tooth pairs j in contact take on their true values, it is necessary to consider the second variation (ref. 22) in ζ_t at the true values of the endpoint positions. For ζ_t to take on such a minimum it is necessary that the second variation be positive, which requires (ref. 22) in our case that

$$\left[\sum_j \sum_k \left(\frac{\partial^2 \zeta_t}{\partial y_{ej} \partial y_{ek}}\right)_{\tau, W_t} \alpha_j \alpha_k\right] > 0 \tag{5.40}$$

for all real numbers α_j and α_k subject to the condition for all j that $|\alpha_j| \leq 1$ and that $\sum_j \alpha_j^2 = 1$. In interpreting y_{ej} (or y_{ek}) here, endpoints y_{Aj} and y_{Bj} on the same tooth pair are treated as y_{ej} for two different values of j; i.e., j and k count endpoints here, two per tooth pair, not tooth pairs. The condition (40) clearly is satisfied if

$$\left(\frac{\partial^2 \zeta_t}{\partial y_{ej} \partial y_{ek}}\right)_{\tau, W_t} = 0 , \quad k \neq j \tag{5.41}$$

and

$$\left(\frac{\partial^2 \zeta_t}{\partial y_{ej}^2}\right)_{\tau, W_t} > 0 \tag{5.42}$$

for both endpoint values $y_{ej} = y_{Aj}$ and $y_{ej} = y_{Bj}$ of all tooth pairs j in contact. It is shown below that the condition (41) always is satisfied, and the condition (42) usually is satisfied and always can be satisfied by a readjustment of the parameter r_o.

Mixed Partial Derivatives of ζ_t. Equation (13) is of the form

$$\left(\frac{\partial \zeta_t}{\partial y_{ej}}\right)_{\tau, W_t} = \frac{N}{D} = D^{-1}N \ . \tag{5.43}$$

Hence,

$$\left(\frac{\partial^2 \zeta_t}{\partial y_{ej}\partial y_{ek}}\right)_{\tau, W_t} = D^{-1}\frac{\partial N}{\partial y_{ek}} - ND^{-2}\frac{2D}{\partial y_{ek}} \tag{5.44a}$$

$$= D^{-1}\left(\frac{\partial N}{\partial y_{ek}} - \frac{\partial \zeta_t}{\partial y_{ej}}\frac{\partial D}{\partial y_{ek}}\right), \tag{5.44b}$$

where equation (43) was used in proceeding from equation (44a) to equation (44b), and τ and W_t are to be treated as constants in evaluating the partial derivatives on the right-hand sides of these equations. Since from equation (26) it follows that $(\partial \zeta_t/\partial y_{ej})_{\tau, W_t} = 0$ at the true endpoint positions, it is necessary here to show only that $(\partial N/\partial y_{ek})_{\tau, W_t} = 0$, provided that $D \triangleq a_1 b_2 - b_1 a_2 \neq 0$.

Continuing to leave off the explicit notation that τ and W_t are to be held constant in forming derivatives, it follows by differentiating the numerator in the right-hand side of equation (13) with respect to y_{ek} that

$$\frac{\partial N}{\partial y_{ek}} = a_1\left(\frac{\partial^2 \eta_{bj}}{\partial y_{ej}\partial y_{ek}} - \frac{\partial b_{2j}}{\partial y_{ej}}\frac{\partial \zeta_t}{\partial y_{ek}} - \frac{\partial^2 b_{2j}}{\partial y_{ej}\partial y_{ek}}\zeta_t - \frac{\partial b_{1j}}{\partial y_{ej}}\frac{\partial \mu}{\partial y_{ek}}\right.$$

$$\left. - \frac{\partial^2 b_{1j}}{\partial y_{ej}\partial y_{ek}}\mu\right) + \frac{\partial a_1}{\partial y_{ek}}\left(\eta'_{bj} - b'_{2j}\zeta_t - b'_{1j}\mu\right)$$

$$- b_1\left(\frac{\partial^2 \eta_{aj}}{\partial y_{ej}\partial y_{ek}} - \frac{\partial a_{2j}}{\partial y_{ej}}\frac{\partial \zeta_t}{\partial y_{ek}} - \frac{\partial^2 a_{2j}}{\partial y_{ej}\partial y_{ek}}\zeta_t - \frac{\partial a_{1j}}{\partial y_{ej}}\frac{\partial \mu}{\partial y_{ek}}\right.$$

$$\left. - \frac{\partial^2 a_{1j}}{\partial y_{ej}\partial y_{ek}}\mu\right) - \frac{\partial b_1}{\partial y_{ek}}\left(\eta'_{aj} - a'_{2j}\zeta_t - a'_{1j}\mu\right) \ , \tag{5.45}$$

where we have recognized that the primes in equation (13) denote partial derivatives with respect to y_{ej}. Since the vanishing of $\partial\zeta_t/\partial y_{ej}$ and $\partial\mu/\partial y_{ej}$ at the true endpoints implied by equations (26) and (28), respectively, applies to any endpoint, we have

$$\frac{\partial\zeta_t}{\partial y_{ek}} = 0 \ , \qquad \frac{\partial\mu}{\partial y_{ek}} = 0 \tag{5.46a,b}$$

at the true endpoints. Furthermore, from the vanishing of $u_{nj}(x,y_{ej})$ at the true endpoints it follows from equations (17) and (25), and (18) and (24) that at the true endpoints we have

$$\eta'_{aj} - a'_{2j}\zeta_t - a'_{1j}\mu = 0, \qquad \eta'_{bj} - b'_{2j}\zeta_t - b'_{1j}\mu = 0 \ . \tag{5.47a,b}$$

Thus, for $\partial N/\partial y_{ek}$ to vanish for different endpoints y_{ej} and y_{ek}, it further is required only that $(\partial^2\eta_{bj}/\partial y_{ej}\partial y_{ek})$, $(\partial^2 b_{2j}/\partial y_{ej}\partial y_{ek})$, $(\partial^2 b_{1j}/\partial y_{ej}\partial y_{ek})$, $(\partial^2\eta_{aj}/\partial y_{ej}\partial y_{ek})$, $(\partial^2 a_{2j}/\partial y_{ej}\partial y_{ek})$, and $(\partial^2 a_{1j}/\partial y_{ej}\partial y_{ek})$ each vanish. Comparing equations (2), (3), (9a,b,c), and (10a,b,c) with equations (3.37), (3.38), (3.36a) through (3.36o), and (3.32a) through (3.32o), we see that each term η_{bj}, b_{2j}, b_{1j}, η_{aj}, a_{2j}, and a_{1j} is a linear combination of integrals of the general form

$$H(x;y_{Aj},y_{Bj}) \triangleq \int_{y_{Aj}}^{y_{Bj}} h(x,y)dy \ , \tag{5.48}$$

where $h(x,y)$ is independent of all endpoints y_{Aj} and y_{Bj} when $K_{nj}^{(\mu)}(x,y)$ and $K_{nj}^{(t)}(x,y)$ are regarded as independent of y_{Aj} and y_{Bj}. Hence, each term η_{bj}, b_{2j}, b_{1j}, η_{aj}, a_{2j}, and a_{1j} also is of the form of equation (48). However, differentiating equation (48) with respect to either $y_{ej} = y_{Aj}$ or $y_{ej} = y_{Bj}$, we obtain

$$\frac{\partial H}{\partial y_{ej}} = \pm h(x,y_{ej}) \ ; \tag{5.49}$$

hence, whenever $y_{ek} \neq y_{ej}$, it follows from equation (49) that

$$\frac{\partial^2 H}{\partial y_{ej}\partial y_{ek}} = 0 \ , \qquad y_{ek} \neq y_{ej} \ . \tag{5.50}$$

Therefore, whenever $y_{ek} \neq y_{ej}$, we have shown that $(\partial N/\partial y_{ek}) = 0$ at the true endpoints, and from this result and the vanishing of $\partial\zeta_t/\partial y_{ej}$ at the true endpoints it follows from equation (44b) that

$$\left(\frac{\partial^2 \zeta_t}{\partial y_{ej}\partial y_{ek}}\right)_{\tau,W_t} = 0 , \qquad y_{ek} \neq y_{ej} . \tag{5.51}$$

Equation (51) is valid at the true endpoints of the lines of contact, provided that $D = a_1b_2 - b_1a_2 \neq 0$.

Unmixed Partial Derivatives of ζ_t. If we set $y_{ek} = y_{ej}$ in equation (44), we can use that result to evaluate $(\partial^2\zeta_t/\partial y_{ej}^2)_{\tau,W_t}$. Since $(\partial\zeta_t/\partial y_{ej}) = 0$ at the true endpoints, we proceed directly to the expression (45) with $y_{ek} = y_{ej}$. Again utilizing equations (46a,b) with $y_{ek} = y_{ej}$ and equations (47a,b), we find at the true endpoints that

$$\frac{\partial N}{\partial y_{ej}} = a_1\left(\eta''_{bj} - b''_{2j}\zeta_t - b''_{1j}\mu\right) - b_1\left(\eta''_{aj} - a''_{2j}\zeta_t - a''_{1j}\mu\right) , \tag{5.52a}$$

$$= -a_1\left(\frac{\partial^2 W_{tj}}{\partial y_{ej}^2}\right)_{\mu,\zeta_t} + b_1\left(\frac{\partial^2 \tau_j}{\partial y_{ej}^2}\right)_{\mu,\zeta_t} , \tag{5.52b}$$

where equations (18) and (17) were used in proceeding to the second line. The right-hand side of equation (52a) is an explicit function of neither τ nor W_t. Differentiating equations (24) and (25) with respect to y_{ej} and evaluating the resulting expressions at the true endpoints where $u_{nj} = 0$, we obtain

$$\left(\frac{\partial^2 W_{tj}}{\partial y_{ej}^2}\right)_{\mu,\zeta_t} = \pm g_{1j}u'_{nj} , \quad \left(\frac{\partial^2 \tau_j}{\partial y_{ej}^2}\right)_{\mu,\zeta_t} = \pm r_o(g_{2j}-g_{1j})u'_{nj} , \tag{5.53a,b}$$

where the primes again denote differentiation with respect to y_{ej}. Let us define

$$A_j(x,y_{ej}) \triangleq \frac{a_1g_{1j}(x,y_{ej}) - r_ob_1[g_{2j}(x,y_{ej})-g_{1j}(x,y_{ej})]}{a_1b_2-b_1a_2} . \tag{5.54}$$

Then, substituting equations (53a,b) into equation (52b) and the resulting expression into equation (44b), and recognizing that $(\partial\zeta_t/\partial y_{ej}) = 0$ at the true endpoints and that $D \triangleq a_1b_2-b_1a_2$, we find using the definition (54) that

$$\left(\frac{\partial^2 \zeta_t}{\partial y_{ej}^2}\right)_{\tau,W_t} = \mp A_j(x,y_{ej}) \frac{\partial u_{nj}(x,y_{ej})}{\partial y_{ej}} , \tag{5.55}$$

where the upper (minus) sign applies to $y_{ej} = y_{Bj}$ and the lower (plus) sign applies to $y_{ej} = y_{Aj}$. Equation (55) is applicable only at the true endpoints y_{Aj} and y_{Bj} where the elastic deformations $u_{nj}(x,y_{ej})$ vanish. The result given by equations (54) and (55) also can be obtained formally by differentiating equation (26) with respect to y_{ej} and setting $u_{nj} = 0$ in the resulting expression.

For ζ_t to take on a minimum value at the true endpoints y_{Aj} and y_{Bj}, equation (42) must be satisfied at each true endpoint position. This criterion is readily understood if we consider the Taylor's series representation of ζ_t as a function of endpoint position y_{ej} about the true endpoint position y^0_{ej}, while holding all other endpoint positions constant. Retaining terms through the second degree in $y_{ej} - y^0_{ej}$, this representation is

$$\zeta_t = \zeta_{t0} + \zeta'_{t0}(y_{ej}-y^0_{ej}) + \frac{1}{2}\zeta''_{t0}(y_{ej}-y^0_{ej})^2 \tag{5.56a}$$

$$= \zeta_{t0} + \frac{1}{2}\zeta''_{t0}(y_{ej}-y^0_{ej})^2 , \tag{5.56b}$$

where primes denote derivatives with respect to y_{ej} while holding τ and W_t fixed, and subscripts 0 denote that ζ_t and its derivatives are evaluated at the true endpoint position y^0_{ej}. Since from equation (26) we have $\zeta'_t = \left(\partial\zeta_t/\partial y_{ej}\right)_{\tau,W_t} = 0$ at the true endpoints, the term proportional to ζ'_{t0} is missing from equation (56b). For ζ_t to increase as y_{ej} is varied in either direction about its true value y^0_{ej}, it is clear from equation (56b) that ζ''_{t0} must be positive. Hence, the condition (42) requires that the right-hand side of equation (55) be positive for every endpoint.

This requirement is readily understood with the aid of Fig. 16, which shows the behavior of the elastic deformation $u_{nj}(x,y)$ of tooth pair j near the true endpoints y_{Aj} and y_{Bj} of the line of contact. This elastic deformation is denoted by the solid lines. Let us assume, now, that the local stiffnesses $K^{(t)}_{nj}(x,y)$, $K^{(\mu)}_{nj}(x,y)$, and $K^{(r)}_{nj}(x,y)$ in equations (37), (23), and (37) are extrapolated beyond the true contact region $y_{Aj} < y < y_{Bj}$ using the stiffness values $K^{(t)}_{nj}(x,y_{ej})$, $K^{(\mu)}_{nj}(x,y_{ej})$,

and $K_{nj}^{(r)}(x,y_{ej})$ at the endpoints, $y_{ej} = y_{Aj}$ or y_{Bj}, as appropriate. Then, if the endpoints y_{Aj} or y_{Bj} used in equations (3.37) through (3.39) are chosen outside the true contact region, the equations will predict the dashed behavior of $u_{nj}(x,y)$ illustrated in Fig. 16, resulting in a prediction of tensile forces between the teeth outside the true contact region. This predicted fictitious behavior can be put to good use in determining the true endpoint positions.

Let us now use this fictitious extrapolated behavior of $u_{nj}(x,y)$ in the neighborhoods of $y = y_{Aj}$ and $y = y_{Bj}$ in our interpretation of equation (55). From Fig. 16 at $y = y_{Bj}$ we have $u'_{nj} < 0$, whereas at $y = y_{Aj}$ we have $u'_{nj} > 0$. Utilizing these signs of u'_{nj}, it follows from the sign convention of equation (55) that $(\partial^2\zeta_t/\partial y_{ej}^2)_{\tau,W_t}$ will be positive if

$$A_j(x,y_{ej}) > 0 \tag{5.57}$$

at all true endpoint positions $y_{ej} = y_{Aj}$ and $y_{ej} = y_{Bj}$, where we recall that $A_j(x,y_{ej})$ is defined by equation (54).

The requirement (57) therefore replaces the requirement (42) for ζ_t to take on a minimum. It is shown in Appendix F that the requirement (57) usually will be satisfied, and that by appropriately adjusting the value of r_o the requirement (57) always can be satisfied. In the computational procedure described next, it is assumed that $A_j(x,y_{ej}) > 0$ since this requirement always can be satisfied by an adjustment in the value of r_o.

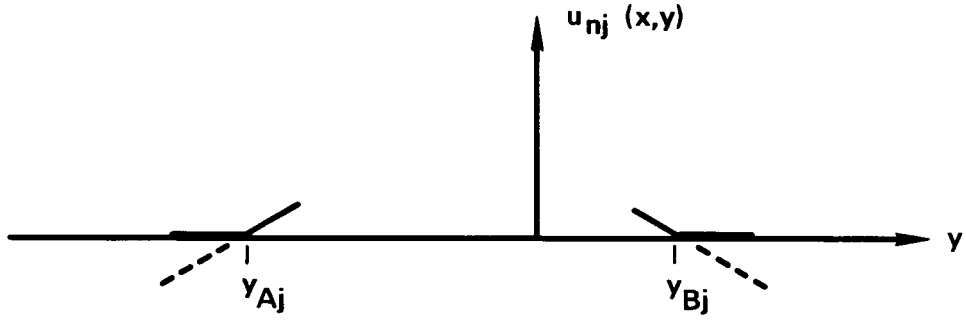

FIG. 16. PREDICTED ACTUAL (SOLID LINES) AND FICTITIOUS (DASHED LINES) LOCAL ELASTIC DEFORMATION OF TOOTH PAIR j NEAR ENDPOINTS y_{Aj} AND y_{Bj} OF LINE CONTACT OF TOOTH PAIR j.

COMPUTATIONAL PROCEDURES

A method is outlined below for numerical computation of the endpoint locations y_{Aj} and y_{Bj} of the lines of tooth contact and the generalized static transmission error components $\zeta_t(x)$ and $\mu(x)$ at a fixed rotational position of the gear pair described by $x = x_k$. The method is based on the intuitively appealing method of steepest descent (ref. 25) sometimes called the gradient method.

Line of Contact Endpoints and Generalized Transmission Error Components for a Fixed Rotational Position of the Gear Pair

The method is based on a very simple idea. For a given rotational position of the gear pair described by the value $x = x_k$, the generalized transmission error component $\zeta_t(x_k)$ is considered to be a function of the two endpoint vectors $\{y_{Aj}(x_k)\}$ and $\{y_{Bj}(x_k)\}$, where the number of elements j in each vector is the number m of tooth pairs j in contact. Thus, we can envision $\zeta_t(x_k)$ to be displayed in a space of 2m+1 dimensions as a function of the 2m variables $y_{Aj}(x_k)$, $y_{Bj}(x_k)$, $j = j_1, j_2, \ldots, j_m$.

Trial vectors $\{y_{Aj}(x_k)\}$ and $\{y_{Bj}(x_k)\}$ are chosen. A suitable choice for these trial vectors is the endpoint values $y_{Aj}(x_k)$ and $y_{Bj}(x_k)$, $j = j_1, j_2, \ldots, j_m$ determined by the geometric zone of tooth contact illustrated in Figs. 3 or 7, as appropriate. Since it was shown above that $\zeta_t(x_k)$ takes on a minimum value when the components of $\{y_{Aj}(x_k)\}$ and $\{y_{Bj}(x_k)\}$ are given their true values, a new trial set of endpoint values is computed next, where the new set is obtained by proceeding in the direction in the 2m+1 dimensional space that maximizes the rate of descent of $\zeta_t(x_k)$ from its initial trial position. This direction is the negative of the gradient of $\zeta_t(x_k)$,

$$-\nabla\zeta_t = \left(-\partial\zeta_t/\partial y_{Aj_1}, \ldots, -\partial\zeta_t/\partial y_{Aj_m}, -\partial\zeta_t/\partial y_{Bj_1}, \ldots, -\partial\zeta_t/\partial y_{Bj_m}\right). \tag{6.1}$$

The components $\partial\zeta_t/\partial y_{Aj}$ and $\partial\zeta_t/\partial y_{Bj}$, $j = j_1, \ldots, j_m$ are computed by equation (5.26), where $u_{nj}(x,y)$ is determined by equation (3.28) after employing equations (3.37) and (3.38) to compute $\zeta_t(x_k)$ and $\mu(x_k)$ for use in equation (3.28). A new pair of generalized mesh force components $W_t(x_k)$ and $\tau(x_k)$ is to be used in the determination of $\zeta_t(x_k)$ and $\mu(x_k)$ by equations (3.37) and (3.38) for each new set of components $\partial\zeta_t/\partial y_{Aj}$ and $\partial\zeta_t/\partial y_{Bj}$, $j = j_1, \ldots, j_m$ as discussed in the next subsection.

A set of 2m increments for the m values of j is computed next,

$$\delta y_{Aj}^{(i)} = -h\partial\zeta_t/\partial y_{Aj}, \qquad j = j_1,\ldots,j_m \tag{6.2a}$$

$$\delta y_{Bj}^{(i)} = -h\partial\zeta_t/\partial y_{Bj}, \qquad j = j_1,\ldots,j_m \tag{6.2b}$$

where for all values of $j = j_1,\ldots,j_m$, h is a constant chosen so as to keep increments δy_{Aj} and δy_{Bj} small in comparison with the largest of the m values of $(y_{Bj}-y_{Aj})$, $j = j_1,\ldots,j_m$. New trial endpoint vectors are then determined by

$$y_{Aj}^{(i+1)} = y_{Aj}^{(i)} + \delta y_{Aj}^{(i)}, \quad j = j_1,\ldots,j_m \tag{6.3a}$$

$$y_{Bj}^{(i+1)} = y_{Bj}^{(i)} + \delta y_{Bj}^{(i)}, \quad j = j_1,\ldots,j_m \tag{6.3b}$$

where i counts iterations. These values provide a new set of trial vectors $\{y_{Aj}^{(i+1)}(x_k)\}$ and $\{y_{Bj}^{(i+1)}(x_k)\}$ from which new values $\zeta_t^{(i+1)}(x_k)$ and $\mu^{(i+1)}(x_k)$ are computed by equations (3.37) and (3.38) using the same generalized mesh force components that were used in computing the derivatives $\partial\zeta_t/\partial y_{Aj}$ and $\partial\zeta_t/\partial y_{Bj}$ in equations (2a) and (2b), respectively.

The new value $\zeta_t^{(i+1)}(x_k)$ should be smaller than its predecessor $\zeta_t^{(i)}(x_k)$, since the negative of the gradient points downhill. If $\zeta_t^{(i+1)}(x_k) < \zeta_t^{(i)}(x_k)$, the above procedure is repeated again with the same value of h, starting with recomputation of the gradient components $\partial\zeta_t/\partial y_{Aj}$, $\partial\zeta_t/\partial y_{Bj}$, $j = j_1,\ldots,j_m$ using new values of the generalized mesh force components, as described above. This computation will result in a new value $\zeta_t^{(i+2)}(x_k)$, and so on. As long as $\zeta_t^{(i+\ell)}(x_k) < \zeta_t^{(i+\ell-1)}(x_k)$, the same value of h is used to produce each new value of $\zeta_t^{(i+\ell)}(x_k)$. However, at some iteration the newest value of $\zeta_t^{(i+\ell)}(x_k)$ will be larger than the prior value $\zeta_t^{(i+\ell-1)}(x_k)$. This will happen when the steps δy_{Aj} and δy_{Bj}, $j = j_1,\ldots,j_m$ computed by equations (2a) and (2b) overshoot the minimum value of $\zeta_t(x_k)$ in our 2m+1 dimensional space.

When the new value of $\zeta_t^{(i+\ell)}(x_k)$ exceeds $\zeta_t^{(i+\ell-1)}(x_k)$, the value of h is substantially reduced, and new values of δy_{Aj} and δy_{Bj}, $j = j_1,\ldots,j_m$ are recomputed

by equations (2a) and (2b) using the last set of already existing derivatives $\partial\zeta_t/\partial y_{Aj}$ and $\partial\zeta_t/\partial y_{Bj}$, $j = j_1,\ldots,j_m$. The iteration procedure then is continued as described above until an increase in the value of $\zeta_t^{(i+\ell)}(x_k)$ again is obtained. At this juncture, the value of h again is substantially reduced.

This procedure is continued until the absolute value of the largest of the set of 2m increments δy_{Aj} and δy_{Bj}, $j = j_1,\ldots,j_m$ that produces an increase in $\zeta_t(x_k)$ is negligible (by several orders of magnitude) in comparison with a typical value of $(y_{Bj} - y_{Aj})$. When this event occurs, the minimum value of $\zeta_t(x_k)$ in our 2m+1 dimensional space effectively has been reached.

Since both $\zeta_t(x)$ and $\mu(x)$ are required to compute $u_{nj}(x,y)$ using equation (3.28), both $\zeta_t(x_k)$ and $\mu(x_k)$ are available at the termination of the above procedure. The values $\zeta_t(x_k)$, $\mu(x_k)$, and the final endpoint vectors $\{y_{Aj}(x_k)\}$ and $\{y_{Bj}(x_k)\}$, $j = j_1,\ldots,j_m$ are to be stored. The third generalized transmission error component $\zeta_r(x_k)$ can be computed from the final endpoint values and $\mu(x_k)$ using equation (3.39). The resulting triad of transmission error components $\mu(x_k)$, $\zeta_t(x_k)$, and $\zeta_r(x_k)$ is the generalized static transmission error evaluated at the rotational position of the gear pair described by $x = x_k$.

When the above procedure is started, care must be taken to insure that the set $j = j_1,\ldots,j_m$ includes all tooth pairs in potential contact. At each iteration, however, there is no guarantee that the new set of endpoints computed by equations (3a) and (3b) will satisfy

$$y_{Bj}^{(i+1)} > y_{Aj}^{(i+1)}, \qquad j = j_1,\ldots,j_m . \tag{6.4}$$

For each value of j not satisfying equation (4), one must set $y_{Bj}^{(i+1)} = y_{Aj}^{(i+1)}$ in the remainder of that iteration, thereby eliminating those lines of tooth contact in the computation of $\zeta_t^{(i+1)}(x_k)$ and $\mu^{(i+1)}(x_k)$.

In related problems, we have found the above-described gradient descent to work very well. It requires a minimum computer programming effort.

Generalized Mesh Force Components

For the same rotational position of the gear pair described by $x = x_k$, the generalized mesh force components $W_t^{(i)}(x_k)$ and $\tau^{(i)}(x_k)$ are required for computation

of $\zeta_t^{(i)}(x_k)$ and $\mu^{(i)}(x_k)$ by equations (3.37) and (3.38) using the endpoint vectors $\{y_{Aj}^{(i)}(x_k)\}$ and $\{y_{Bj}^{(i)}(x_k)\}$, $j = j_1,\ldots,j_m$ as described above. These generalized force components are to be computed using equations (4.24) and (4.19). However, the coefficient matrices $\mathbf{K}(x)$ and $\eta_{\mathbf{K}}(x)$ in equation (4.24), which also appear in the matrix form (3.40) of equations (3.37) through (3.39), depend on the endpoint vectors $\{y_{Aj}^{(i)}(x)\}$, $\{y_{Bj}^{(i)}(x)\}$, $j = j_1,\ldots,j_m$. Hence, generalized mesh force components $W_t^{(i)}(x_k)$ and $\tau^{(i)}(x_k)$ computed using the endpoint vectors $\{y_{Aj}^{(i)}(x_k)\}$ and $\{y_{Bj}^{(i)}(x_k)\}$ should be employed in the above-described gradient descent procedure.

The sequence of steps involved in the iterative portion of the procedure for computing the line of contact endpoints and generalized transmission error components for a given rotational position $x = x_k$ of the gear pair is listed below:

A. Initial trial endpoint set $\{y_{Aj}^{(i)}\}$, $\{y_{Bj}^{(i)}\}$, $j = j_1,\ldots,j_m$.

B. Compute $W_t^{(i)}$ and $\tau^{(i)}$ with equations (4.24) and (4.19) using line of contact endpoints $\{y_{Aj}^{(i)}\}$, $\{y_{Bj}^{(i)}\}$.

C. Compute $\zeta_t^{(i)}$, $\mu^{(i)}$, and $u_{nj}^{(i)}$ at endpoints with equations (3.37), (3.38), and (3.28) using endpoints $\{y_{Aj}^{(i)}\}$, $\{y_{Bj}^{(i)}\}$.

D. Compute $\partial\zeta_t/\partial y_{Aj}$ and $\partial\zeta_t/\partial y_{Bj}$, $j = j_1,\ldots,j_m$ with equation (5.26) using endpoints $\{y_{Aj}^{(i)}\}$, $\{y_{Bj}^{(i)}\}$.

E. Compute new endpoint values $\{y_{Aj}^{(i+1)}\}$, $\{y_{Bj}^{(i+1)}\}$, $j = j_1,\ldots,j_m$ with equations (2a,b) and (3a,b) above.

F. Test: Is $y_{Bj}^{(i+1)} > y_{Aj}^{(i+1)}$, $j = j_1,\ldots,j_m$. If not, set $y_{Bj}^{(i+1)} = y_{Aj}^{(i+1)}$.

G. Compute $\zeta_t^{(i+1)}$ and $\mu^{(i+1)}$ with equations (3.37) and (3.38) using new endpoint values $\{y_{Aj}^{(i+1)}\}$, $\{y_{Bj}^{(i+1)}\}$, $j = j_1,\ldots,j_m$ and values of $W_t^{(i)}$ and $\tau^{(i)}$ computed in step B.

H. Test: Is $\zeta_t^{(i+1)} < \zeta_t^{(i)}$. If yes, delete $\zeta_t^{(i+1)}$, $\mu^{(i+1)}$; increase index i by one and proceed to step B. If no, delete $\zeta_t^{(i+1)}$, $\mu^{(i+1)}$ and test maximum increment magnitude $\left|\delta y_{Aj}^{(i)}\right|$ or $\left|\delta y_{Bj}^{(i)}\right|$ scanned over all $j = j_1,\ldots,j_m$, where $\delta y_{Aj}^{(i)}$ and $\delta y_{Bj}^{(i)}$, $j = j_1,\ldots,j_m$ are those values used in step E. If maximum increment magnitude is negligible (several orders of magnitude) in comparison with typical interval $\left(y_{Bj}^{(i+1)} - y_{Aj}^{(i+1)}\right)$, effective minimum value of $\zeta_t = \zeta_t^{(i)}$ has been achieved. If maximum increment magnitude is not negligible, substantially reduce h and proceed to step E.

Comment: Notice that the comparison test "Is $\zeta_t^{(i+1)} < \zeta_t^{(i)}$." always is made with values of $\zeta_t^{(i+1)}$ and $\zeta_t^{(i)}$ having been computed using the same pair of generalized mesh force components $W_t^{(i)}$ and $\tau^{(i)}$ since minimum property of true value of ζ_t was proved under assumption of constant mesh force components W_t and τ.

Generalized Transmission Error Components and their Spectra

The above procedure generates the generalized static transmission error components $\mu(x)$, $\zeta_t(x)$, and $\zeta_r(x)$ at a single rotational position of the gear pair described by $x = x_k$. By repeating this procedure at an equispaced sequence of values of x_k, the generalized transmission error components (and lines of tooth contact endpoints) are determined as functions of the rotational position of the gears.

If the elastic properties and running surface modifications from perfect equispaced spherical involute surfaces are the same for every tooth on each gear of the gear pair, then the generalized static transmission error components $\mu(x)$, $\zeta_t(x)$, and $\zeta_r(x)$ each is a periodic function of x with period Δ equal to the tooth spacing interval in x (Fig. 3). Thus, minimum definitions of $\mu(x)$, $\zeta_t(x)$, and $\zeta_r(x)$ as functions of x would require the above described procedure to be caried out at about 8 points with spacing in x of $\Delta/8$. An optimum method of interpolating between such equispaced transmission error component computations is described below.

A representation of the transmission error in the frequency domain (refs. 7-9) often is of primary interest. Such a representation can be obtained from the transmission error computed at equispaced intervals using the method of trigonometric

interpolation (ref. 31). Let us denote a generic component $\mu(x)$, $\zeta_t(x)$, or $\zeta_r(x)$ by $\zeta(x)$. Assume that $\zeta(x)$ is periodic with period Δ, as noted above, and that $\zeta(x)$ has been computed at 2n equispaced points x_k, where the spacing between adjacent points is

$$x_k - x_{k-1} = \frac{\Delta}{2n} . \tag{6.5}$$

Let the 2n points x_k at which $\zeta(x_k)$ has been computed be numbered k = -n, -(n-1),...,0,...,n-1. Since $\zeta(x)$ is periodic with period Δ, the value of a 2n+1 st point k = n is provided by the point at k = -n; i.e.,

$$x_n = x_{-n} . \tag{6.6}$$

Let x' denote the independent variable in Lanczos' (ref. 31) treatment of trigonometric interpolation. The period of the periodic function there has been normalized to the interval $[-\pi,\pi]$. To change the interval $[-\pi,\pi]$ to the period Δ in x of our independent variable, we require the transformation

$$x' = 2\pi x/\Delta . \tag{6.7}$$

Incorporating equation (7) into Lanczos' (ref. 31) trigonometric interpolation formula (4-11.24) gives

$$\zeta(x) = \sum_{p=-n}^{n}{}' \alpha_p \exp(i2\pi px/\Delta) , \tag{6.8}$$

where the expansion coefficients α_p are provided by Lanczos' formula (4-11.25),

$$\alpha_p = \frac{1}{2n} \sum_{k=-n}^{n}{}' \zeta(x_k)\exp(-i2\pi px_k/\Delta) , \tag{6.9}$$

where obvious changes in notation have been used. The prime in equation (8) designates (ref. 31) that the two limiting terms α_{-n} and α_n are to be weighted by 1/2 in the summation; similarly, the prime in equation (9) designates that $\zeta(x_{-n})$ and $\zeta(x_n)$ are to be weighted by 1/2 in that summation.

The prime in equation (8) is absent from the corresponding equation (4-11.24) in reference 31. However, the validity of the interpolation formula (8) readily can

be established by substituting equation (9) into equation (8), interchanging the order of summation, and then utilizing equation (4-11.17) of reference 31. Particular attention must be paid to the case where equation (8) is used at $x = x_{-n}$ or $x = x_n$. It follows that the interpolation formula is valid at these endpoints only if $\zeta(x_{-n}) = \zeta(x_n)$, which is satisfied in our application since $\zeta(x)$ is periodic with period Δ. By substituting Lanczos' equation (4-11.20) into his equation (4-11.22), one can see that Lanczos' equation (4-11.22) is not valid for $|j-k| = 2n$. This same conclusion can be reached by using L'Hopital's rule on the right-hand side of Lanczos' equation (4-11.17). Nevertheless, with the prime included, we have shown that equation (8) is an <u>exact</u> interpolation formula when the α_p are computed by equation (9), provided that $\zeta(x_{-n}) = \zeta(x_n)$, which is satisfied in our application.

Equation (8) is identical to the complex Fourier series representation of the transmission error component $\zeta(x)$ (ref. 7, equation (64)) except that (tooth meshing) harmonics p only through order n are included in the representation (8). Thus, from equation (8), we see that the coefficients α_p, $|p| = 0,1,\ldots,n-1$ generated from computations of $\zeta(x_k)$ at the 2n equispaced points x_k, $k = -n,-(n-1),\ldots,0,\ldots,(n-1)$ can be directly interpreted as (approximations to) the complex Fourier series coefficients of the transmission error component $\zeta(x)$. Because of the prime on equation (8), the coefficients α_{-n} and α_n generated by equation (9) ($p = \pm n$) must be divided by 2 to be interpreted as Fourier series coefficients.

The coefficients α_p generated by equation (9) can contain contributions from high-order harmonics $|p| > n$ "impersonating" the lower-order harmonics $|p| \leq n$ (ref. 32, Fig. 8). Such aliasing contamination of the coefficients α_p can be minimized by choosing the number 2n of equispaced points at which $\zeta(x_k)$ is computed to be substantially larger than twice the number of accurately desired harmonics $|p|$.

Conclusion

It has been shown that the traditional definition of the one-component transmission error is unsuitable for accurately characterizing the vibratory excitation arising from meshing pairs of spiral bevel gears. A three-component generalized transmission error definition was introduced that is made up of two orthogonal translational components and one rotational component of relative displacement of the gears with respect to their perfect spherical involute counterparts. All displacements that contribute to these three transmission error components take place in the plane of tooth contact. A transformation of coordinates, equations (2.10) through (2.13), was derived that relates the three generalized transmission error components to the six degree-of-freedom deviations in the positions of the gear shaft centerlines from the positions occupied by their perfect spherical involute counterparts. The methodology is applicable to bevel gear pairs whose actual surface of tooth contact is reasonably well approximated by a plane surface passing through the point occupied by the apexes of the two pitch cones of the mating gears.

In the absence of friction, the forces transmitted by the meshing teeth can be characterized by two orthogonal force components in the plane of tooth contact and one torque component, where the vector describing this torque component is normal to the plane of contact. Equations were derived that relate the three generalized transmission error components to the above-mentioned three generalized mesh force components [equations (3.37) through (3.39)]. These equations include contributions to the transmission error components arising from elastic deformations of the teeth and gear bodies, and contributions from deviations of the running surfaces of the teeth from equispaced perfect spherical involute surfaces. A method was described for incorporating these equations into the equations of motion of a gear system.

When the inertial forces of a meshing gear pair and bearing supports are ignored, the three generalized mesh force components are determined by the tooth/gearbody stiffnesses, deviations of the tooth running surfaces from equispaced perfect spherical involute surfaces, gearshaft bearing support flexibilities, deviations of the bearing centerlines from the positions occupied by the shaft centerlines of rigid perfect spherical involute gears, and the shaft input torque. Equations were derived providing the three generalized mesh force components in terms of the above-described quantities [equations (4.24) and (4.19)]. The three

components of the generalized static transmission error are predicted by equations (3.37) through (3.39) or equation (3.44) when the generalized force components provided by equations (4.24) and (4.19) are used in their evaluation.

Finally, a method was developed for computing the positions of the endpoints of the lines of tooth contact in the plane of contact. These endpoint positions are needed for evaluation of integrals that are required to evaluate coefficients in the above-mentioned equations. The computational procedure developed in the last section provides the three components of the generalized static transmission error at a set of equispaced points taken over one tooth spacing period of the rotational positions of the gears. Equations (6.8) and (6.9) may be employed to provide a smooth interpolation between such points for each of the three generalized transmission error components. When the running surfaces and stiffnesses of all teeth on each gear of a meshing pair are the same, equation (6.9) may be used to provide the Fourier series coefficients of the tooth meshing harmonics of each of the three generalized transmission error components.

APPENDIX A

DERIVATION OF EXPRESSION FOR GENERALIZED TRANSMISSION ERROR IN TERMS OF GEAR DISPLACEMENTS AT SHAFT CENTERLINES

We first express the gear body shaft centerline translations $x_1^{(\cdot)}$, $x_2^{(\cdot)}$, $x_3^{(\cdot)}$ in the y_1, y_2, y_3 coordinates shown in Fig. 6. The y coordinates are obtained by a rotation about the $x_1^{(\cdot)}$ axis through the angle $\gamma_b^{(\cdot)}$. The common plane of the $x_2^{(\cdot)}$, $x_3^{(\cdot)}$, y_2, and y_3 axes is shown in Fig. 17(a), from which it follows directly that

$$\begin{aligned} y_1 &= x_1 \\ y_2 &= x_2\cos\gamma_b - x_3\sin\gamma_b \\ y_3 &= x_2\sin\gamma_b + x_3\cos\gamma_b \end{aligned} \tag{A1}$$

or in matrix notion,

$$\begin{Bmatrix} y_1 \\ y_2 \\ y_3 \end{Bmatrix} = \begin{bmatrix} 1 & 0 & 0 \\ 0 & \cos\gamma_b & -\sin\gamma_b \\ 0 & \sin\gamma_b & \cos\gamma_b \end{bmatrix} \begin{Bmatrix} x_1 \\ x_2 \\ x_3 \end{Bmatrix} , \tag{A2}$$

where the first line in equation (A1) is a consequence of the fact that the rotation was taken about the $x_1^{(\cdot)}$ axis as indicated in Fig. 6, and where the superscripts $(\cdot)$ have been left off. Next, we express the y_1, y_2, y_3 coordinates in terms of the z_1, z_2, z_3 coordinates shown in Fig. 6. The z coordinates are obtained by a rotation about the y_2 axis through the angle $\nu^{(\cdot)}$. The common plane of the y_1, y_3, z_1, and z_3 axes is shown in Fig. 17(b), from which it follows that

$$\begin{aligned} z_1 &= y_1\cos\nu + y_3\sin\nu \\ z_2 &= y_2 \\ z_3 &= -y_1\sin\nu + y_3\cos\nu \end{aligned} \tag{A3}$$

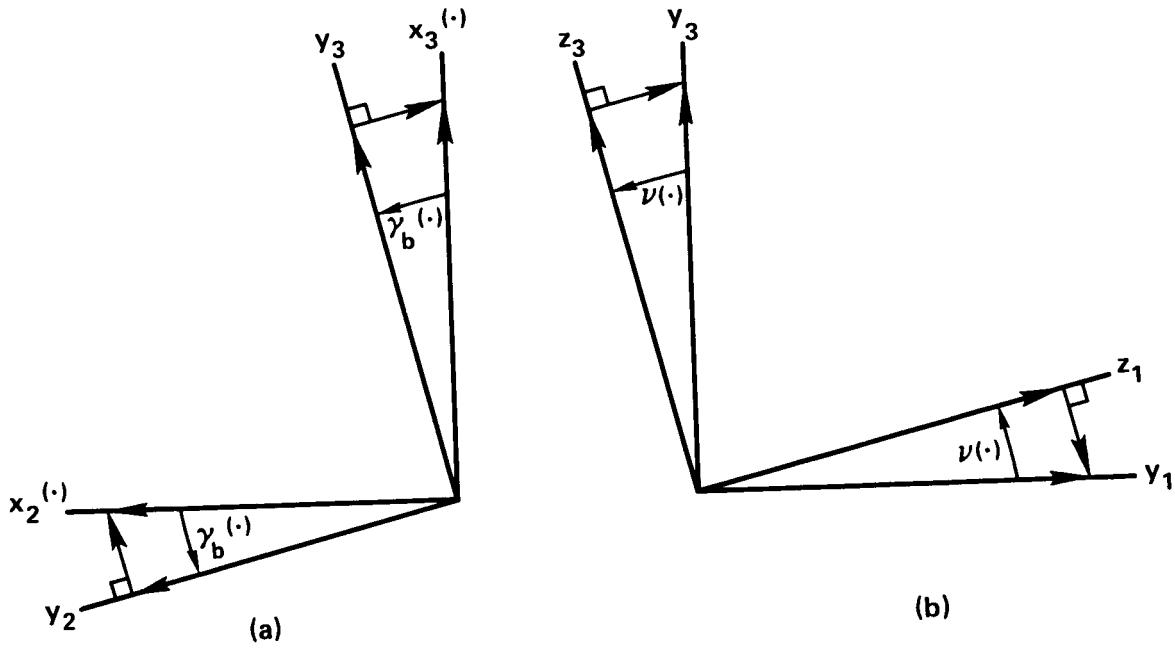

FIG. 17. (a) RESOLVING $x_2^{(\cdot)}$ AND $x_3^{(\cdot)}$ INTO y_2 AND y_3 COMPONENTS.
(b) RESOLVING y_1 AND y_3 INTO z_1 AND z_3 COMPONENTS.

or

$$\begin{Bmatrix} z_1 \\ z_2 \\ z_3 \end{Bmatrix} = \begin{bmatrix} \cos\nu & 0 & \sin\nu \\ 0 & 1 & 0 \\ -\sin\nu & 0 & \cos\nu \end{bmatrix} \begin{Bmatrix} y_1 \\ y_2 \\ y_3 \end{Bmatrix} . \tag{A4}$$

Substituting equation (A2) into the right-hand side of equation (A4) and multiplying the two coefficient matrices yields

$$\begin{Bmatrix} z_1 \\ z_2 \\ z_3 \end{Bmatrix} = \begin{bmatrix} c\nu & s\gamma_b s\nu & c\gamma_b s\nu \\ 0 & c\gamma_b & -s\gamma_b \\ -s\nu & s\gamma_b c\nu & c\gamma_b c\nu \end{bmatrix} \begin{Bmatrix} x_1 \\ x_2 \\ x_3 \end{Bmatrix} , \tag{A5}$$

where the cosine and sine operators have been abbreviated by c ans s respectively (ref. 18, p. 106).

We are concerned with the four possible gear pair configurations listed in Table 1. The configuration represented by the first full line in Table 1 is illustrated in Fig. 3. When gear (2) in Fig. 3 becomes the driver and its direction of rotation is changed from counterclockwise to clockwise, the plane of contact and lines of contact shown in Fig. 3 also apply to this configuration, which is represented by the second full line in Table 1. Thus, in the configurations described by the first two full lines in Table 1, gear (1) in Fig. 3 is represented by the first column in Table 1 entitled "upper sign" and gear (2) in Fig. 3 is represented by the second column entitled "lower sign." Furthermore, the base cone and plane of contact configurations of both gears shown in Fig. 3 are represented by Fig. 6 which, when upright, represents gear (1) and, when upside down, represents gear (2).

From Fig. 6, we can see that gear body translations in the positive z_1 direction are "equivalent" to the addition of material to the running surfaces of perfect involute teeth. Hence, for gears (1) and (2), positive contributions to z_1 are equivalent to negative contributions to the ζ_t component of the generalized transmission error - compare Figs. 5 and 6. It follows from equations (2.10) through (2.13) that the last three elements in the middle row of the right-hand side of equation (2.13) are the negative values of the three elements in the top row of the

coefficient matrix in the right-hand side of equation (A5). Since gear body translations in the z_2 direction are normal to the plane of contact, the middle row of the coefficient matrix in equation (A5) contributes nothing to the generalized transmission error.

From Figs. 5 and 6, we can see that gear body translations in the z_3 direction provide the contributions to ζ_r. A careful examination of Figs. 3 and 6 shows that in the case of gear (1) gear body translations in the positive z_3 direction are equivalent to the addition of material to the running surfaces of the teeth on gear (1); hence, in the case of gear (1) positive contributions to z_3 are equivalent to negative contributions to the ζ_r component of the generatized transmission error. It follows from this fact and equations (2.10) through (2.13) that in the case of gear (1) the last three elements in the third row of the right-hand side of equation (2.13) are the negative values of the three elements in the bottom row of the coefficient matrix in equation (A5). Further careful examination of Figs. 3 and 6 shows that translations of the body of gear (2) in the positive z_3 direction are equivalent to the removal of material from the running surfaces of the teeth on gear (2); hence, in the case of gear (2) positive contributions to z_3 are equivalent to positive contributions to ζ_r. Thus, in the case of gear (2) the last three elements in the third row of the right-hand side of equation (2.13) are the same as the values of the three elements in the bottom row of the coefficient matrix in equation (A5). These facts establish the sign conventions given by the first two full lines in Table 1.

The sign conventions given by the last two full lines in Table 1 are established in a similar manner with the aid of Figs. 7 and 8. The counterpart to Fig. 6 in these considerations is shown in Fig. 8 which is the mirror image of Fig. 6 - i.e., the figure seen by looking through Fig. 6 from its backside. From this fact, it follows that equation (A5) also is valid for the gearing configuration shown in Fig. 7. Consequently, the sign conventions given by the last two full lines in Table 1 can be derived from equation (A5) and Figs. 7 and 8. Furthermore, from the applicability of Fig. 8 to the configurations described by the last two full lines in Table 1 it follows from equation (A5) that the last three elements in the second row of the right-hand side of equation (2.13) also are applicable to the configurations described by the last two full lines in Table 1.

We turn now to the four nonzero elements in the upper left-hand corner of the matrix in equation (2.13). From equations (2.10) through (2.13), we see that the two nonzero elements in the first row represent the coefficients of $\rho_2^{(\cdot)}$ and $\rho_3^{(\cdot)}$, respectively, in their contributions to $\mu(x)$. Taking into account the sign convention for $\mu(x)$ illustrated in Fig. 5, we can readily see from Figs. 6 and 18 that the contribution to $\mu(x)$ from gear $(\cdot)$ is $\rho_2^{(\cdot)} \cos\gamma_b^{(\cdot)} - \rho_3^{(\cdot)} \sin\gamma_b^{(\cdot)}$, from which the first row of the matrix in equation (2.13) follows directly. The first two nonzero elements in the second row of the matrix in equation (2.13) represent the contributions of these rotation components to ζ_t that arise from the shift of the origin through the distance r_o from cone apex to the point $\underline{0}$ on the zone of contact centerline shown in Fig. 6. The signs of these two elements are a consequence of the sign convection illustrated in Fig. 5.

A similar analysis of Fig. 8, which applies to the gearing configuration shown in Fig. 7 and to the last two full rows in Table 1, shows that the four nonzero elements in the upper left-hand corner of the matrix in equation (2.13) also apply to the configurations described by the last two full rows in Table 1.

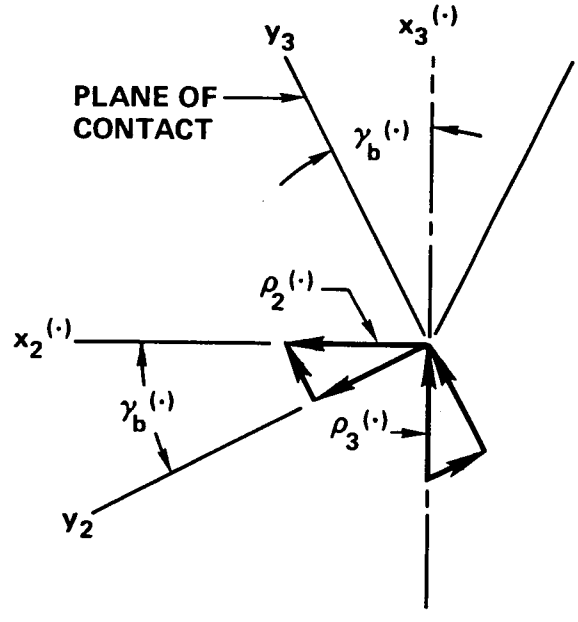

FIG. 18. RESOLVING (SMALL) ROTATION VECTORS $\rho_2^{(\cdot)}$ AND $\rho_3^{(\cdot)}$ INTO COMPONENTS PERPENDICULAR AND PARALLEL TO THE PLANE OF CONTACT. THE PLANE OF THE PAPER CONTAINS THE $x_2^{(\cdot)}$, $x_3^{(\cdot)}$, y_2 AND y_3 AXES SHOWN IN FIG. 6.

C-2

APPENDIX B

DEFINITIONS AND INTEGRAL EQUATIONS FOR LOCAL TOOTH-PAIR STIFFNESSES $K_{nj}^{(\cdot)}(x,y)$

Let $k_j(\nu,\nu';x)$ denote the composite deformation from both teeth at a point ν on the line of contact of tooth pair j due to a unit force applied at point ν' on the line of contact, where force and deformation both are measured in a direction normal to the tooth surfaces and, therefore, in the plane of contact, and x denotes the position of the zone of contact as described by equation (2.8). The influence function $k_j(\nu,\nu';x)$ is assumed to include bending, shear, and Hertzian deformation components of both meshing teeth, as well as the components arising from deformations of the bodies of both meshing gears. The unit force used to define $k_j(\nu,\nu';x)$ is assumed to be applied with uniform intensity to a circular area of diameter equal to the width of the contact line between the two gear teeth. Since the Hertzian deformation component of real teeth is a (weakly) nonlinear function of loading because of dependence of the width of the contact line on loading, specification of the area of applied force implies that our influence function is defined for a given nominal loading condition. The deformation $u_j'(\nu;x)$ at point ν caused by a lineal force density $p_j(\nu';x)$, where ν and ν' are on the line of contact, can be expressed in terms of $k_j(\nu,\nu';x)$ by the line integral

$$u_j'(\nu;x) = \int k_j(\nu,\nu';x)p_j(\nu';x)d\nu' , \tag{B1}$$

where $d\nu'$ denotes differential distance measured along the line of contact and where the integral is taken over the portion of the line of contact contained in the zone of contact.

Equation (B1) may be regarded as a Fredholm integral equation of the first kind for the lineal force density $p_j(\nu';x)$. We may formally invert (ref. 23, pp. 4-9, 351-352) equation (B1) to yield

$$p_j(\nu;x) = \int k_j^{-1}(\nu,\nu';x)u_j'(\nu';x)d\nu' , \tag{B2}$$

where $k_j^{-1}(\nu,\nu';x)$ is the inverse of $k_j(\nu,\nu';x)$.

We shall consider $K_{nj}^{(t)}(x,y)$ first. The differential force increments dW_{nj} normal to the line of contact are related to the force density $p_j(\nu;x)$ by

$$dW_{nj} = p_j(\nu;x)d\nu \ . \tag{B3}$$

From equations (3.5), (3.7), and (B3) we can express the contribution from tooth pair j to the total tangential force W_t illustrated in Fig. 4 by

$$W_{tj}(x) = \int_{\nu} \cos[\psi_b(y_\nu)-\lambda_j(x,y_\nu)]p_j(\nu;x)d\nu \ , \tag{B4}$$

where y_ν is an abbreviation for the coordinate y illustrated in Figs. 3 to 5 expressed as a function of distance ν measured <u>along</u> the line of contact of tooth pair j. From equation (3.3), we have

$$d\nu = \sec\psi_b(y)dy \ ; \tag{B5}$$

hence, ν can be expressed as a function of y by the indefinite integral

$$\nu_y = \int \sec\psi_b(y)dy + C \ , \tag{B6}$$

where C might be chosen by requiring ν_y to be zero at y = 0. For a given value of zone of contact position x, it is obvious from Figs. 3 to 5 that the function $\nu_y = \nu(y)$ also determines the inverse function $y_\nu = y(\nu)$ which is the function used in equation (B4).

Inserting equation (B2) into equation (B4) and using $d\nu' = \sec\psi_b(y)dy$ from equation (B5), we have

$$W_{tj}(x) = \int_{\nu} \cos[\psi_b(y_\nu)-\lambda_j(x,y_\nu)] \int_{\nu'} k_j^{-1}(\nu,\nu';x)u_j'(\nu';x)d\nu'd\nu$$

$$= \int_{\nu'} \{ \int_{\nu} \cos[\psi_b(y_\nu)-\lambda_j(x,y_\nu)]k_j^{-1}(\nu,\nu';x)d\nu \} \ u_j'(\nu';x)d\nu'$$

$$= \int_{y_A}^{y_B} \sec\psi_b(y) \ \{ \int_{\nu} \cos[\psi_b(y_\nu)-\lambda_j(x,y_\nu)]k_j^{-1}(\nu,\nu_y';x)d\nu \}$$

$$\times \ u_j'(\nu_y';x)dy \ , \tag{B7}$$

where in the last line we have considered ν' to be the function of y determined by equation (B6). Since $u'_j(\nu'_y;x)$ and $u_{nj}(x,y)$ both are measured normal to the line of contact, we have

$$u'_j(\nu'_y;x) = u_{nj}(x,y); \tag{B8}$$

hence, requiring that equations (3.13) and (B7) represent identical expressions for arbitrary deformations $u_{nj}(x,y)$, we must have

$$K^{(t)}_{nj}(x,y) \triangleq \{\cos[\psi_b(y)-\lambda_j(x,y)]\}^{-1} \int_\nu \cos[\psi_b(y_\nu)-\lambda_j(x,y_\nu)]k^{-1}_j(\nu,\nu'_y;x)d\nu \ , \tag{B9}$$

which is the definition of the local tooth-pair stiffness $K^{(t)}_{nj}(x,y)$ per unit length of line of contact. The integral with respect to ν in equation (B9) is taken over the full length of line of contact of tooth pair j at zone of contact position x.

It is not necessary to determine the inverse influence function $k^{-1}_j(\nu,\nu';x)$ in order to evaluate the local tooth-pair stiffness $K^{(t)}_{nj}(x,y)$. The symmetry of the influence function $k_j(\nu,\nu';x)$ (Maxwell's reciprocal theorem) implies that $k^{-1}_j(\nu,\nu';x)$ possesses the same symmetry [23, p. 9] - i.e.,

$$k^{-1}_j(\nu,\nu';x) = k^{-1}_j(\nu',\nu;x) \ . \tag{B10}$$

Utilizing the property (B10) in equation (B9) yields

$$\cos[\psi_b(y)-\lambda_j(x,y)]K^{(t)}_{nj}(x,y) = \int_\nu k^{-1}_j(\nu'_y,\nu;x)\cos[\psi_b(y_\nu)-\lambda_j(x,y_\nu)]d\nu \ , \tag{B11}$$

which is of the same general form as equation (B2). Let us define

$$\bar{u}'_{tj}(\nu;x) \triangleq \cos[\psi_b(y_\nu)-\lambda_j(x,y_\nu)] \tag{B12}$$

and

$$\bar{p}_{tj}(\nu'_y;x) \triangleq \cos[\psi_b(y)-\lambda_j(x,y)]K^{(t)}_{nj}(x,y) \ , \tag{B13}$$

which, according to equations (B2) and (B11), are a deformation/force density pair that satisfy equations (B1) and (B2). It follows, then, from equation (B1) that the solution $p_j(\nu'_y;x) = \bar{p}_{tj}(\nu'_y;x)$ to the integral equation (B1) with left-hand side $u'_j(\nu;x) = \bar{u}'_{tj}(\nu;x)$ given by equation (B12) yields the local tooth-pair stiffness

$$K_{nj}^{(t)}(x,y) = \sec[\psi_b(y)-\lambda_j(x,y)]\ \bar{p}_{tj}(\nu_y';x)\ , \tag{B14}$$

where the function $\nu_y' = \nu'(y)$ is determined by equation (B6).

The situation with regard to the local tooth-pair stiffness $K_{nj}^{(r)}(x,y)$ associated with the radial force component $W_{rj}(x)$ is completely analogous to that above for $K_{nj}^{(t)}(x,y)$. Using equations (3.6), (3.8), (3.14), and (B3), we obtain in this case, instead of equation (B9), the definition

$$K_{nj}^{(r)}(x,y) \triangleq \{\sin[\psi_b(y)-\lambda_j(x,y)]\}^{-1} \int_\nu \sin[\psi_b(y_\nu)-\lambda_j(x,y_\nu)]\bar{k}_j^{-1}(\nu,\nu_y';x)d\nu\ . \tag{B15}$$

The local tooth-pair stiffness $K_{nj}^{(r)}(x,y)$ can be obtained from the solution $p_j(\nu_y';x) = \bar{p}_{rj}(\nu_y';x)$ of the integral equation (B1) using for its left-hand side $u_j'(\nu;x) = \bar{u}_{rj}'(\nu;x)$ where

$$\bar{u}_{rj}'(\nu;x) \triangleq \sin[\psi_b(y_\nu)-\lambda_j(x,y_\nu)] \tag{B16}$$

and

$$\bar{p}_{rj}(\nu_y';x) \triangleq \sin[\psi_b(y)-\lambda_j(x,y)]K_{nj}^{(r)}(x,y) \tag{B17}$$

from which one obtains $K_{nj}^{(r)}(x,y)$ by

$$K_{nj}^{(r)}(x,y) = \csc[\psi_b(y)-\lambda_j(x,y)]\bar{p}_{rj}(\nu_y';x)\ , \tag{B18}$$

where the function $\nu_y' = \nu'(y)$ is determined by equation (B6).

The situation with regard to the local tooth-pair stiffness $K_{nj}^{(u)}(x,y)$ appearing in equation (3.16) is slightly more complicated. Inserting equation (B3) into equation (3.9) and then equation (B2) into the resulting expression yields

$$\begin{aligned}\tau_j(x) &= -\int_\nu h(x,y_\nu)\int_{\nu'} \bar{k}_j^{-1}(\nu,\nu';x)u_j'(\nu';x)d\nu'd\nu \\ &= -\int_{\nu'}\Big[\int_\nu h(x,y_\nu)k_j^{-1}(\nu,\nu';x)d\nu\Big]u_j'(\nu';x)d\nu' \\ &= -\int_{y_A}^{y_B}\sec\psi_b(y)\Big[\int_\nu h(x,y_\nu)\bar{k}_j^{-1}(\nu,\nu_y';x)d\nu\Big]u_{nj}(x,y)dy\ ,\end{aligned} \tag{B19}$$

where, in the first line the original integral over y in equation (3.9) has been transformed into an integral over ν, and in the last line the integral over ν' in the second line has been transformed into an integral over y and equations (B5) and (B8) have been used. Substituting equation (3.15) into equation (B19) yields

$$\tau_j(x) = -r_o \int_{y_A}^{y_B} \sec\psi_b(y) \{ \int_\nu \cos[\psi_b(y_\nu)-\lambda_j(x,y_\nu)]k_j^{-1}(\nu,\nu_y';x)d\nu\}$$

$$\times u_{nj}(x,y)dy$$

$$+ \int_{y_A}^{y_B} \sec\psi_b(y)[\int_\nu (r_o-y_\nu)\cos\psi_b(y_\nu)k_j^{-1}(\nu,\nu_y';x)d\nu]u_{nj}(x,y)dy$$

$$= - r_o \int_{y_A}^{y_B} \sec\psi_b(y)K_{nj}^{(t)}(x,y)\cos[\psi_b(y)-\lambda_j(x,y)]u_{nj}(x,y)dy$$

$$+ \int_{y_A}^{y_B} \sec\psi_b(y)[\int_\nu (r_o-y_\nu)\cos\psi_b(y_\nu)k_j^{-1}(\nu,\nu_y';x)d\nu]u_{nj}(x,y)dy \ , \qquad \text{(B20)}$$

where the definition (B9) has been used in going to the second expression. The first lines of equations (3.16) and (B20) are identical. Thus, comparing the second lines of these two equations, we must have

$$(r_o-y)K_{nj}^{(\mu)}(x,y) = \sec\psi_b(y) \int_\nu (r_o-y_\nu)\cos\psi_b(y_\nu)k_j^{-1}(\nu,\nu_y';x)d\nu \qquad \text{(B21)}$$

or

$$K_{nj}^{(\mu)}(x,y)$$

$$\triangleq \{[1-(y/r_o)]\cos\psi_b(y)\}^{-1} \int_\nu [1-(y_\nu/r_o)]\cos\psi_b(y_\nu)k_j^{-1}(\nu,\nu_y';x)d\nu \ , \qquad \text{(B22)}$$

in order that equations (3.16) and (B20) represent identical expressions for arbitrary deformations $u_{nj}(x,y)$. The integral with respect to ν in equation (B22) is taken over the full length of line of contact of tooth pair j at zone of contact position x.

To derive the integral equation whose solution yields $K_{nj}^{(\mu)}(x,y)$, we apply the symmetry of equation (B10) to equation (B22) which gives

$$[1-(y/r_o)]\cos\psi_b(y)K_{nj}^{(\mu)}(x,y) = \int_\nu k_j^{-1}(\nu_y',\nu;x)[1-(y_\nu/r_o)]\cos\psi_b(y_\nu)d\nu \ , \tag{B23}$$

which is of the same general form as equation (B2). It follows from equations (B1), (B2), and (B23) that the local tooth-pair stiffness $K_{nj}^{(\mu)}(x,y)$ can be obtained from the solution $p_j(\nu_y';x) = \bar{p}_{\mu j}(\nu_y';x)$ of the integral equation (B1) using for its left-hand side $u_j'(\nu;x) = \bar{u}'_{\mu j}(\nu,x)$ where

$$\bar{u}'_{\mu j}(\nu;x) \triangleq [1-(y_\nu/r_o)]\cos\psi_b(y_\nu) \tag{B24}$$

and

$$\bar{p}_{\mu j}(\nu_y';x) \triangleq [1-(y/r_o)]\cos\psi_b(y)K_{nj}^{(\mu)}(x,y) \tag{B25}$$

from which one obtains $K_{nj}^{(\mu)}(x,y)$ by

$$K_{nj}^{(\mu)}(x,y) = [1-(y/r_o)]^{-1}\sec\psi_b(y)\bar{p}_{\mu j}(\nu_y';x) \ , \tag{B26}$$

where the function $\nu_y' = \nu'(y)$ is determined by equation (B6).

APPENDIX C

DERIVATION OF EXPRESSION FOR h(x,y) GIVEN BY EQUATION (3.15)

From Fig. 19 and the fact that the sum of the interior angles of a triangle is π radians, we have

$$\gamma = \pi - \left(\frac{\pi}{2} - \psi_b\right) - \lambda_j = \frac{\pi}{2} + \psi_b - \lambda_j \ . \tag{C1}$$

Applying the law of sines to the same triangle in Fig. 19 and using equation (C1), we find

$$\frac{r_o - y'}{\sin\left(\frac{\pi}{2} - \psi_b\right)} = \frac{r_o - y}{\sin\left(\frac{\pi}{2} + \psi_b - \lambda_j\right)} \ . \tag{C2}$$

However,

$$\sin\left(\frac{\pi}{2} - \psi_b\right) = \cos\psi_b \tag{C3}$$

and

$$\sin\left(\frac{\pi}{2} + \psi_b - \lambda_j\right) = \cos(\psi_b - \lambda_j) \ . \tag{C4}$$

Combining equations (C3) and (C4) with equation (C2) gives

$$r_o - y' = \frac{\cos\psi_b}{\cos(\psi_b - \lambda_j)} (r_o - y) \tag{C5}$$

or

$$y' = r_o - \frac{\cos\psi_b}{\cos(\psi_b - \lambda_j)} (r_o - y) \ . \tag{C6}$$

Furthermore, from Fig. 19 and equation (C1), we have

$$\frac{h}{y'} = \sin(\pi - \gamma) = \sin\left[\frac{\pi}{2} - (\psi_b - \lambda_j)\right]$$

$$= \cos(\psi_b - \lambda_j) \ . \tag{C7}$$

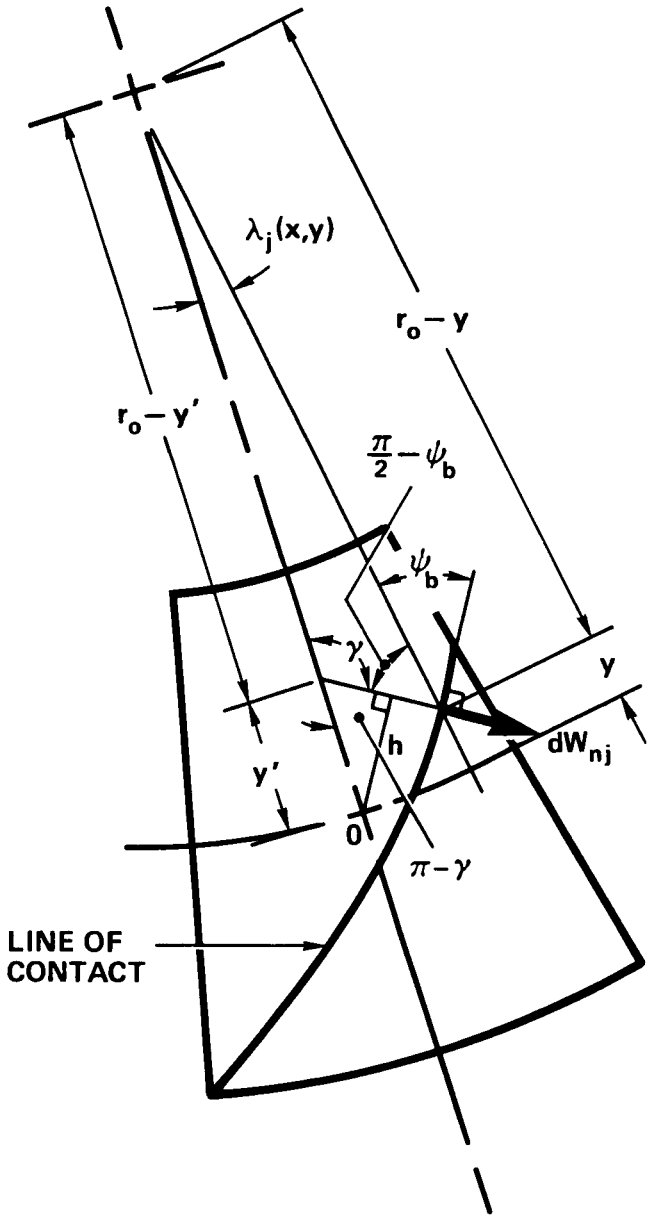

FIG. 19. GEOMETRY REQUIRED FOR DERIVATION OF EXPRESSION FOR h(x,y).

Combining equations (C6) and (C7) yields the desired relationship for h:

$$h = r_o\cos(\psi_b - \lambda_j) - (r_o - y)\cos\psi_b \ . \qquad \text{(C8)}$$

APPENDIX D

INVERSION OF THE MESH STIFFNESS MATRIX K(x)

From equations (2.10) and (3.37) through (3.42), it follows that the coefficient matrix $\mathbf{K}(x)$ in equation (3.40) can be written as

$$\mathbf{K}(x) = \begin{bmatrix} a_1 & a_2 & 0 \\ b_1 & b_2 & 0 \\ c_1 & 0 & c_3 \end{bmatrix}, \tag{D1}$$

when the terms in the matrix (D1) are appropriately identifed. Expressing the inverse $\mathbf{C}(x)$ of $\mathbf{K}(x)$ in terms of the cofactors (ref. 24, p. 17) of the matrix (D1), it can be shown in a straightforward manner that the inverse of the matrix (D1) can be expressed as

$$\mathbf{K}^{-1}(x) \equiv \mathbf{C}(x) = \frac{1}{|\mathbf{K}|} \begin{bmatrix} b_2c_3 & -a_2c_3 & 0 \\ -b_1c_3 & a_1c_3 & 0 \\ -b_2c_1 & a_2c_1 & a_1b_2-a_2b_1 \end{bmatrix}, \tag{D2}$$

where the determinant $|\mathbf{K}|$ of the matrix (D1) is

$$|\mathbf{K}| = c_3(a_1b_2-a_2b_1) . \tag{D3}$$

APPENDIX E

DERIVATION OF EXPRESSION FOR MESH FORCE COMPONENTS IN GEAR COORDINATE SYSTEM

We require the transformation

$$\{x^{(\cdot)}\} = [\ell^{(\cdot)}]\{z^{(\cdot)}\} \tag{E1}$$

that gives the three components $x_i^{(\cdot)}$, i = 1,2,3 of a vector originally expressed in terms of the components $z_i^{(\cdot)}$, i = 1,2,3 where the $x_i^{(\cdot)}$ and $z_i^{(\cdot)}$ coordinate systems are illustrated in Fig. 12 or its mirror image, Fig. 13. The inverse of this transformation normally would be expressed as

$$\{z^{(\cdot)}\} = [\ell^{(\cdot)}]^{-1}\{x^{(\cdot)}\} , \tag{E2}$$

where $[\ell^{(\cdot)}]^{-1}$ is the inverse of the matrix $[\ell^{(\cdot)}]$. However, since both the $x_i^{(\cdot)}$ and $z_i^{(\cdot)}$ coordinate systems are orthogonal, we have (ref. 18, p. 103)

$$[\ell^{(\cdot)}]^{-1} = [\tilde{\ell}^{(\cdot)}] , \tag{E3}$$

where $[\tilde{\ell}^{(\cdot)}]$ is the transpose of the matrix $[\ell^{(\cdot)}]$. From equations (E1) through (E3) and equation (A5), it follows that

$$[\ell^{(\cdot)}] = \begin{bmatrix} c\nu^{(\cdot)} & 0 & -s\nu^{(\cdot)} \\ s\gamma_b^{(\cdot)} s\nu^{(\cdot)} & c\gamma_b^{(\cdot)} & s\gamma_b^{(\cdot)} c\nu^{(\cdot)} \\ c\gamma_b^{(\cdot)} s\nu^{(\cdot)} & -s\gamma_b^{(\cdot)} & c\gamma_b^{(\cdot)} c\nu^{(\cdot)} \end{bmatrix} , \tag{E4}$$

where c and s are abbreviations for cosine and sine operations as in equation (4.5). The angles $\nu^{(\cdot)}$ and $\gamma_b^{(\cdot)}$ are illustrated in Figs. 12 and 13. Using equation (E4), one can readily verify that $[\ell^{(\cdot)}]\,[\tilde{\ell}^{(\cdot)}] = [I]$, where $[I]$ is the identity matrix.

Let $W_z^{(\cdot)}$ denote the six-component generalized force column matrix or vector described in the z_i, i = 1,2,3 coordinate system analogous to the generalized force vector $Q^{(\cdot)}$ defined by equation (4.3) that describes the three torque components and

three force components applied to gear $(\cdot)$ by its mating gear in the $x_i^{(\cdot)}, i = 1,2,3$ coordinate system. Then $Q^{(\cdot)}$ can be obtained from $W_z^{(\cdot)}$ by the transformation,

$$Q^{(\cdot)} = G_1^{(\cdot)} W_z^{(\cdot)} \tag{E5}$$

where the matrix $G_1^{(\cdot)}$ is obtained from equation (E4):

$$G_1^{(\cdot)} = \begin{bmatrix} c\nu^{(\cdot)} & 0 & -s\nu^{(\cdot)} & 0 & 0 & 0 \\ s\gamma_b^{(\cdot)}\, s\nu^{(\cdot)} & c\gamma_b^{(\cdot)} & s\gamma_b^{(\cdot)}\, c\nu^{(\cdot)} & 0 & 0 & 0 \\ c\gamma_b^{(\cdot)}\, s\nu^{(\cdot)} & -s\gamma_b^{(\cdot)} & c\gamma_b^{(\cdot)}\, c\nu^{(\cdot)} & 0 & 0 & 0 \\ 0 & 0 & 0 & c\nu^{(\cdot)} & 0 & -s\nu^{(\cdot)} \\ 0 & 0 & 0 & s\gamma_b^{(\cdot)}\, s\nu^{(\cdot)} & c\gamma_b^{(\cdot)} & s\gamma_b^{(\cdot)}\, c\nu^{(\cdot)} \\ 0 & 0 & 0 & c\gamma_b^{(\cdot)}\, s\nu^{(\cdot)} & -s\gamma_b^{(\cdot)} & c\gamma_b^{(\cdot)}\, c\nu^{(\cdot)} \end{bmatrix}. \tag{E6}$$

The six-component generalized force vector $W_z^{(\cdot)}$ can be obtained from the three-component generalized mesh force vector W defined by equation (4.1) by a further matrix transformation,

$$W_z^{(\cdot)} = G_2^{(\cdot)} W , \tag{E7}$$

which, when combined with equation (E5), yields

$$Q^{(\cdot)} = G^{(\cdot)} W , \tag{E8}$$

where

$$G^{(\cdot)} \triangleq G_1^{(\cdot)} G_2^{(\cdot)} . \tag{E9}$$

We now evaluate the matrices $G_1^{(\cdot)}$, $G_2^{(\cdot)}$, and $G^{(\cdot)}$ for the various gearing configurations listed in Table 1.

Driver clockwise with left-hand spiral or follower counterclockwise with left-hand spiral. Gear (1) shown in Fig. 3 is the clockwise rotating driver of the meshing gear pair shown there. According to the upper portion of the figure, gear (1) has a left-hand spiral (ref. 19, p. 241). The components of the total resultant force exerted on gear (1) by its mate, gear (2), are shown in Fig. 4. These components W_t and W_r and the resultant torque τ taken about the zone of contact center $\underline{0}$ are shown in Fig. 12. The force components W_t and W_r shown in Fig. 12 lie in the plane of contact, which is the plane occupied by the z_1, z_3 and y_1, y_3 axes shown there. Torque τ about the zone of contact center $\underline{0}$ is represented as a vector normal to the plane of contact passing through $\underline{0}$ with its direction governed by the right-hand rule, which is consistent with the sign convention described in the main text since the relationship between the positive direction of each $\rho_i^{(\cdot)}$ and the corresponding $x_i^{(\cdot)}$, i = 1,2,3 in Fig. 12 is governed by the right-hand rule.

To transform this mesh force system to the gear coordinate system $x_i^{(\cdot)}$ and $\rho_i^{(\cdot)}$, i = 1,2,3 illustrated in Fig. 12, we must first express about the origin of the gear coordinate system located at the apex of the base cone shown in Fig. 12 the torque resulting from the total resultant mesh force. This translated torque vector lies along the z_2 axis, and has a value of $\tau + r_o W_t$, positive in the negative z_2 direction as shown in Fig. 12. Since W_t and W_r lie along the z_1 and z_3 axes, respectively, positive in the positive z directions, it follows for this case that the vector $W_z^{(\cdot)}$, defined above, is

$$W_z^{(\cdot)} = \begin{Bmatrix} 0 \\ -(\tau + r_o W_t) \\ 0 \\ W_t \\ 0 \\ W_r \end{Bmatrix}. \tag{E10}$$

From the definition (1) of $\mathbf{W}$, and equations (E7) and (E10), it follows directly that for this case the matrix $G_2^{(\cdot)}$ is

$$G_2^{(\cdot)} = \begin{bmatrix} 0 & 0 & 0 \\ -1 & -r_o & 0 \\ 0 & 0 & 0 \\ 0 & 1 & 0 \\ 0 & 0 & 0 \\ 0 & 0 & 1 \end{bmatrix} . \tag{E11}$$

The validity of equation (E11) can be established by multiplying $G_2^{(\cdot)}$, equation (E11), by W, equation (4.1), which yields $W_z^{(\cdot)}$ as prescribed by equation (E7).

Finally, the matrix $G^{(\cdot)}$ is obtained by multiplying $G_1^{(\cdot)}$ and $G_2^{(\cdot)}$ as indicated by equation (E9):

$$G^{(\cdot)} = \begin{bmatrix} 0 & 0 & 0 \\ -c\gamma_b^{(\cdot)} & -r_o c\gamma_b^{(\cdot)} & 0 \\ s\gamma_b^{(\cdot)} & r_o s\gamma_b^{(\cdot)} & 0 \\ 0 & c\nu^{(\cdot)} & -s\nu^{(\cdot)} \\ 0 & s\gamma_b^{(\cdot)} s\nu^{(\cdot)} & s\gamma_b^{(\cdot)} c\nu^{(\cdot)} \\ 0 & c\gamma_b^{(\cdot)} s\nu^{(\cdot)} & c\gamma_b^{(\cdot)} c\nu^{(\cdot)} \end{bmatrix} . \tag{E12}$$

By comparing equations (4.5) and (E12), one can see that

$$G^{(\cdot)} = -\tilde{T}^{(\cdot)} \tag{E13}$$

when the upper signs in the third column in the right-hand side of equation (4.5) are used, which is consistent with the sign convention described in Table 1. According to equation (E8), equation (E13) verifies equation (4.4) for the case of a driving gear rotating clockwise with left-hand spiral teeth as illustrated in Fig. 3.

Let us turn now to the case of a follower gear rotating counterclockwise with left-hand spiral teeth. This situation is depicted by the follower gear (2) shown in Fig. 3 except that the spiral angle is opposite to that shown in the upper portion of the figure. For this configuration, the total resultant force exerted on the follower gear (2) by the driver gear (1) also is correctly depicted by Fig. 4, and the force system illustrated in Fig. 12 also correctly depicts the forces exerted on the follower gear (2) by the driver gear (1). From this fact, it follows that the results provided by equations (E12) and (E13) also apply to the case of a follower gear rotating counterclockwise as depicted in Fig. 3, but with a left-hand spiral which is the opposite to that illustrated in the figure.

Follower counterclockwise with right-hand spiral or driver clockwise with right-hand spiral. Gear (2) shown in Fig. 3 is the counterclockwise rotating follower of the meshing gear pair shown there. According to the upper portion of the figure, gear (2) has a right-hand spiral. Each force component W_t, W_r, and τ exerted on gear (2) by its mate, gear (1), in this case is directed opposite to that shown in Fig. 4, since that figure illustrates the forces exerted on gear (1) by gear (2).

The configuration shown in Fig. 12 is applicable to the follower gear (2), as well as the driver gear (1). When the above-described mesh force components W_t, W_r, and τ acting on gear (2) are sketched on Fig. 6, one obtains the force system illustrated in Fig. 12 with the exception that the component W_r is directed opposite to that shown in Fig. 12. In this case, consequently, the six-component generalized force vector $\mathbf{W}_z^{(\cdot)}$, which expresses the three torque components and three force components acting on the gear under consideration in the z_i, $i = 1,2,3$ coordinate system, is equal to that given by equation (E10) with the exception that the sign of W_r is reversed:

$$\mathbf{W}_z^{(\cdot)} = \begin{Bmatrix} 0 \\ -(\tau + r_o W_t) \\ 0 \\ W_t \\ 0 \\ -W_r \end{Bmatrix} . \qquad \text{(E14)}$$

From the definition (4.1) and equations (E7) and (E14), it then follows that for the present case the matrix $G_2^{(\cdot)}$ is

$$G_2^{(\cdot)} = \begin{bmatrix} 0 & 0 & 0 \\ -1 & -r_o & 0 \\ 0 & 0 & 0 \\ 0 & 1 & 0 \\ 0 & 0 & 0 \\ 0 & 0 & -1 \end{bmatrix}, \tag{E15}$$

which is the same as equation (E11) except for the sign change in the lowermost element in the third column.

The matrix $G^{(\cdot)}$ is obtained by multiplying the matrices described by equations (E6) and (E15) as indicated by equation (E9). This multiplication yields

$$G^{(\cdot)} = \begin{bmatrix} 0 & 0 & 0 \\ -c\gamma_b^{(\cdot)} & -r_o c\gamma_b^{(\cdot)} & 0 \\ s\gamma_b^{(\cdot)} & r_o s\gamma_b^{(\cdot)} & 0 \\ 0 & c\nu^{(\cdot)} & s\nu^{(\cdot)} \\ 0 & s\gamma_b^{(\cdot)} s\nu^{(\cdot)} & -s\gamma_b^{(\cdot)} c\nu^{(\cdot)} \\ 0 & c\gamma_b^{(\cdot)} s\nu^{(\cdot)} & -c\gamma_b^{(\cdot)} c\nu^{(\cdot)} \end{bmatrix}. \tag{E16}$$

By comparing equations (4.5) and (E16), one can see that equation (E13) is valid in this case also when the lower signs in the third column in the right-hand side of equation (4.5) are used, which is consistent with the sign convention described in Table 1.

We turn now to the case of a driver gear rotating clockwise but with right-hand spiral teeth. This case is depicted by the driver, gear (1), shown in Fig. 3 except that the spiral angle is opposite to that shown in the upper portion of the figure. For this case also, each force component W_t, W_r, and τ exerted on the driver, gear

(1), by the follower, gear (2), is directed opposite to that shown in Fig. 4. Hence, for this case also, the system of forces exerted on the driver, gear (1), by the follower, gear (2), is represented by situation depicted in Fig. 12, with the exception that the component W_r is directed opposite to that shown in Fig. 12. It follows that equations (E14), (E15), and (E16) are valid for this case also, which completes our proof of the validity of equations (4.4) and (4.5) for the last of the four gear element configurations enumerated in the first two lines of Table 1.

Driver counterclockwise with right-hand spiral or follower clockwise with right-hand spiral. Each of the remaining four gear element configuration possibilities delineated in the last two lines in Table 1 represents an exact mirror image of one of the four configurations in the first two lines of the table. Specifically, the third and fourth gear element configurations delineated in each of the two columns in Table 1 represent, respectively, the exact mirror images of the first and second gear element configurations in the same column.

The configuration shown in Fig. 7 is the mirror image of that shown in Fig. 3. The case of a counterclockwise rotating driver with right-hand spiral teeth is illustrated by Gear (1) of Fig. 7. The case of a clockwise rotating follower with right-hand spiral teeth is represented by gear (2) of Fig. 7, except that in this latter case the spiral angle is opposite to that shown in the upper portion of the figure. The forces exerted on the gear under consideration by its mating gear in each of these two cases are represented by the force system shown in Fig. 4. For both cases, this force system also is shown in Fig. 13.

Figure 13 is an exact mirror image of Fig. 12. From Fig. 13, it follows that the expression for the generalized force vector $\mathbf{W}_z^{(\cdot)}$ also is given by equation (E10) for the two gear element configurations under present consideration. Hence, the expressions given by equations (E11) and (E12) for the matrices $\mathbf{G}_2^{(\cdot)}$ and $\mathbf{G}^{(\cdot)}$, respectively, also are applicable to the present two cases, from which it follows that equations (E13), (4.4), and (4.5) also are verified when the upper signs in the third column in the right-hand side of equation (4.5) are used, which is consistent with the sign convention described in Table 1. However, it is important to recognize that for the present two cases, and the two to be described below, the sign convention for each i = 1,2,3 describing the relationship between each rotation component $\rho_i^{(\cdot)}$, and hence, $\tau_i^{(\cdot)}$, and the displacement component $x_i^{(\cdot)}$ is governed by the left-hand rule, as may be seen in Fig. 8 or Fig. 3.

Follower clockwise with left-hand spiral or driver counterclockwise with left-hand spiral. The first of these two cases is represented by gear (2) of Fig. 7, and the second is represented by gear (1) of the same figure except that in this latter case the spiral angle is opposite to that shown in the upper portion of the figure. In each of these two cases, each of the force components exerted on the gear under consideration by its mating gear is directed opposite to that illustrated in Fig. 4. These force components exerted on the gear under consideration are shown in Fig. 13 except that, for the present two cases, the direction of W_r is opposite to that shown in Fig. 13. It follows that, for the present two cases, the generalized force vector $\mathbf{W}_z^{(\cdot)}$ is given by equation (E14); hence, the matrices $\mathbf{G}_z^{(\cdot)}$ and $\mathbf{G}^{(\cdot)}$ are given by equations (E15) and (E16), respectively. Therefore, equation (E13) is valid for these two cases when the lower signs in the third column in the right-hand side of equation (4.5) are used, which is consistent with the sign convention described in Table 1.

APPENDIX F

SIGN OF $A_j(x,y_{ej})$

The definition (5.54) expresses $A_j(x,y_{ej})$ as

$$A_j \triangleq \frac{a_1 g_{1j} - r_o b_1 (g_{2j} - g_{1j})}{a_1 b_2 - b_1 a_2} \quad . \tag{F1}$$

But,

$$a_1 b_2 - b_1 a_2 = a_1 b_2 \left(1 - \frac{b_1 a_2}{a_1 b_2}\right) \quad . \tag{F2}$$

Combining equations (F1) and (F2) gives

$$A_j = \left(1 - \frac{b_1 a_2}{a_1 b_2}\right)^{-1} \left[\frac{a_1 g_{1j} - r_o b_1 (g_{2j} - g_{1j})}{a_1 b_2}\right]$$

$$= \left(1 - \frac{b_1 a_2}{a_1 b_2}\right)^{-1} \frac{1}{b_2} \left[g_{1j} - r_o \frac{b_1}{a_1} (g_{2j} - g_{1j})\right] \quad . \tag{F3}$$

From equation (F3) it is clear that if $b_1 = 0$ and $(g_{1j}/b_2) > 0$, then $A_j > 0$. By comparing equation (5.3) with equation (3.38), we see that $b_2 = \tilde{K}^{(t)}_{c-1}(x;\psi_b)$, which from equations (3.36a) and (3.32a) may be seen always to be positive. Furthermore, it follows from equation (5.22) that g_{1j} always is positive; hence, $(g_{1j}/b_2) > 0$. Therefore, it is necessary to show only that we can set $b_1 = 0$.

The coordinate system we have used was devised to keep equations (3.37) and (3.38) relatively uncoupled. In fact, if $b_1 = 0$, equation (3.38), can be solved for ζ_t independently of the value of μ. From equations (5.3) and (3.38), it follows that

$$b_1 = -\left[\tilde{K}^{(t)}_{yc^{-1}c}(x;\psi_b,\lambda_j) + r_o \tilde{K}^{(t)}_{c^{-1}(1-c)}(x;\psi_b,\lambda_j)\right] \quad , \tag{F4}$$

where the notation is described by equations (3.32g), (3.32d), (3.36g), and (3.36d). The term $\tilde{K}^{(t)}_{c^{-1}(1-c)}(x;\psi_b,\lambda_j)$ in equation (F4) is positive and independent of r_o. Therefore, the magnitude of the positive term $r_o \tilde{K}^{(t)}_{c^{-1}(1-c)}(x;\psi_b,\lambda_j)$ can be adjusted by

changing the value of r_o. The term $\tilde{K}^{(t)}_{yc^{-1}c}(x;\psi_b,\lambda_j)$ can be either positive or negative depending on the value of r_o. However, careful examination of equations (3.32g), (3.32d), and Fig. 11 shows that r_o always can be chosen so that $\tilde{K}^{(t)}_{yc^{-1}c}(x;\psi_b,\lambda_j)$ is made negative with magnitude equal to $r_o\tilde{K}^{(t)}_{c^{-1}(1-c)}(x;\psi_b,\lambda_j)$, which will set $b_1 = 0$. Increasing r_o will decrease the value of b_1, and decreasing r_o will increase the value of b_1.

The value of r_o controls the position of the origin of the coordinate y, as one can see from Fig. 11. We have chosen the value of r_o to position the origin of the coordinate y in the middle of the nominal contact range F, as shown in Fig. 11. This choice tends to keep the magnitude of b_1 very small, as careful examination of equations (3.32g), (3.32d), (3.36g), (3.36d), (F4), and Fig. 11 will show. Thus, with the choice of r_o shown in Fig. 11, we can expect $A_j(x,y_{ej})$ usually to be positive, requiring in these cases no readjustment in the value of r_o.

REFERENCES

1. Buckingham, E., Analytical Mechanics of Gears, McGraw-Hill, New York, 1949. Republished by Dover, New York, 1963.

2. Walker, H., "Gear Tooth Deflection and Profile Modification," The Engineer, October 14, 1938, pp. 409-412; October 21, 1938, pp. 434-436; August 16, 1940, pp. 102-104.

3. Harris, S.L., "Dynamic Loads on the Teeth of Spur Gears," Proceedings of the Institution of Mechanical Engineers, Vol. 172, 1958, pp. 87-100.

4. Gregory, R.W., Harris, S.L., and Munro, R.G., "Dynamic Behavior of Spur Gears," Proceedings of the Institution of Mechanical Engineers, Vol. 178, 1963-1964, pp. 207-218.

5. Niemann, G., and Baethge, J., "Drehwegfehler, Zahnfederhärte und Geräusch bei Stirnrädern, VDI-Z, Vol. 112, 1970, No. 4, pp. 205-214 and No. 8, pp. 495-499.

6. Remmers, E.P., "Analytical Gear Tooth Profile Deisgn," ASME Paper No. 72-PTG-47, 1972.

7. Mark, W.D., "Analysis of the Vibratory Excitation of Gear Systems: Basic Theory," Journal of the Acoustical Society of America, Vol. 63, No. 5, May 1978, pp. 1409-1430.

8. Mark, W.D., "Analysis of the Vibratory Excitation of Gear Systems. II: Tooth Error Representations, Approximations, and Application," Journal of the Acoustical Society of America, Vol. 66, No. 6, Dec. 1979, pp. 1758-1787.

9. Mark, W.D., "Gear Noise Excitation," Engine Noise: Excitation, Vibration, and Radiation, edited by R. Hickling and M.M. Kamal, Plenum, New York, 1982.

10. Welbourn, D.B., "Fundamental Knowledge of Gear Noise - A Survey," Conference on Noise and Vibrations of Engines and Transmissions, Cranfield Institute of Technology, The Institution of Mechanical Engineers, London, July 1979.

11. Smith, J.D., Gears and Their Vibration: A Basic Approach to Understanding Gear Noise, Marcel Dekker, New York, 1983.

12. Mark, W.D., "The Transfer Function Method for Gear System Dynamics Applied to Convential and Minimum Excitation Gearing Designs," NASA Contractor Report 3626, National Aeronautics and Space Administration, Washington, D.C., October, 1982.

13. Sloane, A., Engineering Kinematics, MacMillan, New York, 1941. Republished by Dover, New York, 1966.

14. Baxter, M.L., Jr., "Basic Theory of Gear-Tooth Action and Generation," Chap. 1 in Gear Handbook, D.W. Dudley, editor, McGraw-Hill, New York, 1962.

15. Michalec, G.W., Precision Gearing: Theory and Practice, Wiley, New York, 1966.

16. Ham, C.W., Crane, E.J., and Rogers, W.L., Mechanics of Machinery, 4th edition, McGraw-Hill, New York, 1958.

17. Merritt, H.E., Gears, Pitman, London, 1943.

18. Meirovitch, L., Methods of Analytical Dynamics, McGraw-Hill, New York, 1970.

19. Faires, V.M., and Keown, R.M., Mechanism, 5th edition, McGraw-Hill, New York, 1960. Republished by Krieger, Malabar, Florida, 1980.

20. Remmers, E.P., "The Dynamics of Gear Pair Systems," ASME Paper No. 71-DE-23, 1971.

21. Goldstein, H., Classical Mechanics, Addison-Wesley, Reading, Massachusetts, 1959.

22. Lanczos, C., The Variational Principles of Mechanics, 4th edition, University of Toronto Press, Toronto, 1970. Republished by Dover, New York, 1986.

23. Fung Y.C., Foundations of Solid Mechanics, Prentice-Hall, Englewood Cliffs, New Jersey, 1965.

24. Hildebrand, F.B., Methods of Applied Mathematics, 2nd edition, Prentice-Hall, Englewood Cliffs, New Jersey, 1965.

25. Saaty, T.L. and Bram, J., 1964, Nonlinear Mathematics, McGraw-Hill, New York, pp. 70-76. Republished by Dover, New York, 1981.

26. Seager, D.L., 1970, "Tooth Loading and Static Behavior of Helical Gears," Transactions ASLE, Vol. 13, No. 1, pp. 66-77.

27. Conry, T.F., and Seireg, A., "A Mathematical Programming Method for Design of Elastic Bodies in Contact," ASME Journal of Applied Mechanics, Vol. 38, No. 2, 1971, pp. 387-392.

28. Conry, T.F., and Seireg, A., "A Mathematical Programming Technique for the evaluation of Load Distribution and Optimal Modifications for Gear Systems," ASME Journal of Engineering for Industry, Vol. 95, No. 4, 1973, pp. 1115-1122.

29. Apostol, T.M., Mathematical Analysis, Addison-Wesley, Reading, Massachusetts, 1957, p. 77.

30. Murray, W., Numerical Methods for Unconstrained Optimization, Academic Press, London, 1972, p. 2.

31. Lanczos, C., Applied Analysis, Prentice-Hall, Englewood Cliffs, New Jersey, 1956, pp. 233-235.

32. Bergland, G.D., "A Guided Tour of the Fast Fourier Transform," IEEE Spectrum, Vol. 6, No. 7, 1969, pp. 41-52. Reprinted in Digital Signal Processing, L.R. Rabiner, and C.M. Rader, editors, IEEE Press, New York, 1972, pp. 228-239.

1. Report No.	2. Government Accession No.	3. Recipient's Catalog No.
NASA CR-4081		

4. Title and Subtitle	5. Report Date
Analysis of the Vibratory Excitation Arising From Spiral Bevel Gears	July 1987
	6. Performing Organization Code: 505-42-94

7. Author(s)	8. Performing Organization Report No.
William D. Mark	6451 (E-3580)
	10. Work Unit No.

9. Performing Organization Name and Address	11. Contract or Grant No.
BBN Laboratories Incorporated 10 Moulton Street Cambridge, Massachusetts 02238	NAS3-23703
	13. Type of Report and Period Covered: Contractor Report Final

12. Sponsoring Agency Name and Address	14. Sponsoring Agency Code
National Aeronautics and Space Administration Lewis Research Center Cleveland, Ohio 44135	

15. Supplementary Notes

Project Manager, Fred B. Oswald, Propulsion Systems Division, Lewis Research Center, Cleveland, Ohio 44135.

16. Abstract

This report develops tools required to understand and predict in terms of its underlying causes the vibratory excitation arising from meshing spiral bevel gears. A generalized three-component transmission error of meshing spiral bevel gears is defined. Equations are derived that yield the three components of the generalized transmission error in terms of deviations of tooth running surfaces from equispaced perfect spherical involute surfaces and tooth/gearbody elastic deformations arising from the three components of the generalized force transmitted by the meshing gears. A method for incorporating these equations into the equations of motion of a gear system is described. Equations are derived for the three components of the generalized force transmitted by the gears which are valid whenever inertial effects of the meshing gears and their supports are negligible. Bearing offsets from the positions occupied by the shaft centerlines of perfect spherical involute bevel gears and bearing/bearing support flexibilities enter into the computation of these forces. For given forces transmitted by the gears, the three components of the generalized transmission error are shown to be stationary with respect to small independent variations in the positions of the endpoints of the lines of tooth contact about their true values. One of these transmission error components is shown to take on a minimum value with respect to these variations. A computational procedure based on this extremum principle is described which is suitable for computing the zone of tooth contact in the plane of contact, the three components of the generalized static transmission error, and the Fourier series spectra of these components.

17. Key Words (Suggested by Author(s))	18. Distribution Statement
Spiral bevel gears; Gears; Transmissions; Transmission error; Noise	Unclassified - unlimited STAR Category 37

19. Security Classif. (of this report)	20. Security Classif. (of this page)	21. No. of pages	22. Price*
Unclassified	Unclassified	120	A06

*For sale by the National Technical Information Service, Springfield, Virginia 22161

NASA-Langley, 1987